Forecasting Distributions of Warm-Season Precipitation Associated with 500-hPa Cutoff Cyclones

Abstract of

a thesis presented to the Faculty

of the University at Albany, State University of New York

in partial fulfillment of the requirements

for the degree of

Master of Science

College of Arts & Sciences

Department of Atmospheric and Environmental Sciences

Matthew A. Scalora
2009

ABSTRACT

The forecasting of heavy precipitation and severe weather associated with warm-season 500-hPa cutoff cyclones is a challenge over the northeastern United States (U.S.). Numerical weather prediction models have difficulty predicting aspects of the evolution of cutoff cyclones, such as their deepening or filling rates and tracks. In particular, forecasting the distribution of precipitation in cutoff cyclones can be challenging. The purpose of this research is to increase the understanding of the structure and evolution of cutoff cyclones from which improvements in the skill of forecasting cutoff cyclones can follow. This research was conducted under the National Weather Service Collaborative Science, Technology, and Applied Research (CSTAR) program. The results of this research are intended to provide forecast methodologies and contribute to increased situational awareness concerning cutoff cyclones over the northeastern U.S. during the warm season.

A 61-year (1948–2008) global climatology of objectively identified 500-hPa cutoff cyclones is presented to document the frequency of cutoff cyclones on both hemispheric and regional scales. A cutoff cyclone is defined as a 500-hPa geopotential height minimum possessing at least a 30-m geopotential height rise in all directions for at least 12 h. Major influences on cutoff cyclone development were found to include orography, upper-level jets, and baroclinicity along coasts. Minima in cutoff cyclone frequency are related to either high terrain or to semipermanent high pressure systems.

This study also discusses findings from an in-depth review of 20 warm-season cases of cutoff cyclones passing through the northeastern U.S. Cases were chosen that illustrate the various operational challenges associated with forecasting heavy

precipitation and severe weather in conjunction with cutoff cyclones. Common tropospheric fields and features, including low-level temperature and moisture, low-level jets, and upper-level jet streaks, were composited along with selected parameters used in warm-season precipitation forecasting. A total of 45 cutoff cyclone days, termed storm days, occurring in conjunction with the 20 cutoff cyclone cases were selected for examination. The 45 storm days were examined for evidence of distinctive synoptic-scale flow patterns in order to stratify the datasets based on the tilt of the 500-hPa trough and embedded cutoff, termed a cutoff–trough system. Schematic figures were derived from composites of various meteorological fields and features for the storm days that fit into each cutoff–trough system tilt category. Five distinct patterns of lower-, middle-, and upper-level features were deduced based on the evolution and shape of the 500-hPa cutoff cyclone. These five patterns can be used as a means of pattern recognition when a cutoff cyclone is forecasted to occur over the northeastern U.S.

A diagnostic analysis of two 500-hPa cutoff cyclone cases from the 2008 warm season was also performed. These two cases were selected due to their difficult-to-forecast nature and widespread high-impact weather conditions across the northeastern U.S. One case occurred in June (16–20 June 2008) and the other occurred in July (23–25 July 2008). Although both cases had over 100 severe storm reports, only the July case had widespread flash flooding. Forecast challenges arose from the presence of multiple precipitation modes, including convective lines/bow echoes, heavy-precipitation supercells, and stratiform rain regions.

ACKNOWLEDGEMENTS

I would like to first thank my co-advisors, Lance Bosart and Dan Keyser, for making it possible for me to pursue this research opportunity. They consistently held me to high standards and offered me insight and guidance which helped me to develop skills that will prove useful in my future endeavors. I thank NOAA for their funding of this research through the Collaborative Science, Technology, and Applied Research (CSTAR) program (Grant #NA07NWS4680001). The CSTAR program allows valuable collaboration between student research and National Weather Service operations.

My interactions with NWS focal points Neil Stuart and Tom Wasula from NWS-Albany, NY really helped drive this research. I benefited from their willingness to meet, exchange e-mails, and participate in the Northeast CSTAR online forum. They were also extremely instrumental in the beginning stages of this research by pointing me in the right direction. Other NWS personnel that contributed to this research include Warren Snyder from NWS-Albany, NY and Dan St. Jean from NWS-Gray, ME.

I would also like to thank Kevin Tyle and David Knight for their technical support and dedication to the department. Their willingness to exchange e-mails, even if it was in the evening or on the weekend, helped me to complete this research efficiently. Celeste Iovinella, Barbara Zampella, and Patricia Seguin were all extremely helpful with administrative issues.

The graduate students and professors deserve much recognition for helping me with my coursework and research. I came to school at UAlbany without ever taking a course on meteorology and the department was extremely helpful as I adjusted to the

program here. In particular, I would like to thank Chris Thorncroft for his willingness to meet with me regarding questions and concerns I had during my first semester as a graduate student. I am also grateful to Anantha Aiyyer and Brandon Smith for creating the programs I needed to perform an updated global cutoff cyclone climatology. Fellow graduate students, Alan Srock, Gareth Berry, and Kay Shelton, are thanked for helping me with issues concerning FORTRAN programming.

Finally, I would like to thank my family and girlfriend, Allison, for their love and support over my two years here at UAlbany. My father and mother have always been great role models and encouraged me to pursue whatever interests I had. Their support has helped me to stay motivated and complete my research in a timely manner. I thank Allison for the fun times we've shared over the past two years and always supporting me with the decisions I've made.

TABLE OF CONTENTS

LIST OF FIGURES

1. Introduction

1.1 Overview

The forecasting of precipitation distributions associated with warm-season 500-hPa cutoff cyclones is a challenge over the northeastern United States (U.S.). Numerical weather prediction models have difficulty predicting aspects of the evolution of cutoff cyclones, such as their deepening or filling rates and tracks (e.g., Hawes and Colucci 1986). Cutoff cyclones are generally displaced from the mean steering flow aloft, which leads to a slower forward speed than a typical open wave (Palmén 1949; Bell and Bosart 1989, hereafter referred to as BB). Resulting slow-moving cutoff cyclones can lead to blocking patterns, which slow the forward speed of upstream systems and create stagnant weather patterns within the blocking region (e.g., Rex 1950; Colucci 1985, 1987). Long-lasting cutoff cyclones are generally associated with continual negative 500-hPa geopotential height anomalies (Dole and Gordon 1983; Dole 1986). Cutoff cyclones form either to the north or south of the main branch of the westerlies in the Northern Hemisphere. Those developing to the north, also referred to as closed lows, are associated with deepening cold-core troughs (e.g., Rogers and Bosart 1986). Those forming to the south of the westerlies occur more frequently, are more barotropic in nature, and may be associated with blocking patterns (e.g., Palmén 1949; BB).

The need for improvement in quantitative precipitation forecasts (QPFs) has often been cited (e.g., Anthes 1983; Jensenius 1990; Junker and Hoke 1990; Fritsch et al. 1998; Fritsch and Carbone 2004). Cutoff cyclones have been documented to produce about

30% of the annual precipitation over the northeastern U.S. (Atallah and Aiyyer 2002). Their structure and slow speed creates difficulties in precipitation forecasts (Hawes and Colucci 1986). Precipitation distributions can be a challenge to predict in models as forcing for ascent (e.g., vorticity or thermal advections) tends to be weaker and less widespread than in typical open-wave cyclones. In addition, the complex terrain over the northeastern U.S. modulates these precipitation distributions. For example, the orientation of low-level flow with respect to terrain features can affect which locations get the heaviest precipitation (Smith 2003). The high-impact nature of cutoff cyclones is shown by both the flooding and severe weather threat these systems pose. The difficult-to-forecast nature of 500-hPa cutoff cyclones is the basis for further research on such systems. The purpose of this research, through use of climatologies and case studies, is to improve the skill in forecasting cutoff cyclones.

1.2 Literature Review

1.2.1 Theory of Formation and Evolution of Cutoff Cyclones

Crocker et al. (1947) studied the formation of an upper-level cold pool and theorized that flow deformation in the middle and upper troposphere can result in the separation of a cold (warm) pool equatorward (poleward) of the mean flow. Figure 1.1, taken from Fig. 2 of Palmén and Nagler (1949), displays the process of isolated cold pool formation. As cold pools migrate equatorwards they undergo subsidence and associated stretching and horizontal convergence in upper levels. Vorticity then increases at the

level of maximum convergence which induces a cyclonic circulation that can act to deform the mean flow in a way that will isolate and "cut off" the cold pool from its polar source region. These ideas were supported and further explored in Palmén (1949) and Eliassen and Kleinschmidt (1957).

The formation of a cutoff cyclone can also be explained using the principle of potential vorticity (PV) conservation in a barotropic atmosphere as shown by Rossby (1940):

$$\frac{\zeta + f}{\Delta p} = \text{constant.} \qquad (1)$$

Here, ζ is the relative vorticity, f is the Coriolis parameter, and Δp is the column depth in pressure coordinates. As discussed in Palmén and Newton (1969, hereafter referred to as PN), as a column of air travels equatorwards it undergoes stretching (an increase in Δp) and a decrease in planetary vorticity (f). For the relationship in Eq. (1) to hold true, relative vorticity (ζ) must increase. An increase in relative vorticity will lead to a cyclonic circulation that may deform the mean flow if strong enough.

As cutoff cyclones evolve they oftentimes can be associated with blocking regimes. Figures 1.2a–c, taken from Figs. 26a–c of Berggren et al. (1949), show a series of schematics of unstable wave development as a cutoff cyclone forms equatorward of the mean flow. Disturbances amplify as strong zonal flow upstream from the blocking region approaches the block from the west and slows down (Berggren et al. 1949). Rex (1950) explained how such a blocking pattern can lead to complicated forecasts, as several different structures can form. PN (sec. 10.4) described these various structures other than cutoff cyclones that can result from significantly amplifying upper-level waves

(Figs. 1.3a–e, taken from Figs. 10.4a–e of PN). Figure 1.3d most clearly depicts a cutoff cyclone.

Hsieh (1949) studied the development and evolution of a cutoff cyclone over North America from March 1948. He observed that a rapid intrusion of polar air into an upper-level jet can lead to the formation of a cold dome of air "cut off" from the mean flow. Keyser and Shapiro (1986, sec. 2d), Bell and Bosart (1993), and Bell and Keyser (1993) all examined how a preexisting trough and upstream wind maximum can interact to form a cutoff cyclone. They found that as the wind maximum reaches the base of the upper-level trough, absolute vorticity is concentrated at the base of the trough and creates a closed cyclonic circulation.

A PV framework can also be used to explain cutoff cyclone formation and evolution. PN studied a cutoff cyclone over North America that was first analyzed by Palmén and Nagler (1949). PN described the cutoff cyclone as a self-sustaining cold vortex but still attached to a polar source region to the north by an "umbilical cord" cold shear line. Hoskins et al. (1985) used PV formulated in isentropic coordinates to show that this "umbilical cord" consisted of a high PV region as is the cold pool. The poleward cold air source region acts as a high PV reservoir. A later study by Thorncroft et al. (1993) showed that isolated pockets of high PV air constituting a cutoff cyclone can form as a result of two different nonlinear life cycles of baroclinic waves [Figs. 1.4a–b, taken from Figs. 12a–b of Thorncroft et al. (1993)]. The LC1 life cycle (Fig. 1.4a) involves anticyclonic wrapping of PV and forms a cutoff cyclone on the equatorward side of the mean jet. The LC2 life cycle (Fig. 1.4b) involves cyclonic wrapping of PV and forms a cutoff cyclone on the poleward side of the mean jet. Cutoff cyclones formed in the LC2

life cycle can be associated with "bombs" (rapidly deepening low-level cyclones), as seen, e.g., in Sanders and Gyakum (1980) and Konrad and Colucci (1998).

1.2.2 Structure of Cutoff Cyclones

It was originally believed that upper-level cutoff cyclones were separate entities from low-level cyclones (Hsieh 1949; Palmén 1949; Palmén and Nagler 1949). Peltonen (1963) observed structural similarities at various levels in a cutoff cyclone case study that occurred in Europe on 8–20 November 1959. Figures 1.5a–d, taken from Figs. 7a–d of Peltonen (1963), shows the system at levels ranging from the surface through 300 hPa. The cyclone centers become more symmetric in upper levels, where temperature distributions are fairly symmetric as well. Figure 1.6, taken from Fig. 8a of Peltonen (1963), shows a vertical cross-section along line *a–a* in Fig. 1.5c. The thick solid line denotes the "tropopause funnel" within the cutoff circulation (PN). Below this "tropopause funnel" there are upward (downward) sloping isentropes (isotherms) approaching the cutoff cyclone from both sides. The depressed isotherms found under the "tropopause funnel" signify the cold-core structure of the cutoff cyclone. Above the tropopause and into the lower stratosphere, the isentropes (isotherms) bulge downward (upward) above the tropospheric cold-core cutoff cyclone, indicative of a warm-core structure.

The structure of a cutoff cyclone is characterized by a symmetric distribution of temperature and geopotential height where values decrease inwards with minima at the center of the cyclonic circulation. The symmetry of cutoff cyclones can also be shown by

overlaying PV on potential temperature surfaces. Hoskins et al. (1985) showed how cutoff cyclones consist of anomalously high values of PV in their cores. Thorpe (1986) also used the PV framework to explain cutoff cyclone structure. He used the invertibility principle formulated by Eliassen and Kleinschmidt (1957), which applies to the PV structures of balanced disturbances. Figure 1.7, taken from Fig. 1 of Thorpe (1986), shows the vertical structure of an idealized cutoff cyclone. Noteworthy is the presence of the "tropopause funnel" and upward sloping isentropes towards the cutoff cyclone core. The strongest winds are found above regions where potential temperature contours slope the most, consistent with thermal wind balance. Bell and Keyser (1993) also noted that cutoff cyclones are associated with anomalously high PV.

1.2.3 Cutoff Cyclone Climatologies

1.2.3a Cutoff Cyclone Distribution and Genesis/Lysis

Studies of the global distribution of cutoff cyclones are less common relative to studies of cutoff cyclone structure. The first studies of cutoff cyclone distributions focused on the Southern Hemisphere and showed that cutoff cyclones commonly form in association with a blocking regime over eastern Australia and New Zealand (e.g., Kerr 1953; van Loon 1956). PN examined the Northern Hemisphere and found that cutoff cyclones occur preferentially along sections of the westerlies (e.g., western U.S. and southwestern Europe). Parker et al. (1989) performed a comprehensive study of cutoff cyclones over the west half of the Northern Hemisphere over a 36-year period. They

found that cutoff cyclone frequency increases over the North Pacific Ocean during summer. BB completed the first cutoff cyclone climatology that spanned the entire Northern Hemisphere. They used a 15-year dataset derived from National Meteorological Center (NMC) analyses (2° × 5° grid) to obtain an objective distribution of cutoff cyclones. Cutoff cyclones were found to commonly occur north of and within the mean westerlies. Areas of maximum genesis include the North Pacific Ocean and Gulf of Alaska, north-central Canada and Hudson Bay region, northeastern U.S. through Greenland, and southern Europe. Cutoff cyclones are also favored south of the mean belt of westerlies (e.g., eastern Atlantic Ocean eastwards to central Asia). Another important finding in BB was that lysis areas were documented to be generally near or just downstream of genesis areas, consistent with the slow movement of cutoff cyclones. Other areas, e.g., southern Europe and the northwest Atlantic Ocean, were favored for more mobile systems.

Bell and Bosart (1994) continued BB's study of cutoff cyclone distributions by focusing on the dynamical precursors (e.g., significant downstream planetary-scale ridge amplification) that lead to common areas of cutoff cyclone genesis in the Northern Hemisphere (e.g., southwestern and eastern U.S., lee of Alps). Smith (2003) found much in common between his cutoff cyclone distributions (e.g., areas of genesis and lysis) and those in Parker et al. (1989) and BB. Figure 1.8, taken from Fig. 3.2 of Smith (2003), shows a plot representing the frequency of cutoff cyclone occurrence over the Northern Hemisphere. Maxima correspond to those found in BB, and include the North Pacific Ocean, north-central Canada, off the southern coast of Greenland, and southern Europe.

Several studies link cutoff cyclone formation to topography. Tennant and Van Heerden (1994) noted that topography was at least partially responsible for cutoff cyclone formation over southern Africa. The effect of topography on cutoff cyclone genesis over the North Atlantic Ocean was examined by Doyle and Shapiro (1999). They discovered that cutoff cyclones developed in response to an orographically induced jet off of southern Greenland.

1.2.3b Cyclone Tracking

Early cyclone tracking techniques were mainly subjective and relied on synoptic reasoning due to the absence of large datasets and sufficient computer power (e.g., Bowie and Weightman 1914; Reitan 1974). Moreover, observational data were lacking prior to the International Geophysical Year in 1957–1958. Objective cyclone tracking methods were eventually implemented to perform more thorough and reliable climatologies (e.g., König et al. 1993; Hodges 1994; Sinclair 1997; Blender and Schubert 2000; Geng and Sugi 2001). Results from these objective cyclone tracking studies led to the conclusion that there are three main surface cyclone tracks across North America: 1) northeastward moving cyclones that form over the southwestern U.S.; 2) east-southeastward moving cyclones that form over western and central Canada; and 3) northeastward moving cyclones that form near the mid-Atlantic region. Alpert et al. (1990) identified intermonthly track variations within seasons in his study of surface cyclones over the Mediterranean Sea. Geng and Sugi (2001) addressed winter surface cyclone variability in terms of speed, intensity, and deepening rates over the North Atlantic Ocean. They

found that stronger cyclones have faster speeds and deepening rates than weaker cyclones. Hoskins and Hodges (2002) used both quasi-geostrophic and PV frameworks to study winter cyclone tracks across the Northern Hemisphere, from which they found that lower- and upper-level disturbances occur preferentially along a northeastward oriented band over the North Atlantic Ocean.

Novak et al. (2002) and Smith (2003) performed comprehensive studies of upper-level cyclones (i.e., 500-hPa cutoff cyclones) using an objective tracking scheme and methodologies set forth in Geng and Sugi (2001). Novak et al. (2002) created warm-season tracks, while Smith (2003) created cool-season tracks. Mean warm-season tracks were subjectively drawn [Fig. 1.9, taken from Fig. 2 of Novak et al. (2002)] using the objectively produced tracks to identify particular "cutoff cyclone freeways". These tracks include: 1) the Southwest track, which forms in the southern Great Plains and tracks through northern New England; 2) the Zonal track, originating in the central Great Plains and extending through the mid-Atlantic; 3) the Great Lakes track, extending from central Canada through northern New England; 4) the Northwest track, which originates over Hudson or James Bay; and 5) the Atlantic/Coastal track, running northeastward along the eastern U.S. coast. The Great Lakes track is the most common, followed closely by the Northwest track. The Atlantic/Coastal track is sometimes associated with tropical cyclones undergoing extratropical transition.

1.2.4 Precipitation in Cutoff Cyclones

Before the advent of real-time upper-air data, precipitation was not thought to have much association with upper-level features (Jorgensen 1963). Studies on precipitation processes dealt mainly with surface data, and because of this focus, it was generally accepted that precipitation in midlatitudes was mostly tied to surface cyclones or baroclinic zones. Hsieh (1949) was one of the first investigators to address precipitation distributions associated with cutoff cyclones [Fig. 1.10, taken from Fig. 13 of Hsieh (1949)]. Hsieh noted that although geopotential height and temperature are nearly symmetric about the cutoff cyclone, precipitation is maximized to the east and southeast of the cutoff cyclone center. This location is where upper-level divergence would be favored as described in PN (sec. 12.6).

Jorgensen et al. (1967) performed a precipitation climatology for 700-hPa closed cyclones over the intermountain western U.S. over a 39-month period. They found that areas receiving the most significant precipitation were situated just to the southeast of the centers of these cyclones. Weaker cyclones tend to produce lighter precipitation amounts and exhibit a pattern whereby the heaviest precipitation is shifted to the south and west of the cyclone center. Klein et al. (1968) and Korte et al. (1972) expanded upon this precipitation climatology by using the same period of time and studying precipitation distributions with respect to cutoff cyclones at various levels in the troposphere. Figure 1.11 [taken from Fig. 8 of Klein et al. (1968)] showed that the highest frequency of measurable precipitation associated with 500-hPa cutoff cyclones is about 2.5° south and 3.5° east of the cyclone center. This result confirms the earlier finding by Hsieh (1949) that precipitation is most commonly found in the southeastern quadrant of a cutoff cyclone. Klein et al. (1968) and Korte et al. (1972) also found that precipitation occurs

with about half of 500-hPa cutoff cyclones over the western U.S. states. Taljaard (1985) found that orography can have an effect on the distribution of light-to-moderate precipitation associated with cutoff cyclones.

More recently, Fracasso (2004) and Najuch (2004) performed 51-year (1948–1998) climatologies of precipitation associated with 500-hPa cutoff cyclones based on tracks and months. Fracasso (2004) focused on the cool season (October–May) and found that heaviest precipitation amounts occur along coastal areas and near the higher elevations of the northeastern U.S. Lighter precipitation amounts are found to the south and west of these areas and in the lower elevations away from the coast. Fracasso (2004) also noted that monthly precipitation amounts associated with cutoffs decrease from October until January, and then increase to a maximum in April. Najuch (2004) complemented the Fracasso (2004) study by focusing on the warm season (June–September). She found that the heaviest precipitation amounts in cutoffs were again located along the Atlantic Coast. Najuch (2004) also found that the most intense precipitation occurs in the month of August when it is believed that late warm-season warm coastal waters and warm air temperatures likely enhance convective activity, leading to much higher daily rainfall amounts in the northeastern U.S. Orographic lift was also found to enhance precipitation from the coastal plains to the intermountain regions of the northeastern U.S.

1.3 Study Goals and Organization of Thesis

The main goals of this thesis are threefold: 1) to diagnose and display the climatological behavior of cutoff cyclones on hemispheric and regional scales; 2) to examine several warm-season cutoff cyclones for evidence of distinctive synoptic-scale flow patterns and stratify the resulting patterns; and 3) to analyze two warm-season cutoff cyclone cases that illustrate the various problems with forecasting heavy precipitation and severe weather associated with cutoff cyclones. The results of this research are intended to provide forecast methodologies and contribute to increased situational awareness concerning cutoff cyclones over the northeastern U.S. during the warm season.

The first part of this study updates the global climatology performed by Smith (2003) that documents the frequency of cutoff cyclones on both hemispheric and regional scales. Data are presented in the form of maps and histograms of frequency for selected geographical areas.

The second part of this study discusses findings from an in-depth study of 20 warm-season cutoff cyclones. All these systems tracked through the northeastern U.S. and affected the region with varying amounts of precipitation and severe weather.

The third part of this study examines two representative case studies from the 2008 warm season. These cases were difficult to forecast and produced high-impact weather conditions across the northeastern U.S. Both cases involved several severe storm reports, while only one had widespread flash flooding.

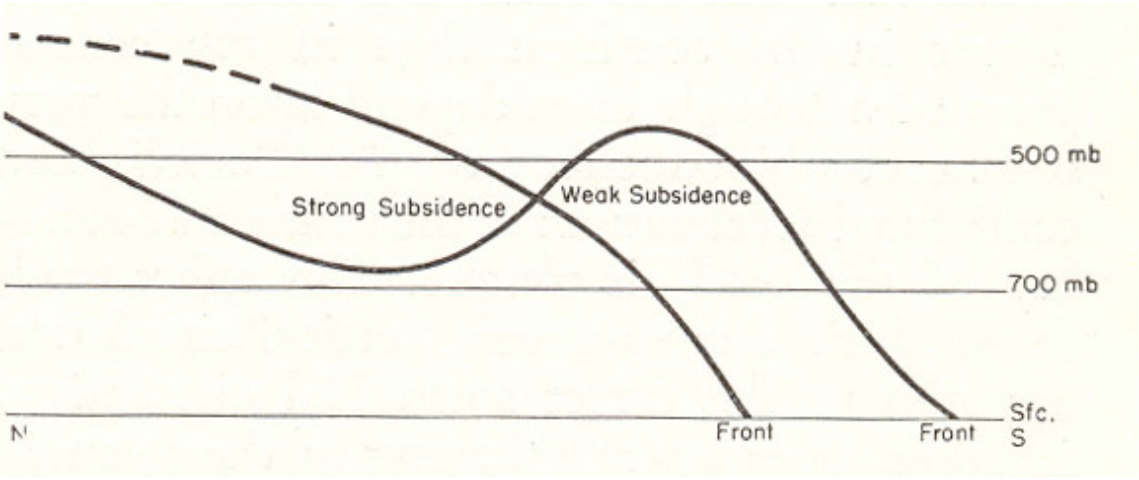

Fig. 1.1. Schematic meridional cross section through an upper-level trough showing the profile of the polar air before and after the formation of a cutoff cyclone. Source: Palmén and Nagler (1949), Fig. 2.

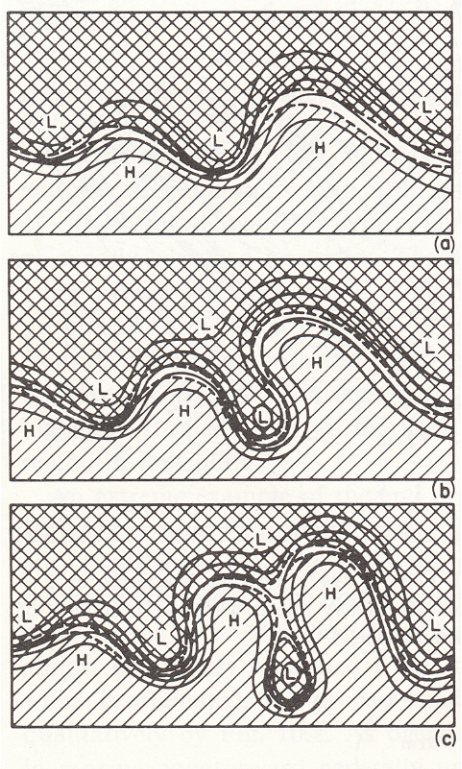

Figs. 1.2a–c. Idealized schematics of the development of unstable waves at 500 hPa, in association with the establishment of a blocking anticyclone at high latitudes and a cutoff cyclone at low latitudes. Warm air (hatched) is separated from cold air (cross-hatched) by frontal boundaries (dashed lines). Solid lines represent streamlines. Source: Berggren et al. (1949), Figs. 26a–c.

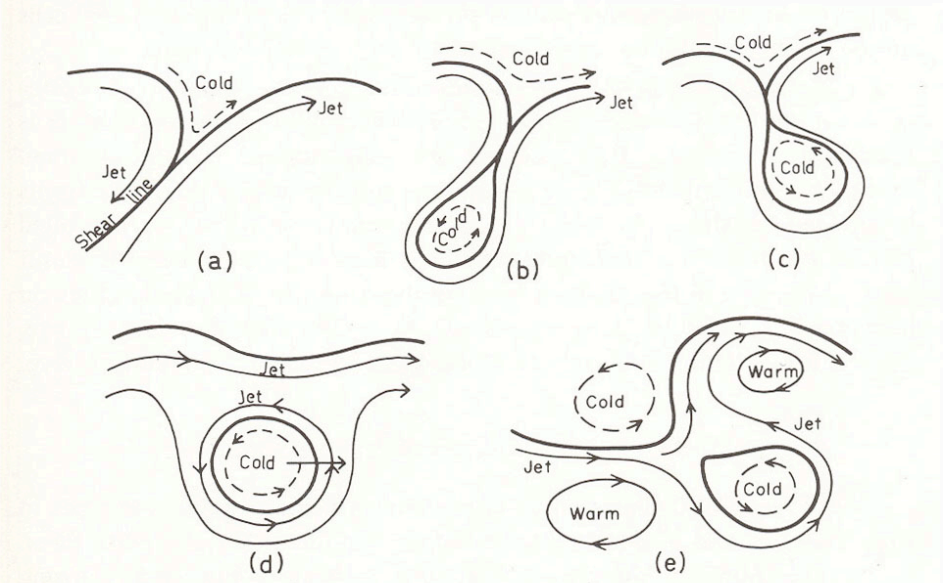

Figs. 1.3a–e. Five characteristic types of disturbances resulting from the extreme growth of upper-level waves. Thick solid lines represent fronts. Streamlines in warm (cold) air are represented by solid (dashed) arrows. Source: Palmén and Newton (1969), Figs. 10.4a–e.

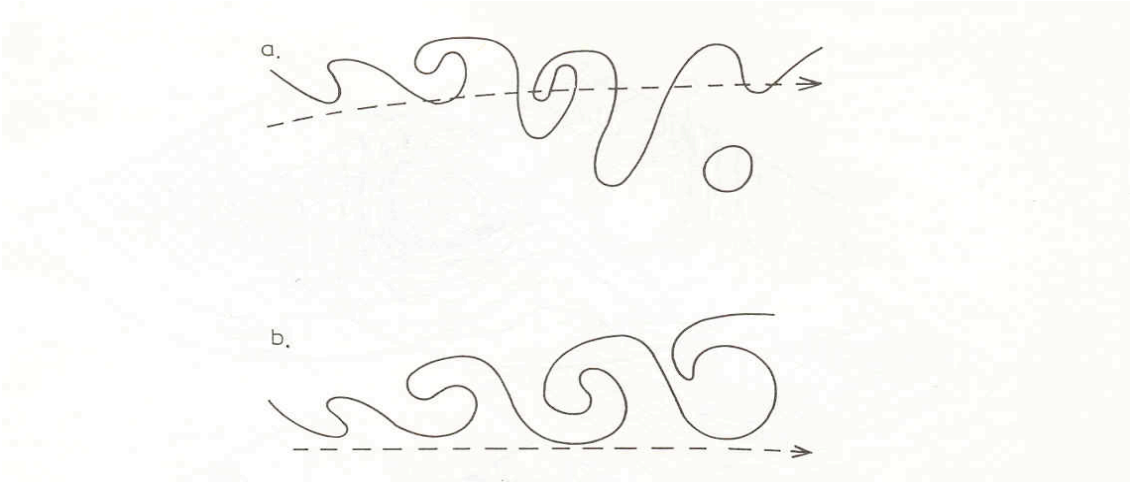

Figs. 1.4a–b. Schematic of a PV–θ contour (solid line) in an Atlantic storm track sharing its main characteristics with (a) an LC1-type life cycle and (b) an LC2-type life cycle. The mean jets are represented by the dashed arrows. Source: Thorncroft et al. (1993), Figs. 12a–b.

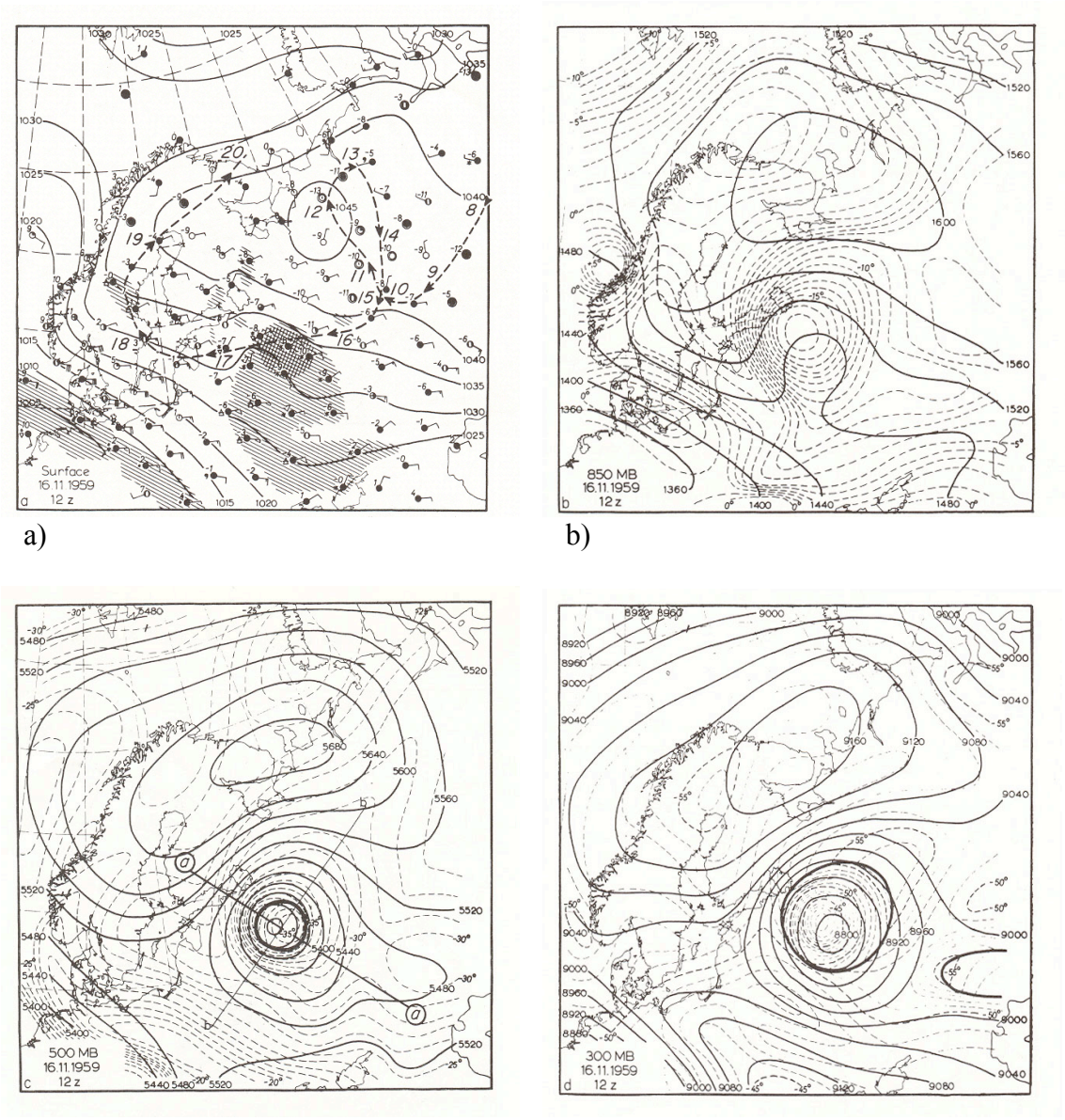

a) b)

c) d)

Figs. 1.5a–d. (a) surface, (b) 850 hPa, (c) 500 hPa, (d) 300 hPa level for 1200 UTC 16 November, 1959. In (a), temperatures are in °C; precipitation areas are hatched, with areas exceeding 1 mm × 12 h^{-1} cross-hatched. In other charts, isotherms are at 1°C intervals and geopotential height contours are at 40 m intervals. Thick lines in (c) and (d) are the tropopause intersections. The path of the 500-hPa cyclone center is shown in (a) with the arrowheads indicating its location at 0000 UTC on the dates given. Source: Peltonen (1963), Figs. 7a–d.

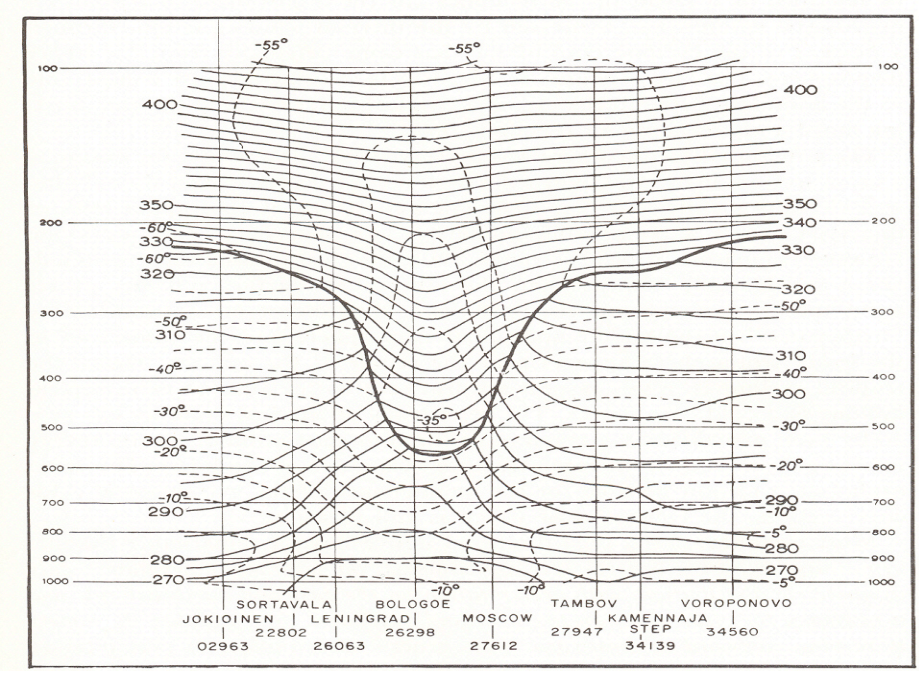

Fig. 1.6. Vertical cross section along line *a–a* in Fig. 1.5c. Shown is the tropopause (thick solid line), isotherms (dashed lines, contour interval is 5°C), and isentropes (solid lines, contour interval is 5 K). Source: Peltonen (1963), Fig. 8a.

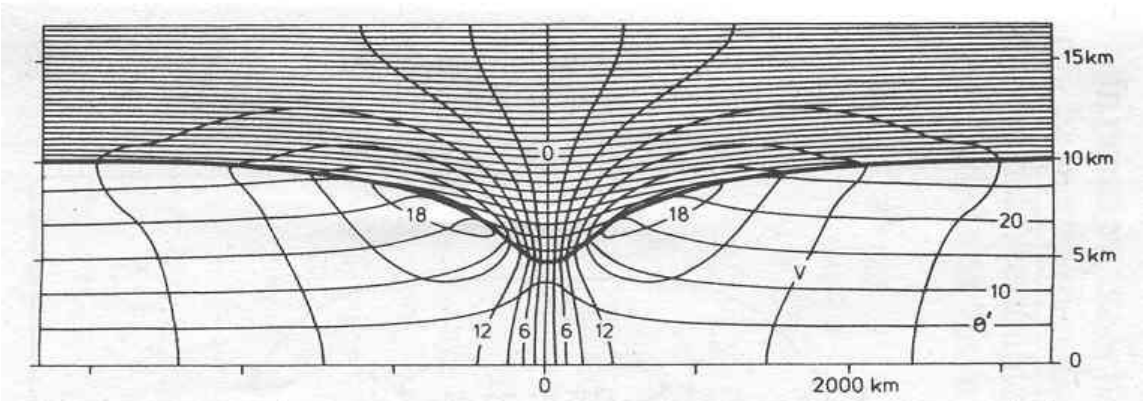

Fig. 1.7. Idealized vertical cross section for a cold core, upper-level cyclone. Shown are isotachs (v, solid lines, contour interval is 3 m s^{-1}), isentropes (θ', solid lines, contour interval is 5 K), the tropopause (thick solid line), and the axis of symmetry (represented by the "0" label in the horizontal axis). Source: Thorpe (1986), Fig. 1.

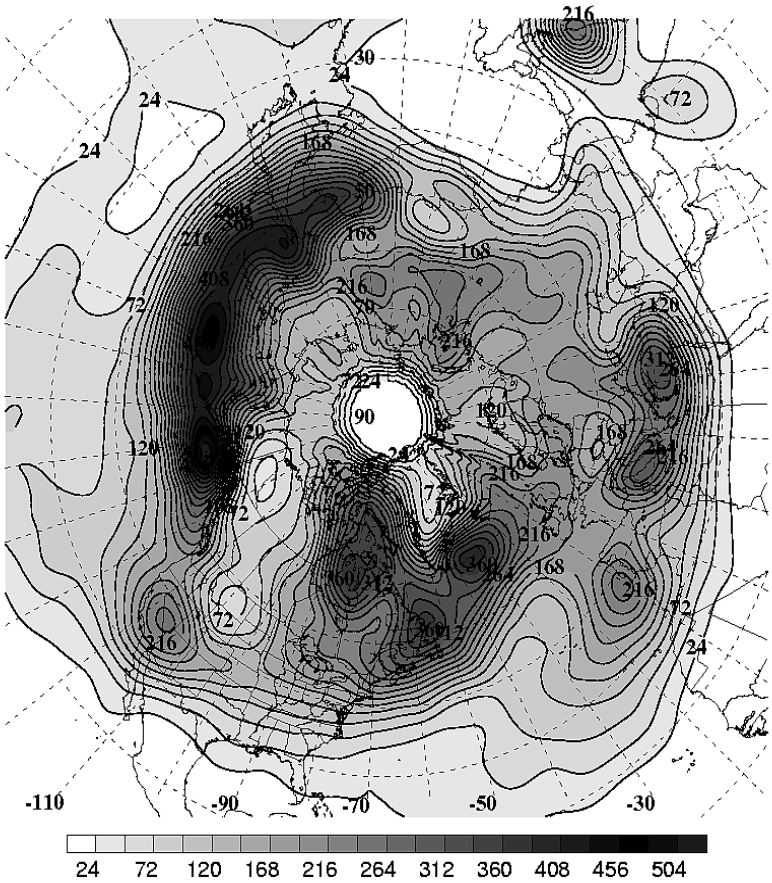

Fig. 1.8. Total number of cutoff cyclone events (shaded and contoured every 24 events) per grid point for the Northern Hemisphere for 1948–2001. Source: Smith (2003), Fig. 3.2.

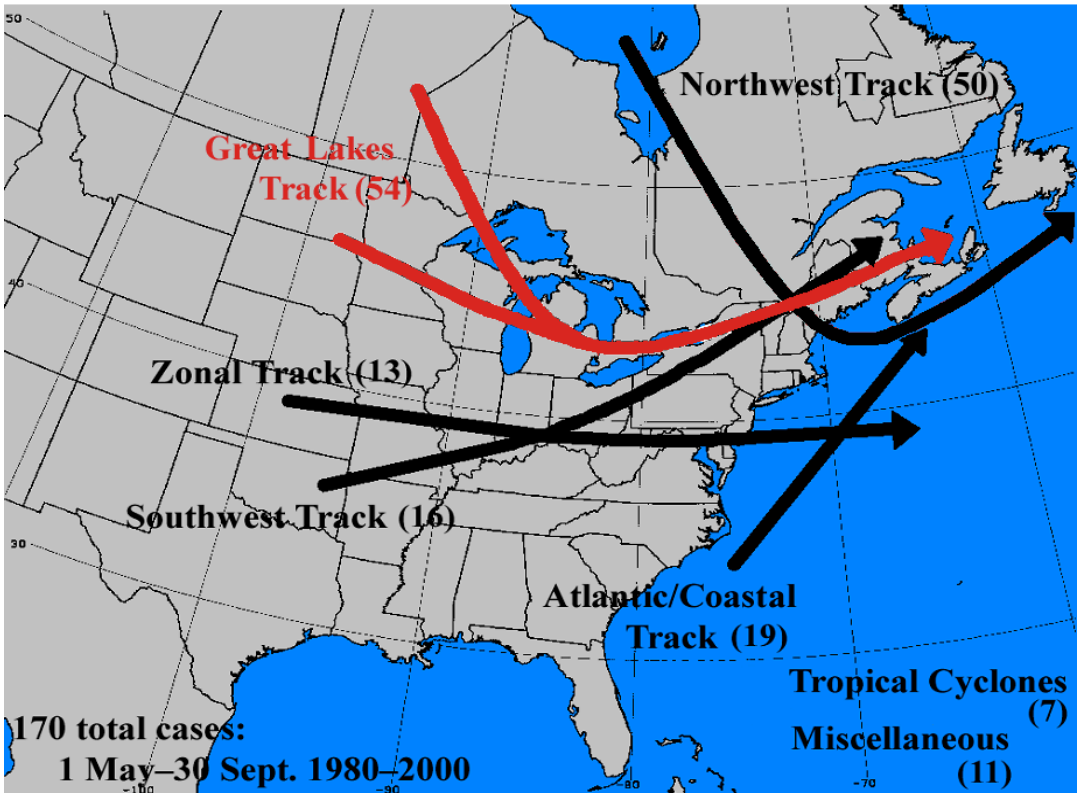

Fig. 1.9. Five main tracks followed by 500-hPa cutoff cyclones during warm-season months (May–September) derived from a subjective tracking scheme. The dataset ranges from 1980 through 2000 for a total of 170 cutoff cyclones cases. Source: Novak et al. (2002), Fig. 2.

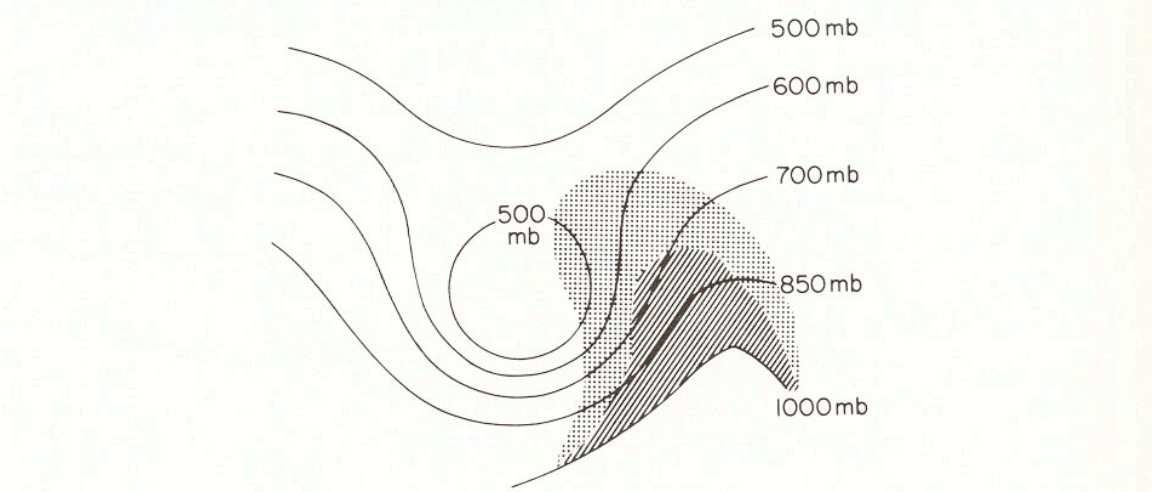

Fig. 1.10. Schematic representation of precipitation relative to upper-level geopotential height contours (solid lines). Heavier precipitation is hatched, lighter precipitation is stippled. Source: Hsieh (1949), Fig. 13.

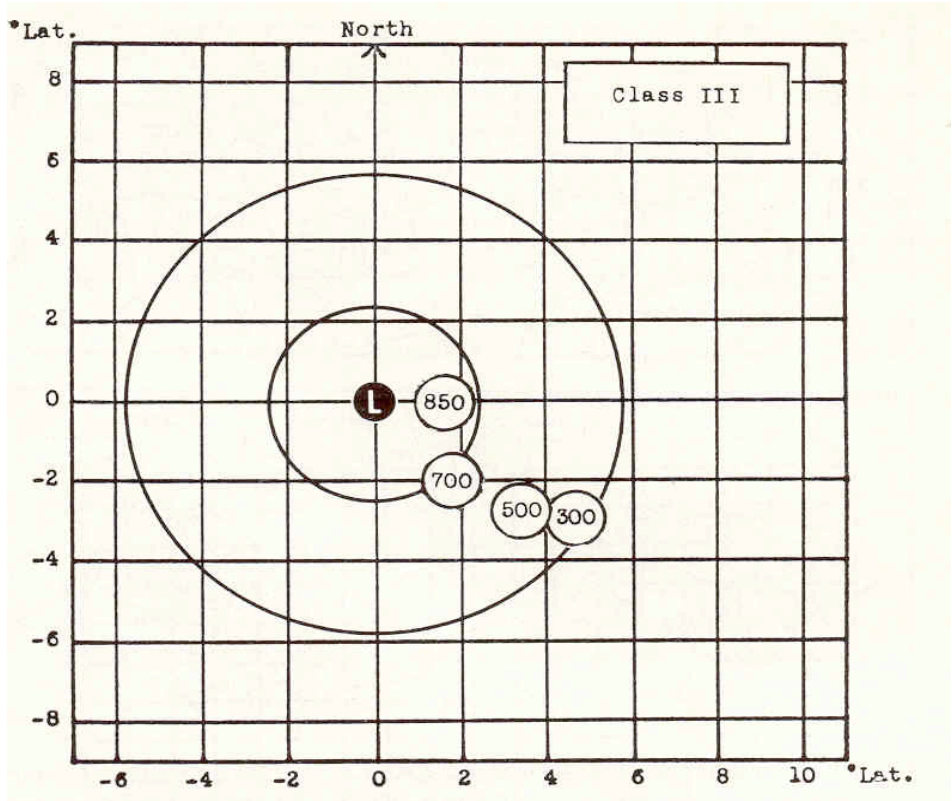

Fig. 1.11. Areas of maximum frequency of occurrence of measurable precipitation associated with the most intense (Class III) cyclones, centered at the origin for 850, 700, 500, and 300 hPa. Symmetrical circles represent idealized contours about the cyclone center at any level. Source: Klein et al. (1968), Fig. 8.

2. Data and Methodology

2.1 Data Sources

2.1.1 Climatology

The climatology portion of this research made use of the National Centers for Environmental Prediction (NCEP)–National Center for Atmospheric Research (NCAR) global gridded reanalysis dataset (Kalnay et al. 1996; Kistler et al. 2002). The NCEP–NCAR reanalysis has a 2.5° latitude–longitude grid and 6-h temporal resolution. Four-times-daily gridded 500-hPa geopotential height analyses for the period 1 January 1948 through 31 December 2008 were utilized to construct appropriate climatological fields.

2.1.2 Case Studies

Several sources of data were used for the overview of 20 case studies and the detailed diagnostic analyses of two cases from 2008. The four-times-daily NCEP Global Forecast System (GFS) (Environmental Modeling Center 2003) 1.0° × 1.0° final analyses were used to assess the synoptic-scale and mesoscale weather conditions for cutoff cyclone cases that occurred during 2000–2006. The 0.5° × 0.5° GFS initialized analyses became available starting 7 November 2006 and were used to study 2007–2008 cutoff cyclone cases with increased grid resolution.

The NCEP Climate Prediction Center Unified Precipitation Dataset (UPD) (Higgins et al. 1996) was used to obtain 24-h (1200–1200 UTC) precipitation amounts for the 2000 cases. The UPD is a 0.25° latitude–longitude gridded dataset derived from three sources: National Climatic Data Center (NCDC) daily cooperative observer (COOP) stations, River Forecast Center data, and daily accumulations from the NCDC Hourly Precipitation Dataset. The UPD is available online at http://www.cdc.noaa.gov/. Because of the tendency of the UPD to underestimate precipitation amounts (e.g., Atallah et al. 2007), the National Precipitation Verification Unit (NPVU) quantitative precipitation estimates (QPEs), which became available starting August 2000, were utilized for the 2001–2008 cases. This 10-km resolution dataset encompasses both rain gauge and radar-estimated precipitation amounts (McDonald and Baker 2001). In addition, National Weather Service (NWS) COOP reports were included in the NPVU dataset starting in 2004. The NPVU dataset is available online at http://www.hpc.ncep.noaa.gov/npvu/.

Surface observations obtained from NWS Automated Surface Observing System (ASOS) sites and buoy and ship observations were plotted using plotting routines at the Department of Atmospheric and Environmental Sciences, University at Albany. Weather Services International Corporation NOWrad regional 2-km radar composites were obtained from the Mesoscale and Microscale Meteorology Division of NCAR archives (available online at http://www.mmm.ucar.edu/imagearchive/). Radiosonde data were acquired from the Department of Atmospheric Science, University of Wyoming, webpage (http://weather.uwyo.edu/upperair/sounding.html).

2.2 Methodology

2.2.1 Climatology

The first part of this study updates the global climatology of 500-hPa cutoff cyclones performed by Smith (2003). The climatology focuses on the frequencies of cutoff cyclones for each grid point of the NCEP–NCAR reanalysis between 80°S and 80°N for 1948–2008. Areas poleward of 80°S and 80°N are ignored because of significant data compression arising from the proximity of grid points in the zonal direction. A cutoff cyclone is defined as a geopotential height minimum with at least a 30-m geopotential height rise in all directions for at least 12 h (three consecutive 6-h analyses). Geopotential height minima are located by finding grid points that have lower geopotential height values than the values at the eight surrounding grid points. These geopotential height minima grid points are evaluated in terms of a 30-m geopotential height-rise requirement. Figure 2.1, taken from BB, shows examples of a geopotential height minimum that meets the cutoff selection criterion (Fig. 2.1a), and a minimum that fails to meet this criterion (Fig. 2.1b). For the aforementioned step, an algorithm is employed that extends radial arms every 20° from the geopotential height minimum and looks for a 30-m geopotential height rise every 40 km along the arm or until the distance along the arm from the geopotential height minimum reaches 500 km. Smith (2003) documented that when the geopotential height-rise requirement was forced for all 18 radial arms (e.g., in BB), the algorithms were missing cyclones that were cutoff according to NWS DIFAX maps. Therefore, in Smith (2003) and this study, a

geopotential height minimum passes the aforementioned test if the procedure works for at least 16 of the 18 arms. Finally, a tracking algorithm was implemented that checks if the radial arm test works for at least three consecutive 6-h analyses. A detailed discussion of this tracking algorithm is found in Smith (2003). Cutoff cyclones that opened up and then closed off again are counted as two distinct cutoff cyclones.

The General Meteorological Package (GEMPAK) (desJardins et al. 1991), version 5.9.3, was utilized to display selected results of the climatology. The climatology data are presented in the form of event frequency (the number of cutoff cyclones passing through each grid point) for both hemispheres, the Tropics, and eastern North America. Time scales include annual, seasonal, and monthly frequencies. Graphs are included to show frequencies and trends in cutoff cyclones for specific geographical areas. In addition, the "cutoff grid point of the year" is plotted to show which grid point had the highest number of cutoff cyclones annually during 1948–2008 for the Northern Hemisphere. The "cutoff day of the year" is shown in a graph representing the day of the year when the most cutoff cyclones occurred over the Northern Hemisphere.

2.2.2 Standardized Anomalies

The use of standardized anomalies is an effective approach for analyzing and forecasting weather events (e.g., Grumm and Hart 2001; Chan et al. 2003; Junker et al. 2008, 2009). Standardized anomalies allow the forecaster to use the degree of departure from normal of weather parameters to assess the potential impact and significance of an event. The methodology in this study used to calculate standardized anomalies starts

with computing centered 15-day (6-h intervals) means of various fields over a 30-year period (1979–2008) using the NCEP–NCAR reanalysis. This period is felt to be long enough to establish representative means and standard deviations. The fields considered include 500-hPa geopotential height, 500-hPa temperature, 700–500-hPa lapse rate, 850-hPa wind speed, and precipitable water (PWAT). The 1.0° GFS analyses (2000–2006 cases) and 0.5° GFS analyses (2007–2008 cases) were used to calculate standardized anomalies with respect to the climatological fields created from the NCEP–NCAR reanalysis.

2.2.3 Overview of 20 Case Studies

An important component of this thesis was the study of 20 warm-season (June–September) cases of cutoff cyclones passing through the CSTAR domain (Fig. 1.2). This task was accomplished using the 1.0° GFS analyses (2000–2006 cases) and 0.5° GFS analyses (2007–2008 cases). Cases were chosen that illustrate the various operational challenges associated with forecasting heavy precipitation and severe weather in conjunction with cutoff cyclones. Common tropospheric fields and features, including low-level temperature and moisture, low-level jets, and upper-level jet streaks, were composited along with selected parameters used in warm-season precipitation forecasting.

A total of 45 cutoff cyclone days, termed storm days, occurring in conjunction with 20 cutoff cyclone cases over the 2000–2008 warm seasons were selected for examination as part of the case study research. Days were defined as 1200–1200 UTC.

The 45 storm days were first ranked by precipitation amounts. These rankings were constructed by ranking the fraction of New England, New York, Pennsylvania, and New Jersey that received at least 25 mm of precipitation in the 24-h period. The areal fractions were objectively determined using Adobe Photoshop software. Standardized PWAT anomalies were averaged over the precipitating areas for the two 6-h times of heaviest precipitation for each of the 45 storm days (usually 1800 and 0000 UTC).

The 45 storm days were also examined for evidence of distinctive synoptic-scale flow patterns in order to stratify the datasets based on the tilt of the 500-hPa trough and embedded cutoff, termed a cutoff–trough system. A visual inspection of the 500-hPa geopotential height field was used to assign negative, neutral, and positive tilts for each cutoff–trough system (Fig. 1.3). Note that it was possible that cutoff cyclones spanning multiple days could have varying tilts over their life cycles. Schematic figures were derived from composites of various tropospheric fields and features for the storm days that fit into each cutoff–trough system tilt category.

2.2.4 Analyses of Two 2008 Cases

Two 500-hPa cutoff cyclone cases from the 2008 warm season were chosen for detailed diagnostic analysis due to their difficult-to-forecast nature and widespread high-impact weather conditions across the northeastern U.S. One case occurred in June (16–20 June 2008) and the other occurred in July (23–25 July 2008). Both cases had over 100 severe storm reports, while the July case also had widespread flash flooding. The following maps were produced for each cutoff cyclone case:

1) 24-h and storm-total precipitation amounts to locate the areas of heaviest precipitation produced by the cutoff.
2) 500-hPa geopotential height, absolute vorticity, and wind speed and direction, to track the cutoff cyclone, show its tilt, and illustrate its vorticity structure.
3) Mean sea level pressure (SLP), 1000–500-hPa thickness, and 250-hPa wind speed to assess surface low development, areas of thermal advections, and upper-level jet dynamics.
4) 850-hPa equivalent potential temperature (θ_e) and wind speed and direction to locate θ_e ridges and evaluate low-level warm moist air availability.
5) 1000–500-hPa and 1000–700-hPa wind shear and convective available potential energy (CAPE) to assess the likely mode of convection.
6) Maps of surface observations with temperature and SLP contoured to analyze surface boundaries.
7) Maps of standardized anomalies of 500-hPa geopotential height, 500-hPa temperature, 700–500-hPa lapse rate, 850-hPa wind speed, and PWAT to assess the degree of departure from normal of these fields.
8) Vertical cross sections of potential temperature (θ), vertical velocity (ω), frontogenesis, absolute vorticity, and normal wind component to illustrate the vertical structure of the cutoff.

GEMPAK, version 5.9.3, was used to produce the aforementioned maps.

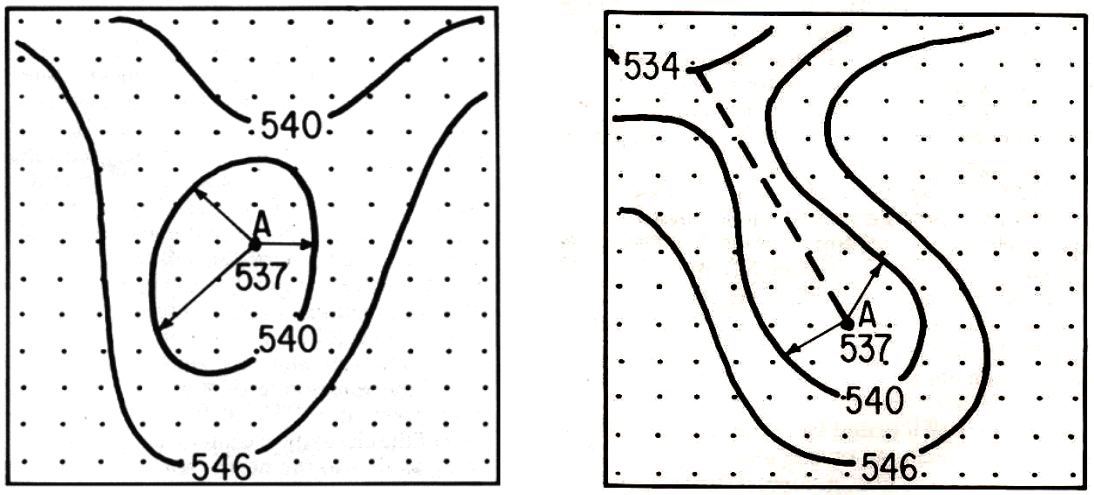

a) b)

Fig. 2.1. Sample 500-hPa geopotential height analyses illustrating the objective method used to identify cutoff cyclones: (a) Three sample radial arms out of the actual 20 used to identify a 30-m closed contour around the center grid point of a cutoff cyclone. A geopotential height rise of at least 30 m occurs before a decrease along all arms. (b) As in (a), except that geopotential heights along the dashed radial arm do not exceed 30 m higher than at point A before decreasing. Source: Bell and Bosart (1989), Figs. 1a–b.

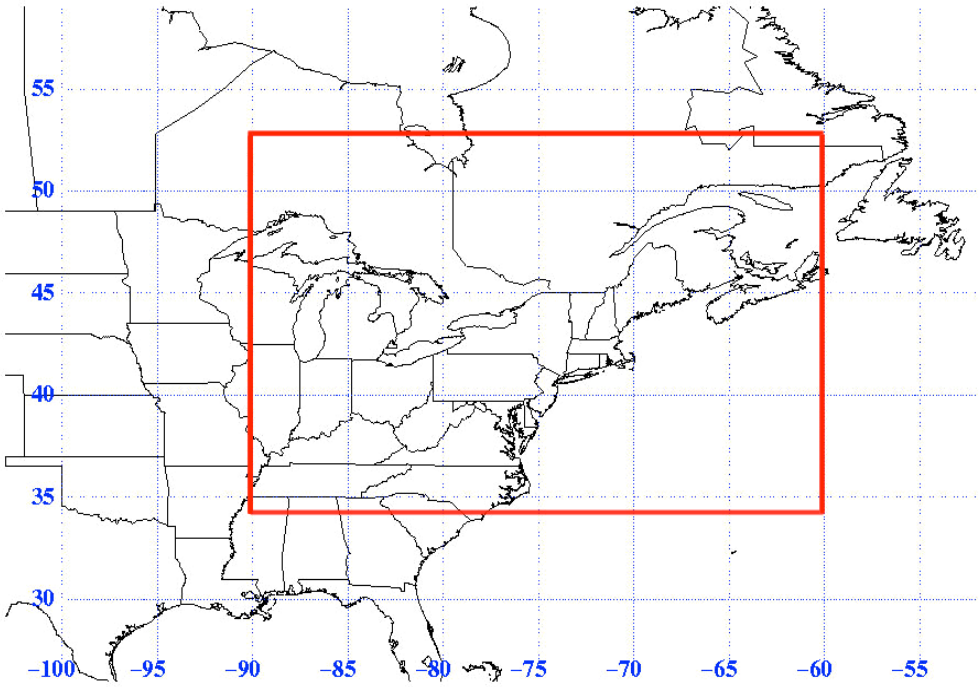

Fig. 2.2. CSTAR domain bounding the northeastern U.S.

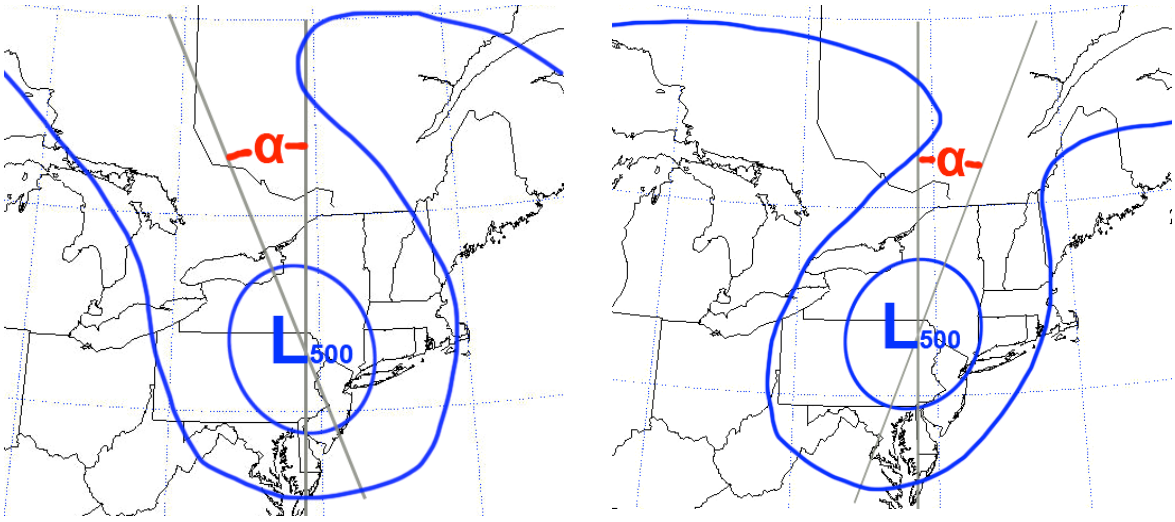

Fig. 2.3. Schematics displaying the methodology for assigning tilt to a 500-hPa cutoff–trough system.

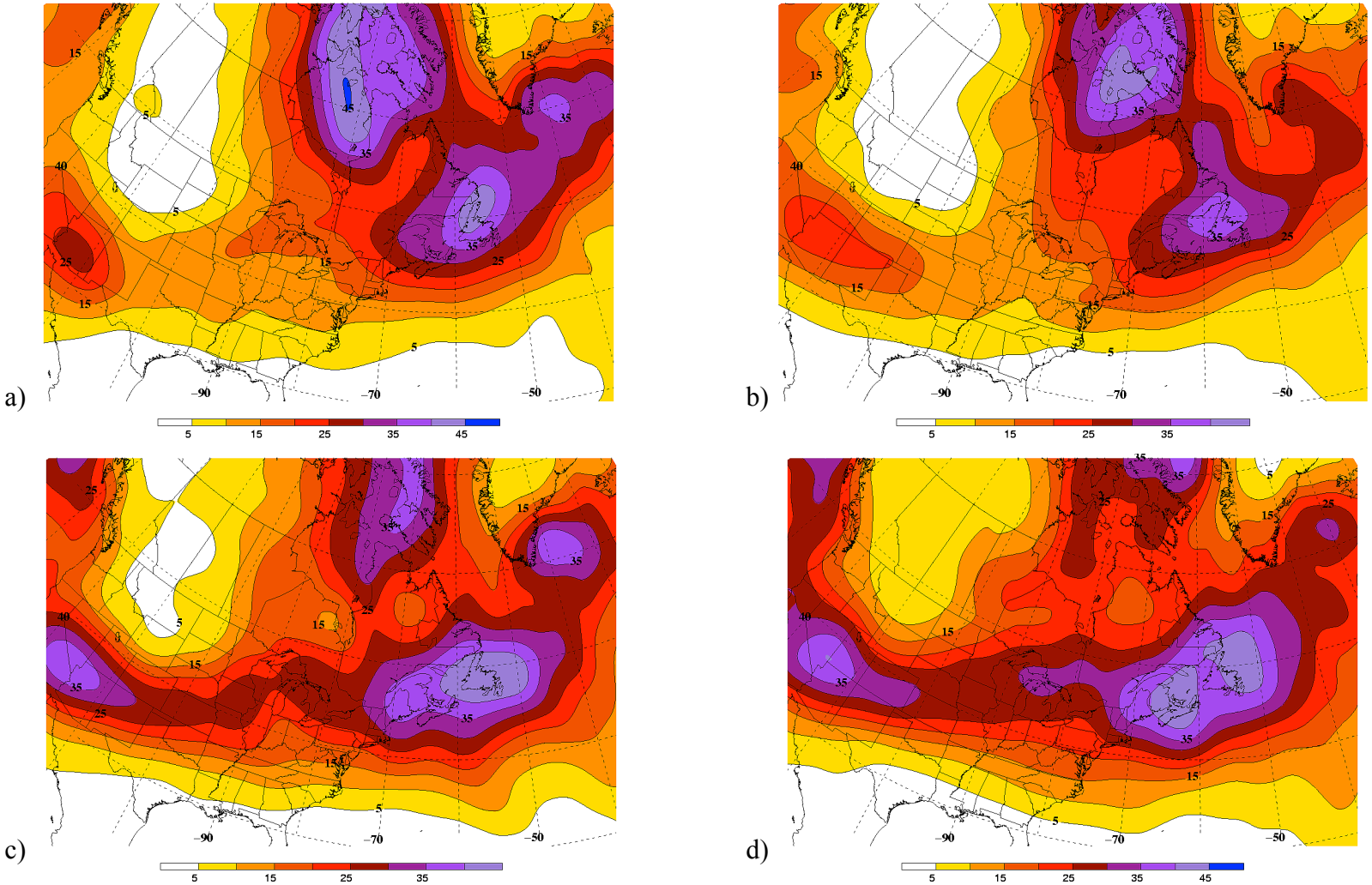

Fig. 3.17. Number of 500-hPa cutoff cyclone events (shaded and contoured every 5) per grid point for eastern North America for (a) January, (b) February, (c) March, (d) April, (e) May, (f) June, (g) July, (h) August, (i) September, (j) October, (k) November, and (l) December 1948–2008.

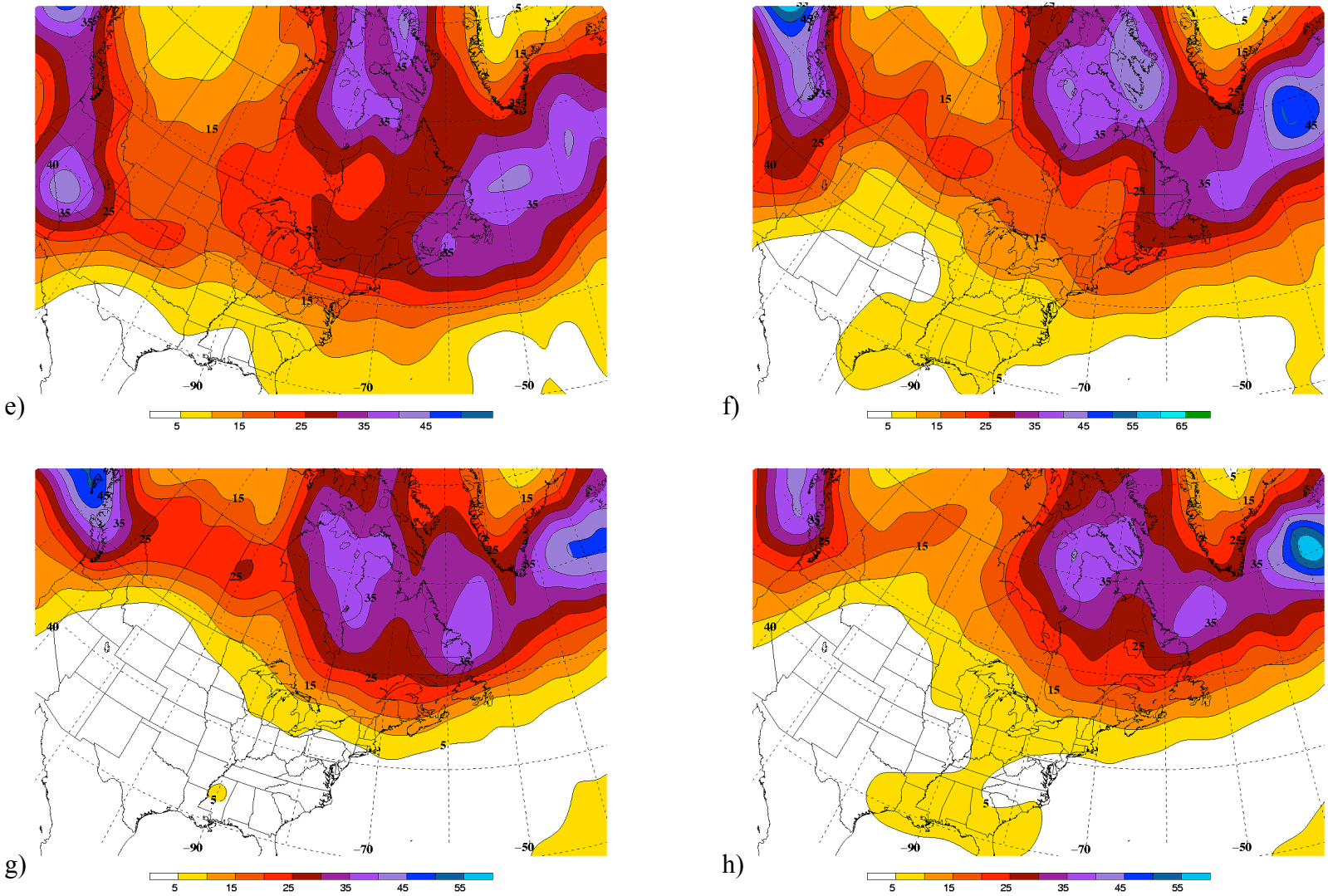

Fig. 3.17 *continued.*

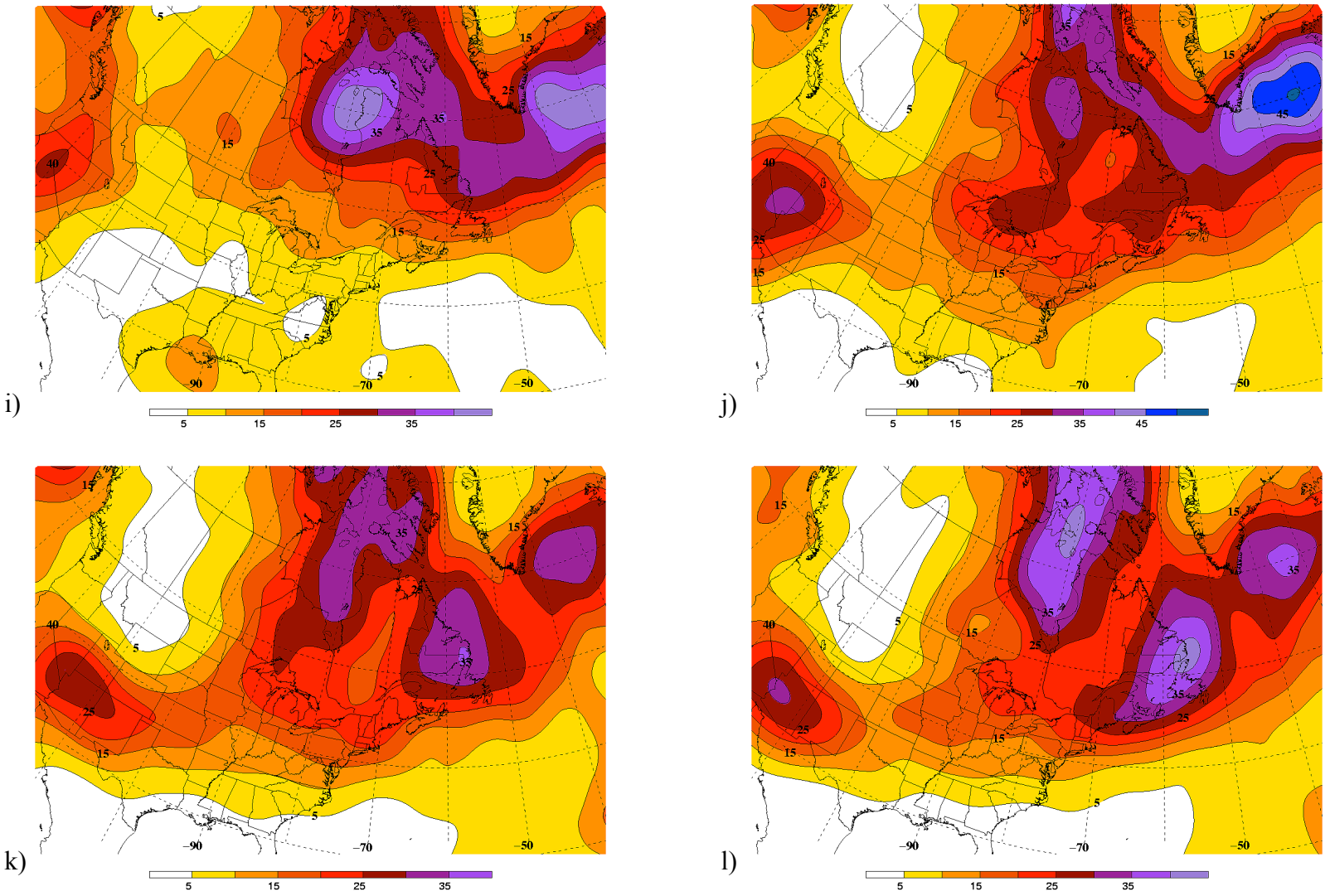

Fig. 3.17 *continued.*

3. Results: Climatology

The NCEP–NCAR reanalysis dataset and algorithms discussed in sec. 2.2.1 were used to objectively identify all 500-hPa cutoff cyclones during the 61-year period from 1 January 1948 through 31 December 2008. During this period a total of 348,950 cutoff cyclones were identified between 80°S and 80°N for all longitudes. A total of 209,570 of these cutoff cyclones occurred in the Northern Hemisphere (hereafter NH).

3.1 Northern Hemisphere

3.1.1 Total Cutoff Cyclone Events, Cutoff Day/Grid Point of the Year

The total number of 500-hPa cutoff cyclone events per year for the NH is shown in Fig. 3.1a. An average of about 3,440 events and a standard deviation of about 220 events are found over the 61-year period. Noteworthy is the increase in events during 1948–1957. Observational data were lacking in spatial and temporal resolution prior to the International Geophysical Year (IGY) in 1957–1958, and may have inhibited the detection of cutoff cyclones during 1948–1957. Removing these first 10 years from the climatology leads to a fairly uniform distribution of about 3,510 events per year and a standard deviation of about 130 events. Recently, there was a period of increased cutoff cyclone occurrence over the NH. The period from 2004 through 2008 has an average of about 3,730 events per year.

The average number of cutoff cyclones per day during 1948–2008 over the NH is displayed in Fig. 3.1b. The most prominent maximum (minimum) occurs in late spring/early summer (winter). Almost 11 cutoff cyclones occur per day in the months of May and June, while only about eight or nine cutoff cyclones occur per day during the cool season. There is a gradual increase (decrease) of cutoff cyclone activity from winter (summer) through early summer (winter).

Figure 3.1c shows the days of the year, averaged from the 61-year period, when the highest number of cutoff cyclones occurs over the entire NH. These "cutoff days of the year" generally occur from January through August, with the majority in May through July. Figure 3.1d shows the grid points in the NCEP–NCAR reanalysis over the NH that had the greatest number of observed cutoff cyclone events in a given year. The most prominent area of frequent cutoff cyclone activity is over the northern Pacific Ocean. Other notable areas include Hudson Bay, southeast of Greenland, southern Europe, and eastern India. These areas will be discussed in detail throughout this chapter.

A map of the total number of cutoff cyclone events for the NH is shown in Fig. 3.2. The most prominent region of cutoff cyclone activity in the NH is over the northern Pacific Ocean, shown by a band that extends from northeastern Asia to the Gulf of Alaska. The greatest cutoff cyclone frequency within this band and throughout the entire NH is found in the Gulf of Alaska. The semipermanent Aleutian Low near the Gulf of Alaska renders this region conducive to storm tracks and cutoff cyclone occurrences. Other favorable areas for cutoff cyclones include the southwestern U.S., Hudson Bay region, U.S./Canadian Maritimes, off the coast of southeastern Greenland, the western Iberian Peninsula, and from southern Europe eastward through Turkey. Noticeable

minima in cutoff cyclone frequency occur over a large portion of China, Saudi Arabia, Greenland, the Rocky Mountains, and the subtropical central Atlantic and central Pacific. These cutoff cyclone minima are likely due either to high terrain or the presence of semipermanent high pressure systems (e.g., the Bermuda High).

3.1.2 Seasonal Cutoff Cyclone Events

Seasonal frequency distributions of 500-hPa cutoff cyclone events are shown in Figs. 3.3–3.7. Note that for the NH (Southern Hemisphere, hereafter SH), the first complete fall (spring) in the climatology is September, October, and November 1948, the first winter (summer) is December 1948 and January and February 1949, the first spring (fall) is March, April, and May 1948, and the first summer (winter) is June, July, and August 1948. Figure 3.3 shows the frequency distribution of cutoff cyclones for the NH fall. The distribution shows similar regions favorable for cutoff cyclones as in Fig. 3.2. Areas of most common cutoff cyclone occurrence include the northern Pacific Ocean, Hudson Bay, southeast of Greenland, and southern Europe.

Figure 3.4 shows the frequency of cutoff cyclones for the NH winter. The maxima in cutoff cyclone frequency over the North Pacific and U.S./Canadian Maritimes are shifted slightly equatorwards from their positions in the fall months. This shift is likely due to the equatorward transition of the mean westerlies into the winter months. Also of interest is the increase (decrease) in cutoff cyclone activity over the northwestern (northeastern) Pacific.

The spring frequencies of cutoff cyclone occurrence are shown in Fig. 3.5. Relative to the winter, cutoff cyclone activity during the spring increases throughout the majority of the NH. Most frequent cutoff cyclone occurrence is still found in a band ranging from northeastern Asia to the Gulf of Alaska. Cutoff cyclones also occur more frequently over the southwestern U.S., with a "cutoff cyclone freeway" showing up from the southwestern U.S. northeastward through the U.S./Canadian Maritimes. Cutoff cyclone frequency also increases throughout much of Europe with a maximum over the eastern Mediterranean Sea and Turkey.

Finally, Fig. 3.6 shows the frequency of cutoff cyclones for the NH summer. The high levels of cutoff cyclone frequency during the spring continue into the summer over the northern Pacific, Hudson Bay, and southeast of Greenland. Cutoff cyclones occur least frequently over the U.S. during the summer than any other season, as the mean westerlies are positioned farther poleward than in any other season. The frequency maxima near the Canadian Maritimes and eastern Mediterranean Sea are also shifted poleward.

3.1.3 Specific Areas of Cutoff Cyclone Activity

As previously shown and discussed in Fig. 3.2, 500-hPa cutoff cyclones occur in preferred regions of the NH. Regional analysis boxes shown in Fig. 3.7 were positioned to focus in on selected areas in and around North America where cutoff cyclones are common. Trends in cutoff cyclone activity throughout the year for each box are presented in Figs. 3.8a–d. The red lines represent the average number of cutoff cyclone

events occurring in 14-day bins during 1948–2008 within each boxed region. The dashed blue lines indicate the number of 6-h analyses with a cutoff cyclone in the region. As discussed in sec. 2.2.1, it takes three consecutive 6-h analyses of the radial arm criterion being met to count the cyclone as a cutoff. The third 6-h analysis and each subsequent 6-h analysis where the cutoff criterion is still met for the cutoff cyclone event is counted in the dashed blue lines. This measure makes it possible to distinguish where systems tend to be stationary or mobile. Regions with more mobile cutoff cyclones are more likely to exhibit fewer 6-h analyses with cutoff cyclones since the cyclones may leave the enclosed designated box. In addition, weaker cutoff cyclones may exist for fewer 6-h analyses since they often "open-up" shortly after becoming cutoff cyclones. The green lines in Figs. 3.8a–d represent the ratio of the numbers of 6-h analyses to cutoff cyclone events. This ratio serves as a physical measure of cutoff cyclone mobility and duration relative to the number of cutoff cyclone events within each box. For example, regions with higher ratios will tend to have slower-moving, longer-lasting cutoff cyclones than regions with lower ratios.

Box A, located over the Gulf of Alaska, is represented in Fig. 3.8a. Cutoff cyclones occur least frequently during the winter and most frequently in late spring and summer. Cutoff cyclones also appear to be more quasi-stationary in late spring and summer. More mobile systems occur during the cool season.

The southwestern U.S. (box B) cutoff cyclone activity is shown in Fig. 3.8b. A strong seasonal dependence also exists in this region. Cutoff cyclones occur most (least) frequently in early spring (summer). A sharp decline in activity occurs from May through July. The ratios of the numbers of 6-h analyses to cutoff cyclone events is lowest

in late winter and early spring, as mobile systems track across the cutoff cyclone freeway of the U.S. Over the summer, the region tends to be dominated by a continental anticyclone. The low number of cutoff cyclone events during the summer months may skew the results of the ratios of the numbers of 6-h analyses to cutoff cyclone events during the summer months.

Box C represents the Hudson Bay region of North America. Less seasonal dependence is seen in this region than in the other regions previously discussed. Cutoff cyclones are generally quite common throughout the year in this area. Quasi-stationary cutoff cyclones commonly occur in this region, especially from spring through mid-summer.

The area of activity near the U.S./Canadian Maritimes (box D) is shown in Fig. 3.8d. Cutoff cyclone frequency is greatest in spring and gradually decreases through the summer to a minimum in late summer/early fall. Cutoff cyclones appear to be most mobile in fall and winter, consistent with the active North Atlantic storm track in the region.

3.2 Southern Hemisphere

3.2.1 Total Cutoff Cyclone Events

The total number of 500-hPa cutoff cyclone events per year for the SH is shown in Fig. 3.9a. An average of about 2,280 events and a standard deviation of about 150 events are found over the 61-year period from 1 January 1948 through 31 December

2008. Also noteworthy is the consistency of year-to-year event totals dating back to even before the IGY, unlike what is seen in the NH. Recently, there were several years of increased cutoff cyclone occurrence over the SH. The period from 2000 through 2008 has an average of about 2,560 events per year. The average number of cutoff cyclones per day from 1948–2008 over the SH is shown in Fig. 3.9b. Cutoff cyclones generally tend to occur more often during the warm season (about seven per day) than the cool season (about six per day). January is the most active month of the year, while September is the least active. A secondary frequency maximum occurs during the late fall/early winter.

The total number of 500-hPa cutoff cyclone events for the SH is shown in Fig. 3.10. The frequency distributions indicate particular regions favorable for cutoff cyclone occurrence. The most common large area of cutoff cyclone episodes in the SH is seen along a 15°-latitude-wide band surrounding Antarctica. Cutoff cyclones most commonly occur within this band from 20°W through 120°E longitude. Other distinct maxima are located near the Lars Christensen Coast (65°E), Mawson Peninsula (155°E), and the Ross Sea (170°W). Although less common than in the polar regions, cutoff cyclones do occur in the SH middle latitudes. Areas between southeastern Australia and New Zealand average more than two cutoff cyclones per year. Cutoff cyclones also tend to occur along a band from New Zealand east to 140°W. Weaker frequency maxima than the aforementioned maxima are found both southwest and southeast of the South American and African mainlands.

3.2.2 Seasonal Cutoff Cyclone Events

Seasonal frequency distributions of 500-hPa cutoff cyclone events for the SH are shown in Figs. 3.11–3.14. The SH fall frequencies (Fig. 3.11) resemble the annual frequencies (Fig. 3.10), with the highest concentration of cutoff cyclones occurring near the Lars Christensen Coast. Figure 3.12 shows that during the SH winter cutoff cyclones occur more frequently than in the SH fall near the Mawson Peninsula and between Australia and New Zealand. Cutoff cyclone activity near the Lars Christensen Coast decreases from fall to winter. The SH spring frequencies (Fig. 3.13) are similar to those of the SH winter, with the exception of decreased activity along the band from southeastern Australia east to 140°W longitude. Cutoff cyclones increase in frequency into the SH summer (Fig. 3.14) within the maximum frequency band surrounding Antarctica from 20°W through 120°E longitude. Additional areas of increased activity from spring to summer include the Mozambique Channel and northern Australia.

3.3 Tropics

3.3.1 Total Cutoff Cyclone Events

The total number of 500-hPa cutoff cyclone events for the Tropics is shown in Figs. 3.15–3.16. For viewing purposes, the Tropics plots are divided into a Western Hemisphere (WH) plot (Fig. 3.15) and an Eastern Hemisphere (EH) plot (Fig. 3.16). Cutoff cyclones are not nearly as common in the Tropics as in the middle and polar latitudes. There are, however, regions in the tropics more conducive to cutoff cyclone

formation than others. For example, Fig. 3.15 shows that cutoff cyclones preferentially occur in certain regions of the WH Tropics. The areas from Hawaii east-northeastward to western Mexico receive on average at least one cutoff cyclone per year. The cutoff cyclones that affect Hawaii with high-impact weather conditions are referred to as Kona lows (e.g., Simpson 1952; Businger et al. 1998; Otkin and Martin 2004). The small protrusion of cutoff cyclone activity south of the California Baja is likely associated with transitioning tropical cyclones. Cutoff cyclones also tend to occur on both sides of the southern Andes Mountains. Frequency maxima are seen in the eastern North Atlantic and eastern South Pacific. The EH Tropics plot (Fig. 3.16) shows several maxima in cutoff cyclone activity. The most prominent maximum is seen over the eastern Indian subcontinent and Bay of Bengal region. This region is dominated by the Indian Monsoon that peaks in the summer. Cutoff cyclones also occur over the northeastern Arabian Sea and within a band ranging from the northern South China Sea east to about 140°W longitude. In the SH Tropics, cutoff cyclones occur most frequently in the Mozambique Channel and over northern Australia.

3.4 Eastern North America

3.4.1 Total Cutoff Cyclone Events

Monthly totals of 500-hPa cutoff cyclone events for eastern North America are shown in Figs. 3.17a–l. January, shown in Fig. 3.17a, has maxima in cutoff cyclone activity over the Hudson Bay region, the Canadian Maritimes, and southeast of

Greenland. Also noteworthy is the presence of the cutoff cyclone freeway introduced in sec. 3.1.2 encompassing the southwestern U.S. northeastward through the Great Lakes and northeastern U.S. Cutoff cyclones in February (Fig. 3.17b) tend to occur in the same regions as in January, but slightly less frequently.

By March (Fig. 3.17c), cutoff cyclone frequencies increase in most locations. There are stronger signals for cutoff cyclone occurrence over the southwestern U.S., U.S./Canadian Maritimes, and southeast of Greenland. The cutoff cyclone freeway is also more active now. In April (Fig. 3.17d), the distributions shift a little poleward as the cool season transitions towards the warm season. Cutoff cyclones now occur more (less) frequently over the U.S./Canadian Maritimes (Hudson Bay region). The cutoff cyclone freeway is now even more active and shifted northwards.

May (Fig. 3.17e) shows some distinct differences from April (Fig. 3.17d). Cutoff cyclone frequency has increased (decreased) over the Hudson Bay region (U.S./Canadian Maritimes). The maximum in cutoff cyclone frequency over the southwestern U.S. has shifted northward. The cutoff cyclone freeway has also shifted northward and appears to be much weaker than it was in April. Cutoff cyclone activity has declined over the southern Great Plains as spring low-level heating has set in. June (Fig. 3.17f) features an increase in cutoff cyclone activity over northeastern Canada and southeast of Greenland. The maximum over the southwestern U.S. is absent as storm tracks are confined to the north and ridging aloft develops in response to strong low-level heating.

July (Fig. 3.17g) and August (Fig. 3.17h) see continued cutoff cyclone activity over the Hudson Bay region and southeast of Greenland. Cutoff cyclones do not occur over the majority of the U.S. with the exception of the Northwest and Northeast. Cutoff

cyclones also occur over the southeastern U.S. in August in association with landfalling tropical cyclones.

By September (Fig. 3.17i), cutoff cyclones start occurring more frequently over the U.S. The maximum over the western U.S. returns and more cutoff cyclones occur over the southeastern U.S. in association with transitioning tropical cyclones. October (Fig. 3.17j) sees a further increase in cutoff cyclone activity over the southwestern and northeastern U.S. The cutoff cyclone freeway through the central U.S. returns as well.

In November (Fig. 3.17k), cutoff cyclones occur more frequently over the Canadian Maritimes in association with an early winter storm track. The cutoff cyclone freeway shifts equatorward and starts to become better defined. The trends seen in November continue through December (Fig. 3.17l). The winter storm track through the U.S./Canadian Maritimes is well defined, as are the maxima over the southwestern U.S. and Hudson Bay region.

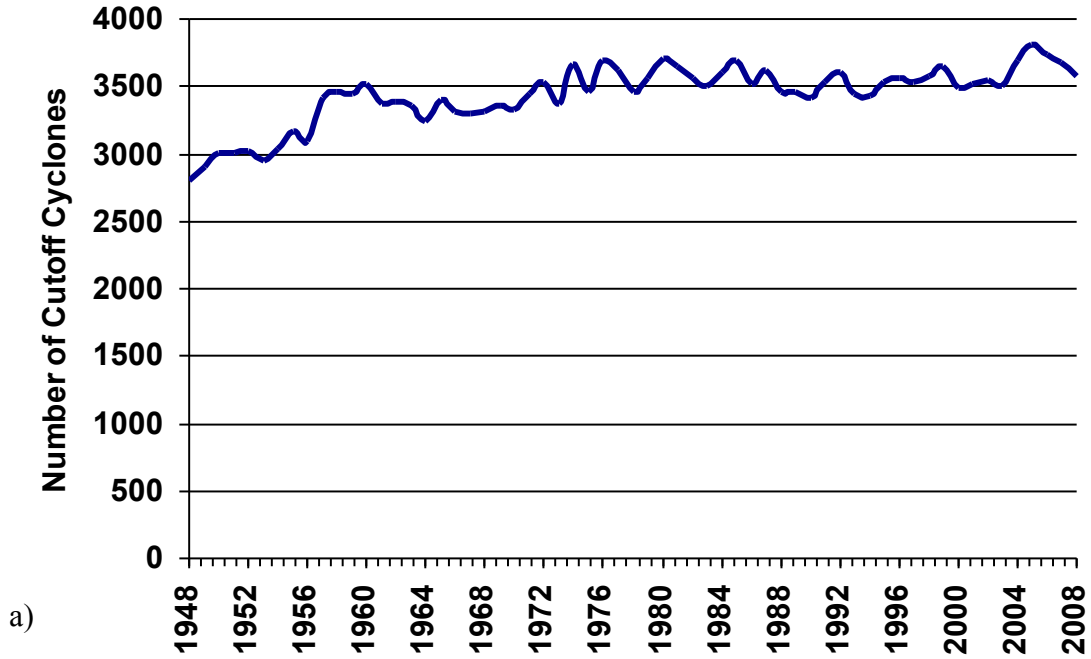

a)

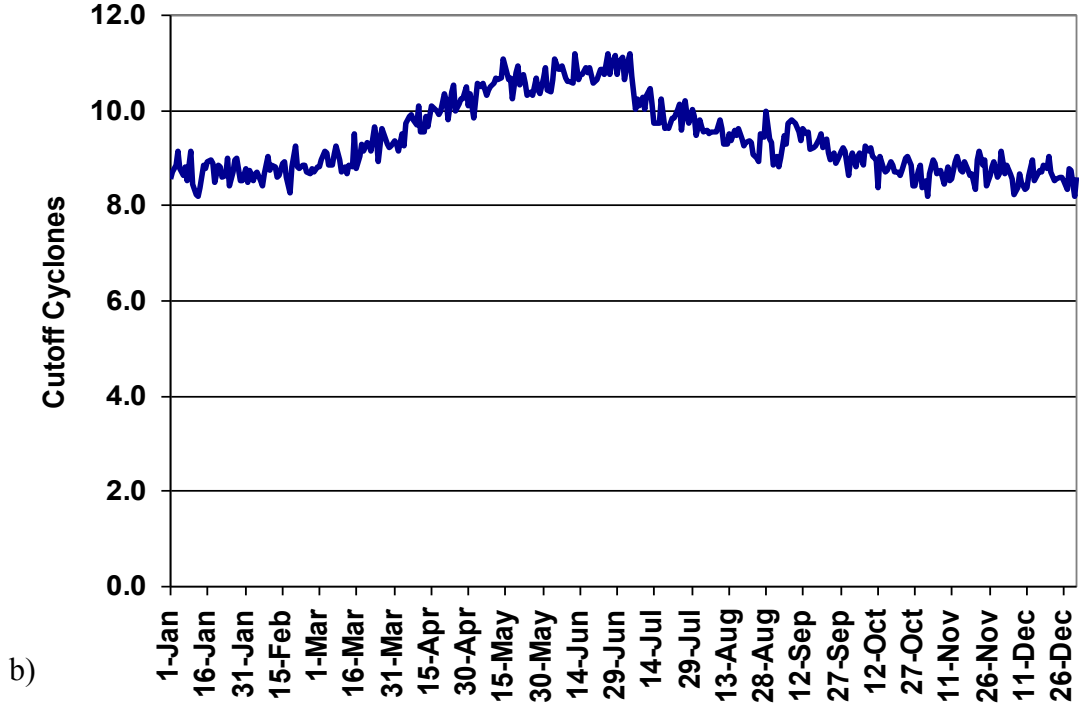

b)

Fig. 3.1. For the NH, (a) annual number of 500-hPa cutoff cyclone events for 1948–2008, (b) average number of 500-hPa cutoff cyclones per day, (c) day of the year when most 500-hPa cutoff cyclones occur for each year, (d) grid point with the greatest number of observed 500-hPa cutoff cyclones for each year.

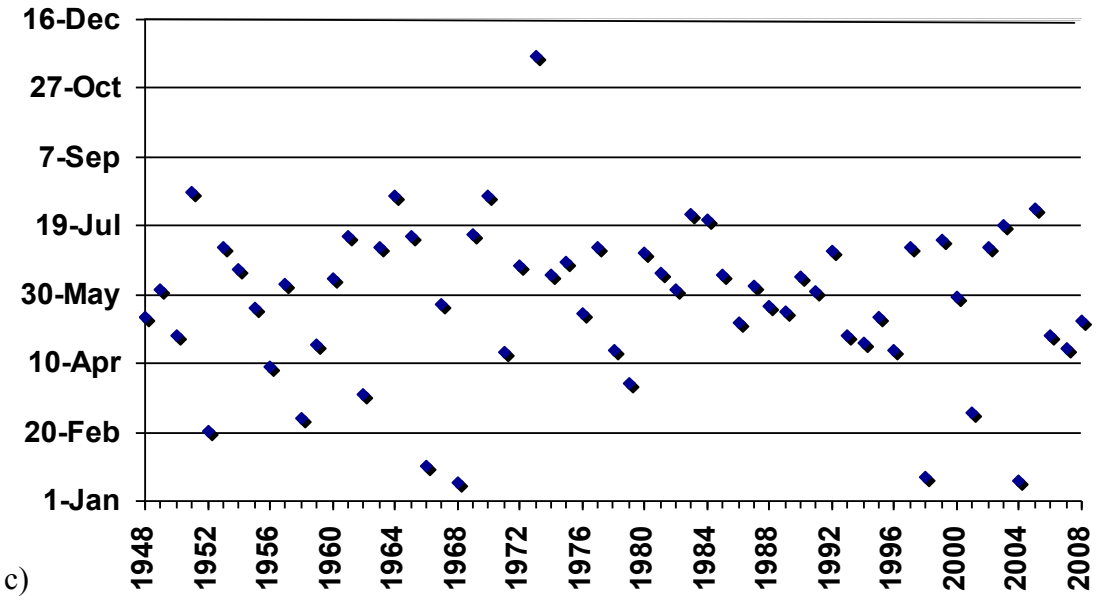

c)

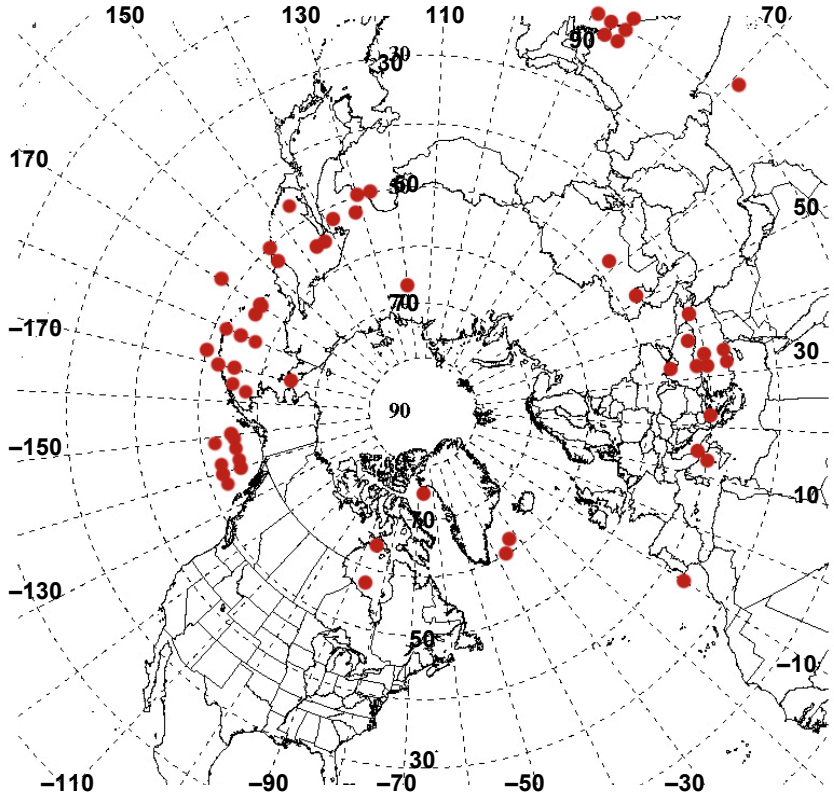

d)

Fig. 3.1. *continued.*

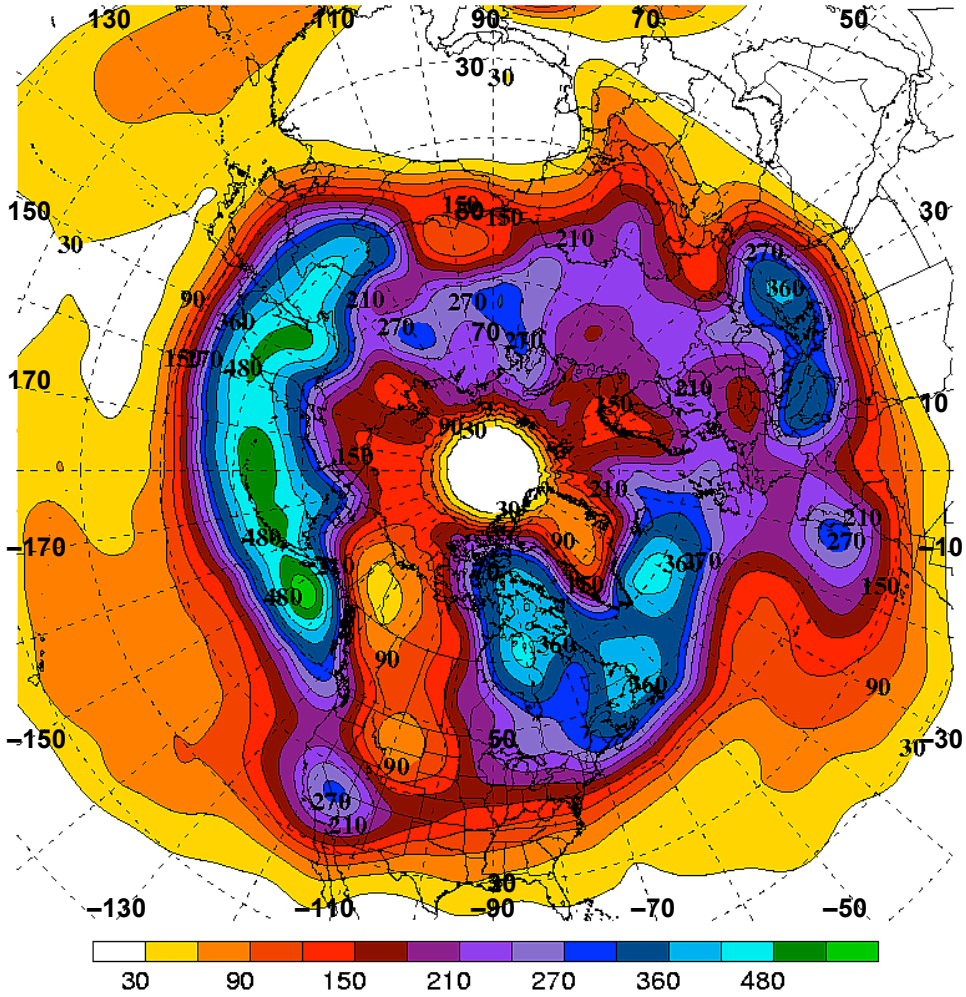

Fig. 3.2. Total number of 500-hPa cutoff cyclone events (shaded and contoured every 30 through 300, then every 60) per grid point for the NH for 1948–2008.

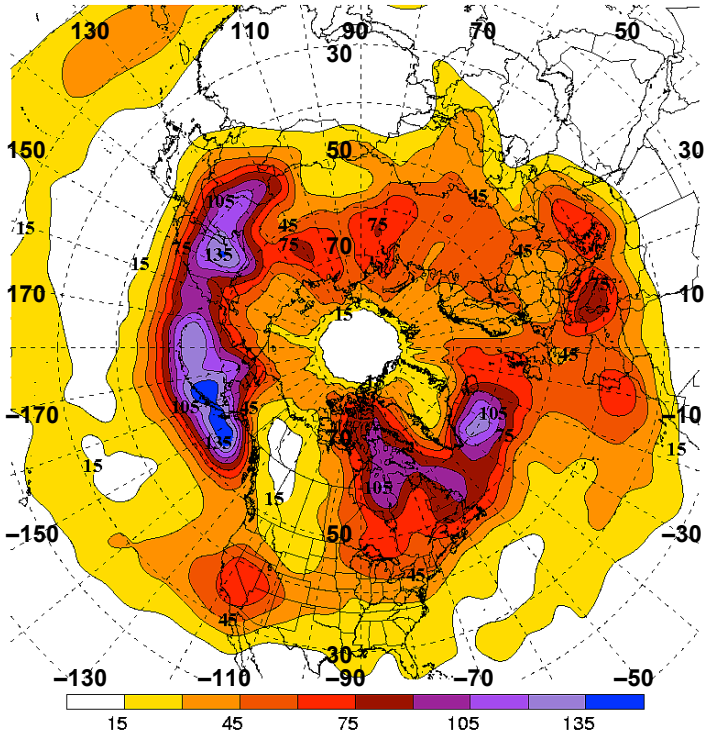

Fig. 3.3. Total number of 500-hPa cutoff cyclone events (shaded and contoured every 15) per grid point for NH fall.

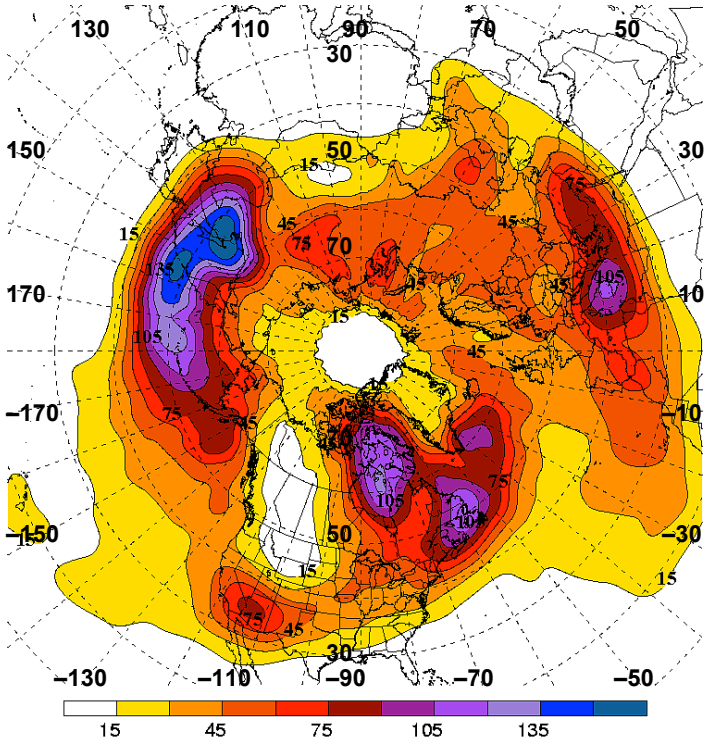

Fig. 3.4. As in Fig. 3.3 but for NH winter.

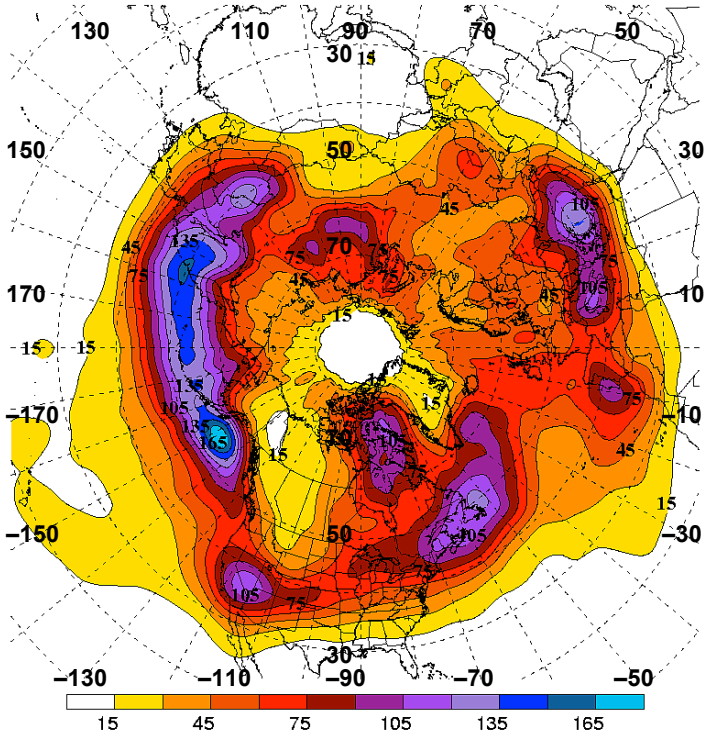

Fig. 3.5. As in Fig. 3.3 but for NH spring.

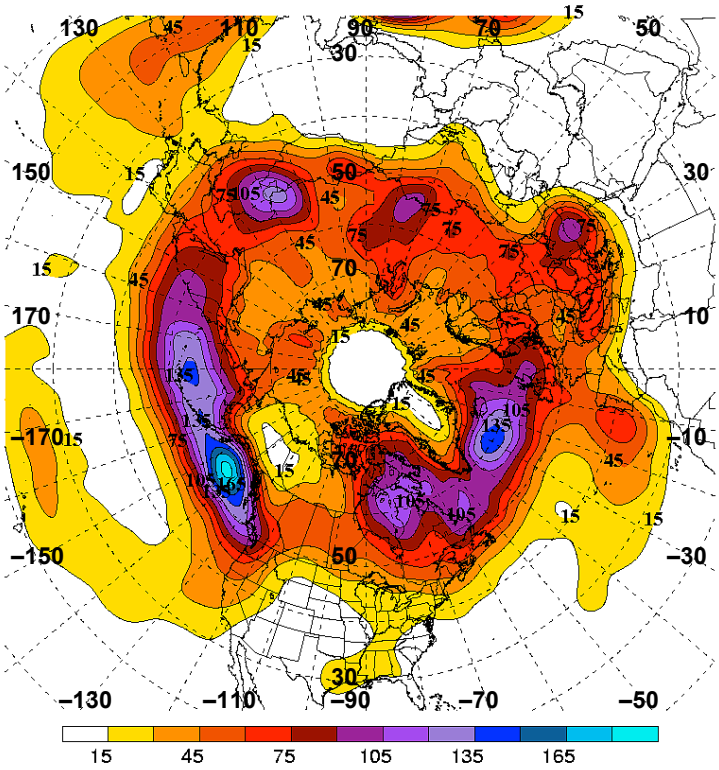

Fig. 3.6. As in Fig. 3.3 but for NH summer.

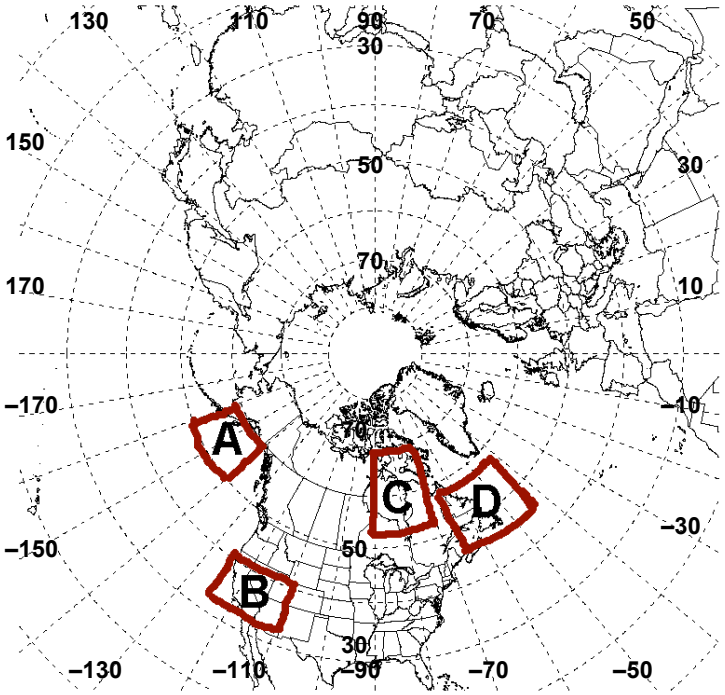

Fig. 3.7. Favored areas of 500-hPa cutoff cyclone activity in and around North America.

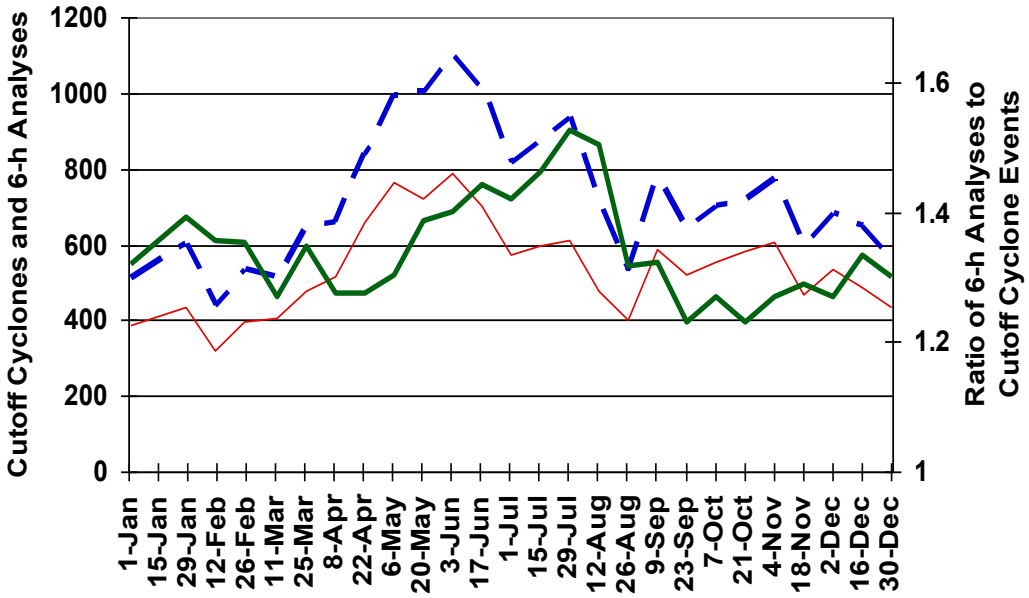

a)

Fig. 3.8. Number of 500-hPa cutoff cyclones (red line), 6-h analyses with a 500-hPa cutoff cyclone (dashed blue line), and ratio of the numbers of 6-h analyses to cutoff cyclone events (green line) for (a) box A, (b) box B, (c) box C, and (d) box D, as defined in Fig. 3.7.

b)

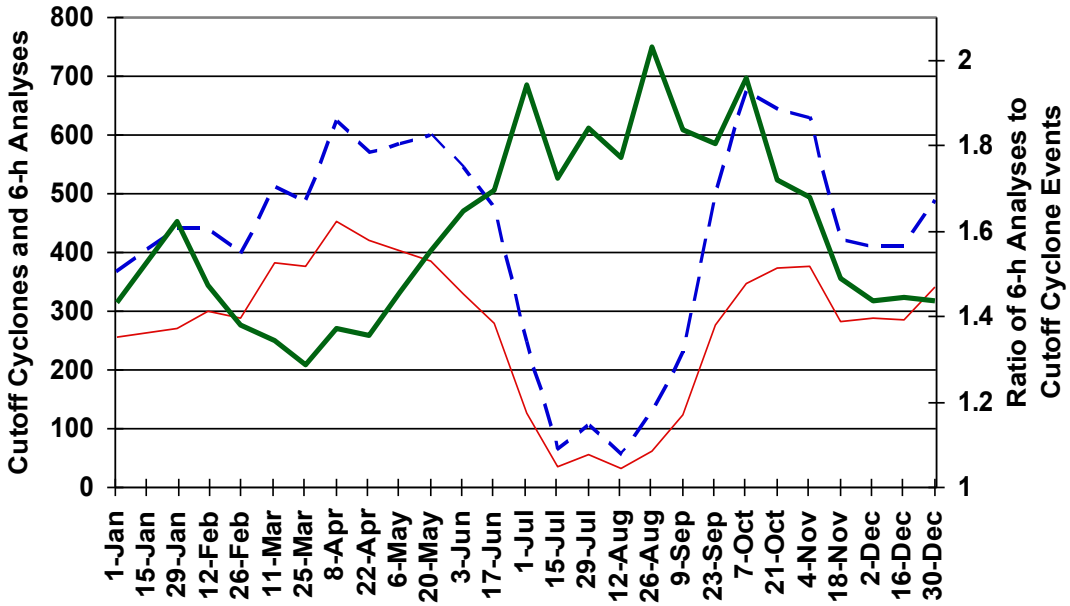

c)

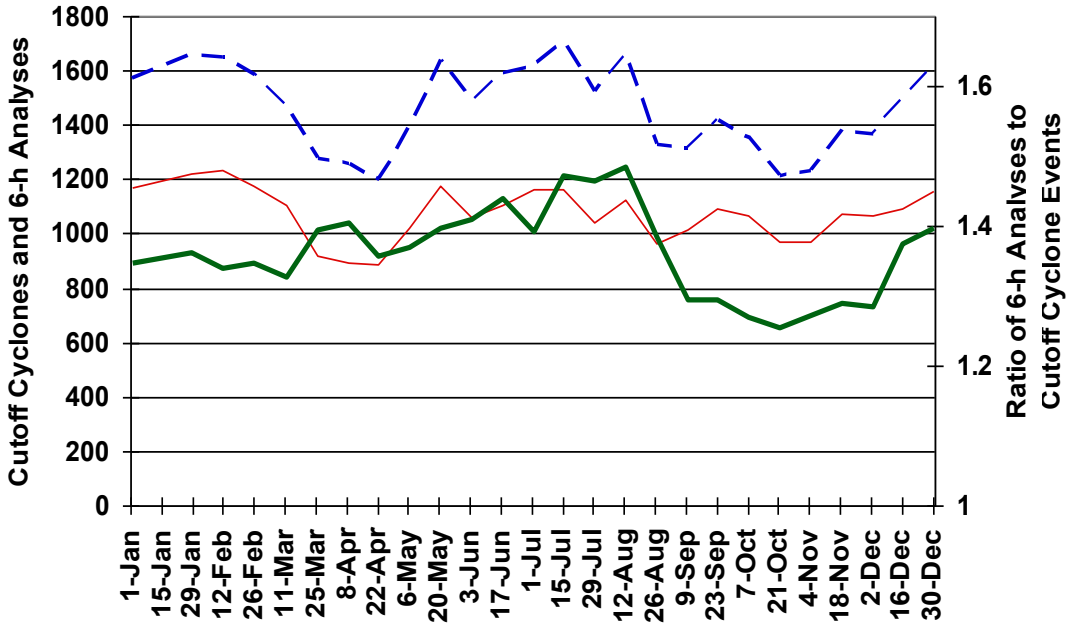

Fig. 3.8. *continued.*

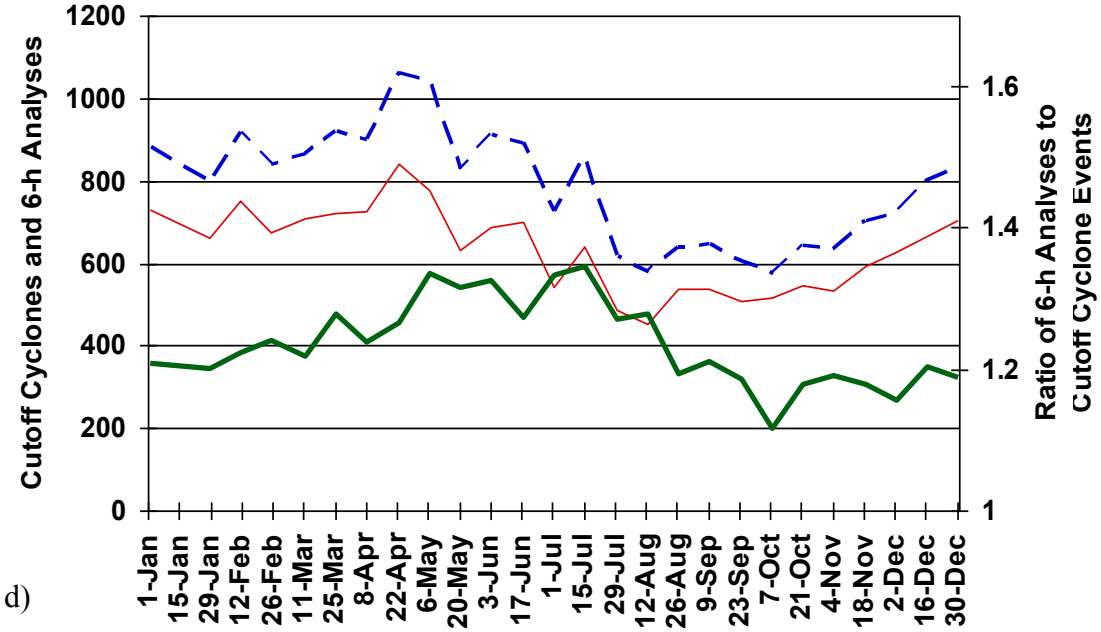

d)

Fig. 3.8. *continued.*

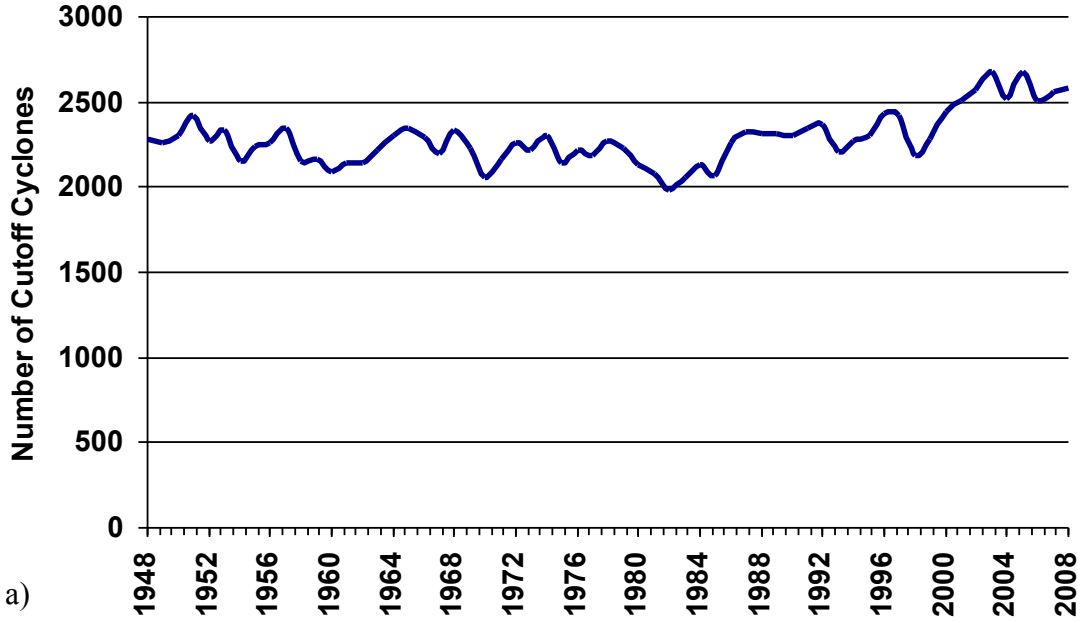

a)

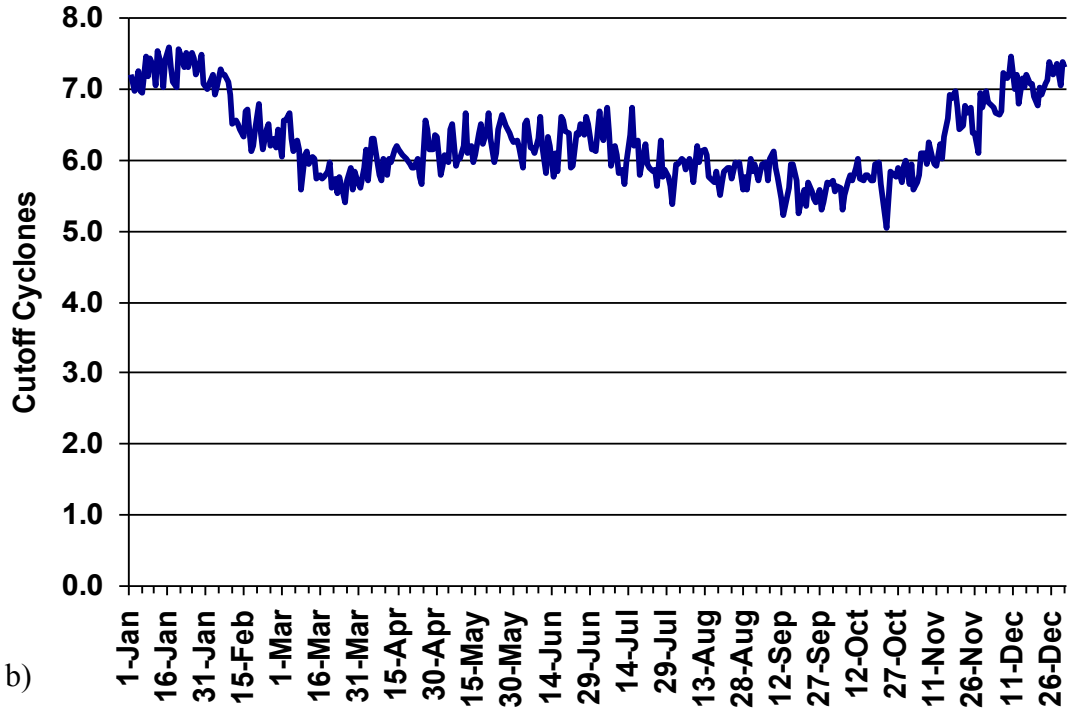

b)

Fig. 3.9. As in Figs. 3.1a–b but for the SH.

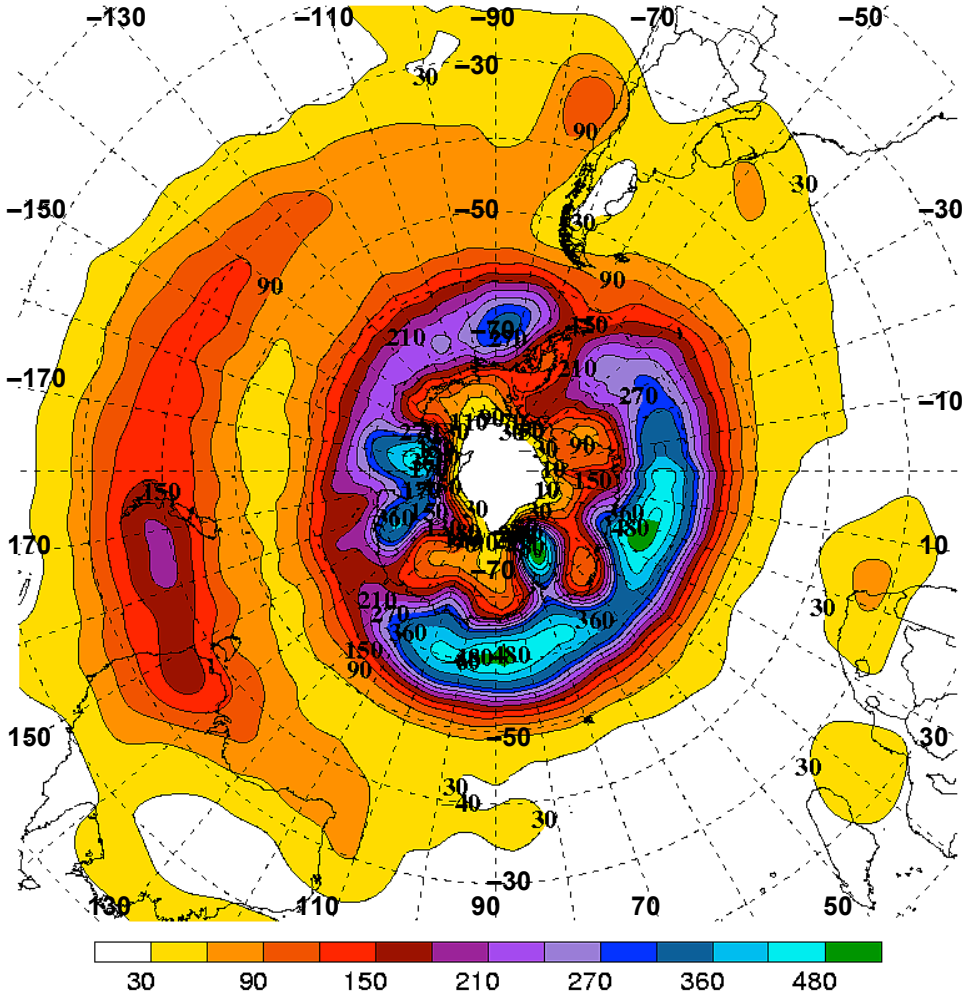

Fig. 3.10. As in Fig. 3.2 but for the SH.

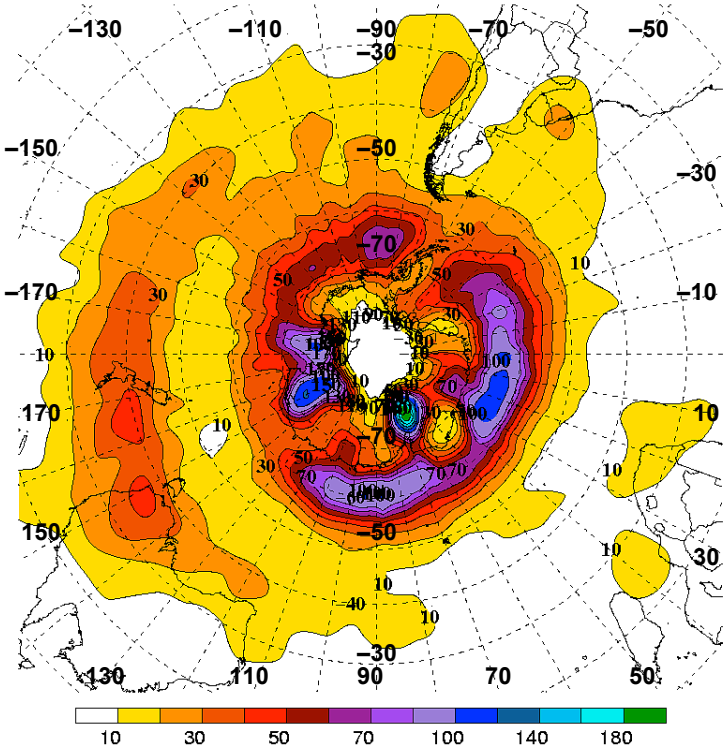

Fig. 3.11. As in Fig. 3.3 but for SH fall. Shaded and contoured every 10 events through 80 events, then every 20 events.

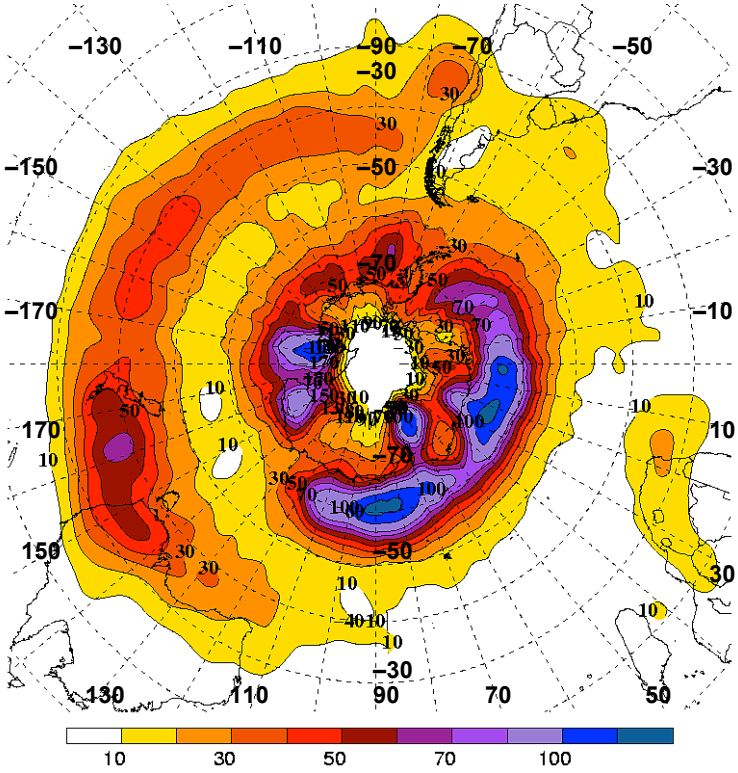

Fig. 3.12. As in Fig. 3.11 but for SH winter.

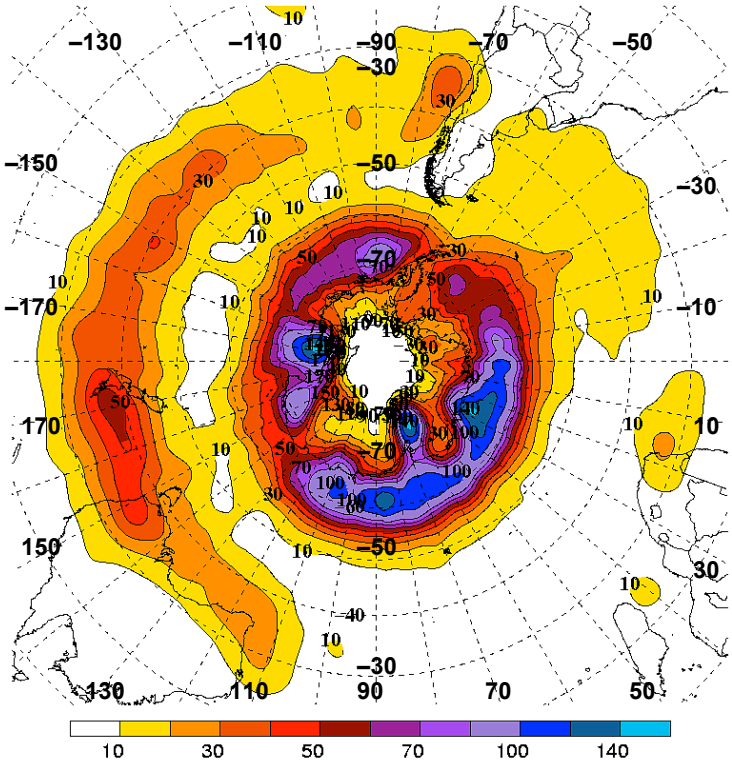

Fig. 3.13. As in Fig. 3.11 but for SH spring.

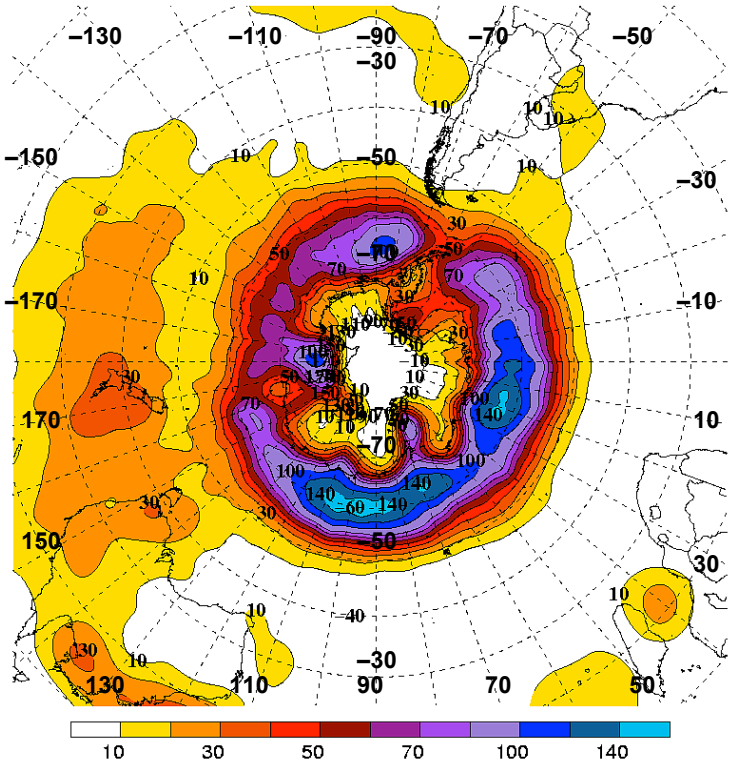

Fig. 3.14. As in Fig. 3.11 but for SH summer.

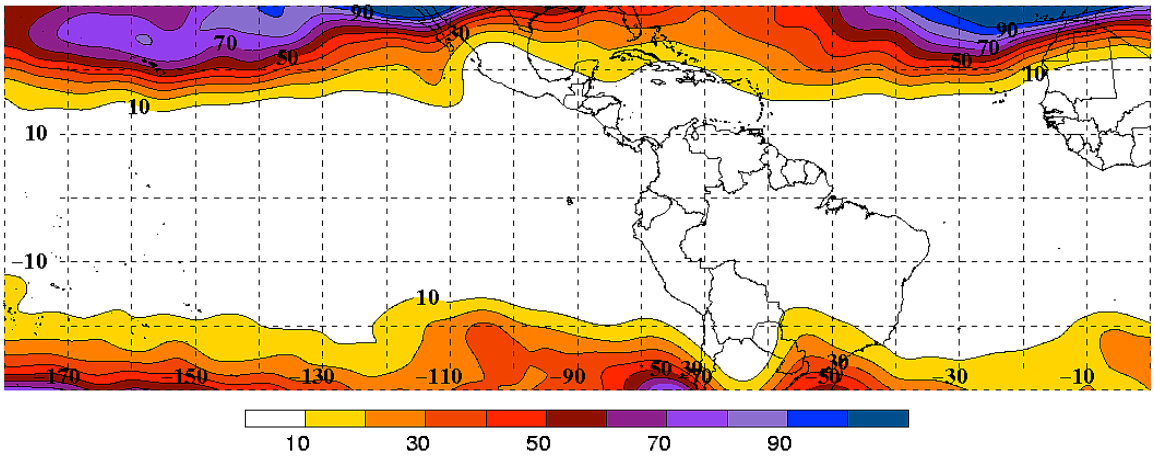

Fig. 3.15. As in Fig. 3.2 but for the Western Hemisphere Tropics. Shaded and contoured every 10 events.

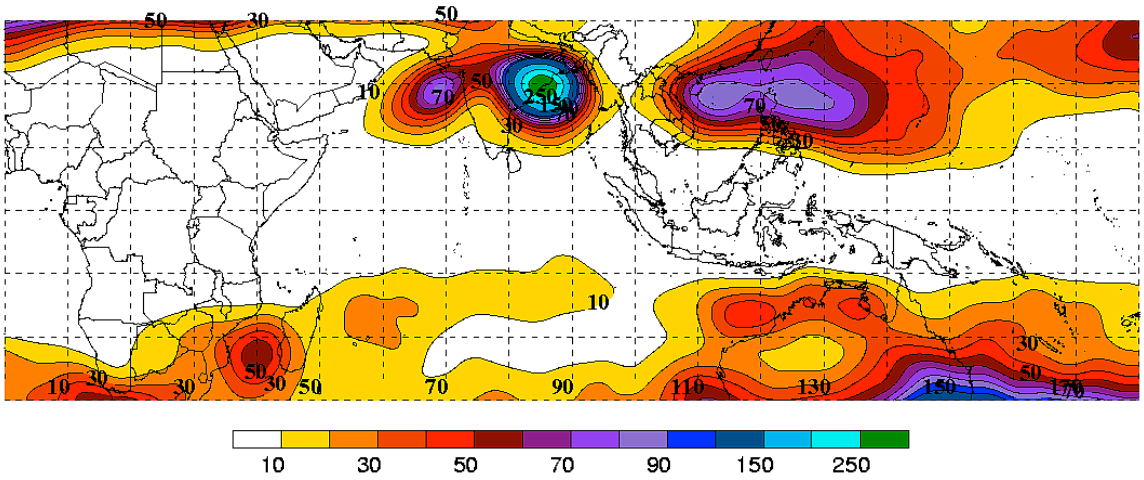

Fig. 3.16. As in Fig. 3.2 but for the Eastern Hemisphere Tropics. Shaded and contoured every 10 events through 100 events, then every 50 events.

4. Results: Overview of 20 Case Studies

4.1 Five Synoptic-Scale Flow Patterns

An important component of this research was the analysis of 20 warm-season cases of 500-hPa cutoff cyclones that tracked through the CSTAR domain and affected the northeastern U.S. with varying amounts of precipitation and severe weather. A selection of 45 storm days in conjunction with 20 cutoff cyclone cases over the 2000–2008 warm seasons were analyzed. As explained in sec. 2.2.3, the 45 storm days were first examined for evidence of distinctive synoptic-scale flow patterns and stratified based on the 500-hPa cutoff–trough system tilt. Schematic figures were derived from composites of various tropospheric fields and features for the storm days that fit into each cutoff–trough system tilt category. Samples of these composites will be shown to lead into the first schematic discussed. Five distinct patterns of lower-, middle-, and upper-level features were deduced based on 500-hPa cutoff–trough system tilt (two positive tilts: types "A" and "B," two neutral tilts: types "A" and "B," and one negative tilt).

4.1.1 Positive Tilt "Type A"

The synoptic-scale flow for the positive tilt "type A" pattern includes strong southerly low-level flow east of the 500-hPa cutoff cyclone and a zonal upper-level jet along the downstream upper-level ridge. Figure 4.1 shows composites of 500-hPa geopotential height and PWAT. The positively tilted cutoff cyclone is located near the

Great Lakes region. PWAT values are largest to the east of the cutoff cyclone, in an area of deep southerlies that are advecting western North Atlantic and/or Gulf of Mexico moisture poleward. PWAT values are at least 40–50 mm over much of Pennsylvania and New York. Figure 4.2 shows additional composite fields associated with the positive tilt "type A" pattern. A surface cyclone is located east of the 500-hPa cutoff cyclone near Lake Erie. A relatively zonal, 80–100 kt 250-hPa jet streak is seen over northern New England/southern Quebec. In the southerly flow ahead of the surface cyclone, high 850-hPa θ_e air streams northwards across Pennsylvania and New York. A θ_e ridge is a common signature in these flow regimes and signifies the axis of warm and moist low-level air.

A schematic for the positive tilt "type A" pattern is shown in Fig. 4.3. This pattern occurred in four of the 20 cases studied. The main forcing mechanisms that lead to the area of heaviest precipitation include warm-air advection and a surface warm front and/or prefrontal trough. Sometimes this area of precipitation is co-located with the equatorward-entrance region of the aforementioned upper-level jet streak to the northeast, a region favorable for the occurrence of upper-level divergence and associated midlevel upward vertical motion. PWAT anomalies in the areas of heaviest precipitation tend to be greater than one, and sometimes two, standard deviations (SDs) above normal. Precipitation occurs in the convective and stratiform modes with the positive tilt "type A" pattern. There was an average of eight severe storm reports per day with this pattern, most of which were wind reports.

4.1.2 Positive Tilt "Type B"

Figure 4.4 shows a schematic of a positive tilt "type B" pattern. This scenario occurred in six of the 20 cases studied. The 500-hPa cutoff cyclone is located south of Lake Erie and follows a Great Lakes track (Novak et al. 2002). This pattern consists of easterly low-level flow, southwesterly upper-level flow, and an upper-level jet streak within the eastern/southeastern side of the trough that envelops the cutoff cyclone. Upper-level jet dynamics may affect precipitation distributions, as portions of the northeastern U.S. may lie in the poleward-exit region of the upper-level jet streak. An inverted surface trough and differential cyclonic vorticity advection associated with a midlevel vorticity maximum swinging around the cutoff cyclone can serve as lifting mechanisms. The southeasterly-to-easterly low-level flow draws in moisture from the western North Atlantic and enhances instability. Stratiform bands with embedded convection commonly occur with this flow pattern. There was an average of six severe storm reports per day with this pattern.

4.1.3 Neutral Tilt "Type A"

A schematic of a neutral tilt "type A" pattern is shown in Fig. 4.5. This scenario occurred in seven of the 20 cases studied. This pattern consists of southerly low-level flow and an associated low-level jet, generally over southern New England. Warm-air advection and differential cyclonic vorticity advection associated with a midlevel vorticity maximum swinging around the cutoff cyclone serve as lifting mechanisms. A sea-breeze front and a surface trough associated with a surface cyclone to the southeast of

the 500-hPa cutoff cyclone may provide additional lifting mechanisms. The southerly-to-southeasterly low-level flow off the western North Atlantic draws in moisture that can lead to precipitation in conjunction with the aforementioned lifting mechanisms. Stratiform and convective bands commonly occur with this flow pattern. Severe weather is more common with this flow pattern than with the two positive tilt patterns, with an average of 33 severe storm reports per day.

4.1.4 Neutral Tilt "Type B"

Figure 4.6 shows a schematic of a neutral tilt "type B" pattern. This scenario occurred in four of the 20 cases studied. The 500-hPa cutoff cyclone is located near James Bay and follows a Northwest track (Novak et al. 2002). Upward vertical motion is associated with differential cyclonic vorticity advection and an elongated surface trough in an area of strong diurnal surface heating. A low-level jet increases the threat for convection to organize. The combination of daytime heating and a large cold pool coinciding with the 500-hPa cutoff cyclone contributes to steep midlevel lapse rates, oftentimes greater than 6.5 °C km^{-1}. The Storm Prediction Center (SPC) usually issued a slight or moderate risk of severe thunderstorms for the regions most conducive for severe weather with this pattern. PWAT values across the northeastern U.S. are normal or below-normal, as air advecting from the west and northwest is relatively dry. Precipitation is mostly in the convective mode with this flow pattern. There was an average of 57 severe storm reports per day with this pattern, most of which were hail reports.

4.1.5 Negative Tilt

A schematic of a negative tilt pattern is shown in Fig. 4.7. This scenario occurred in three of the 20 cases studied. The 500-hPa cutoff cyclone is located near Maine and southern Quebec and is oftentimes transitioning from a neutral tilt "type B" flow pattern. Upward vertical motion is associated with differential cyclonic vorticity advection along a surface trough and/or sea-breeze front. A low-level jet out of the northwest can help to organize convection, but precipitation amounts are generally light. Midlevel lapse rates greater than 6.5 °C km^{-1} tend to occur over parts of the northeastern U.S., and lead to an area of focus for a SPC-issued slight risk of severe thunderstorms. PWAT values across the northeastern U.S. are normal to below-normal as in the neutral tilt "type B" pattern, as air advecting from the northwest is relatively dry. Precipitation occurs only in the convective mode with this flow pattern. There was an average of 21 severe storm reports per day with this pattern, most of which were hail reports.

4.2 Precipitable Water Anomalies

The 45 storm days were ranked by the fraction of New England, New York, Pennsylvania, and New Jersey receiving at least 25 mm of precipitation in the 24-h period. PWAT anomalies were then averaged over precipitating areas. Figure 4.8 shows a direct relationship with strong correlation (R^2>0.7) between standardized PWAT anomalies and ranked precipitation days. PWAT anomalies generally range from –0.5 to

+2.5 SD from normal for all days. Values greater than 2 SD above normal are fairly uncommon but yield heavy precipitation over a large area. Days within the positive (negative) tilt "type A" pattern have heavy precipitation over the largest (smallest) area out of all five patterns. Further discussion of how the days from all five synoptic-scale flow patterns fit into the precipitation day rankings will be presented in chapter 6.

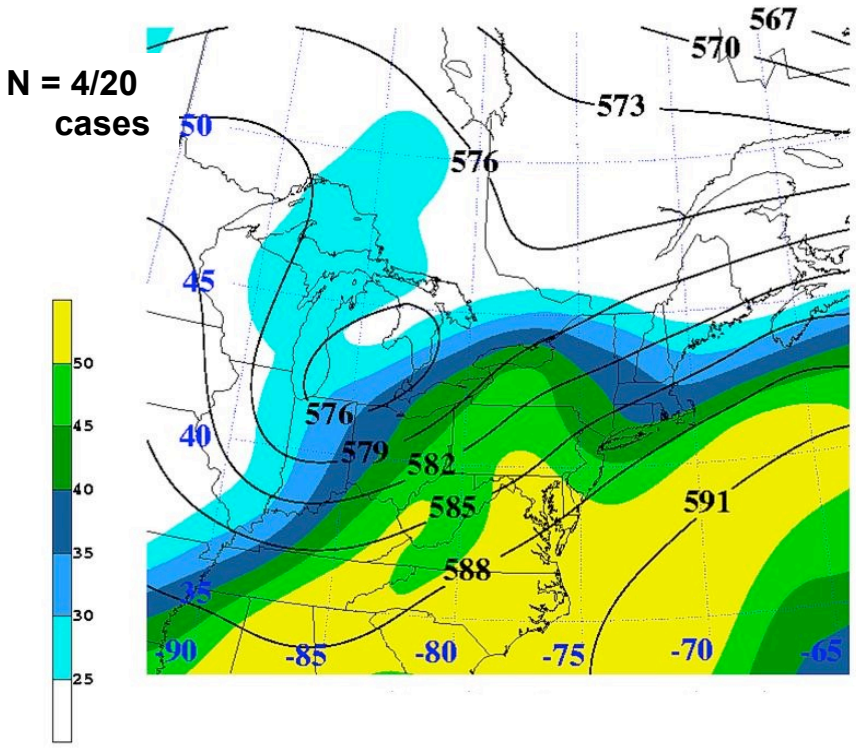

Fig. 4.1. Positive tilt "type A" pattern composites of 500-hPa geopotential height contoured every 3 dam, and PWAT shaded according to the color bar every 5 mm.

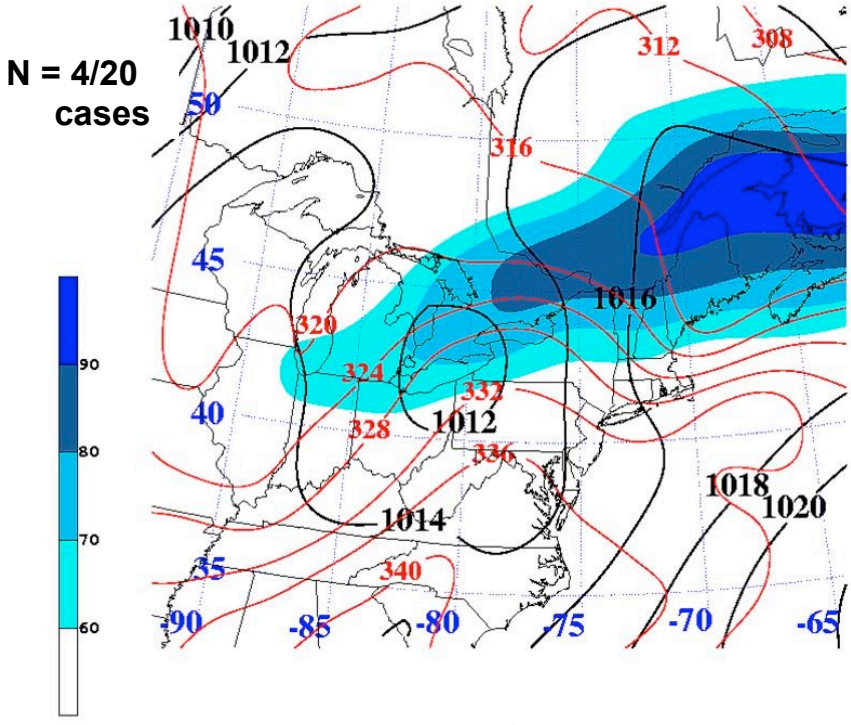

Fig. 4.2. Positive tilt "type A" pattern composites of sea level pressure contoured every 2 hPa in black, 850-hPa θ_e contoured every 4 K in red, and 250-hPa wind speed shaded according to the color bar every 10 kt.

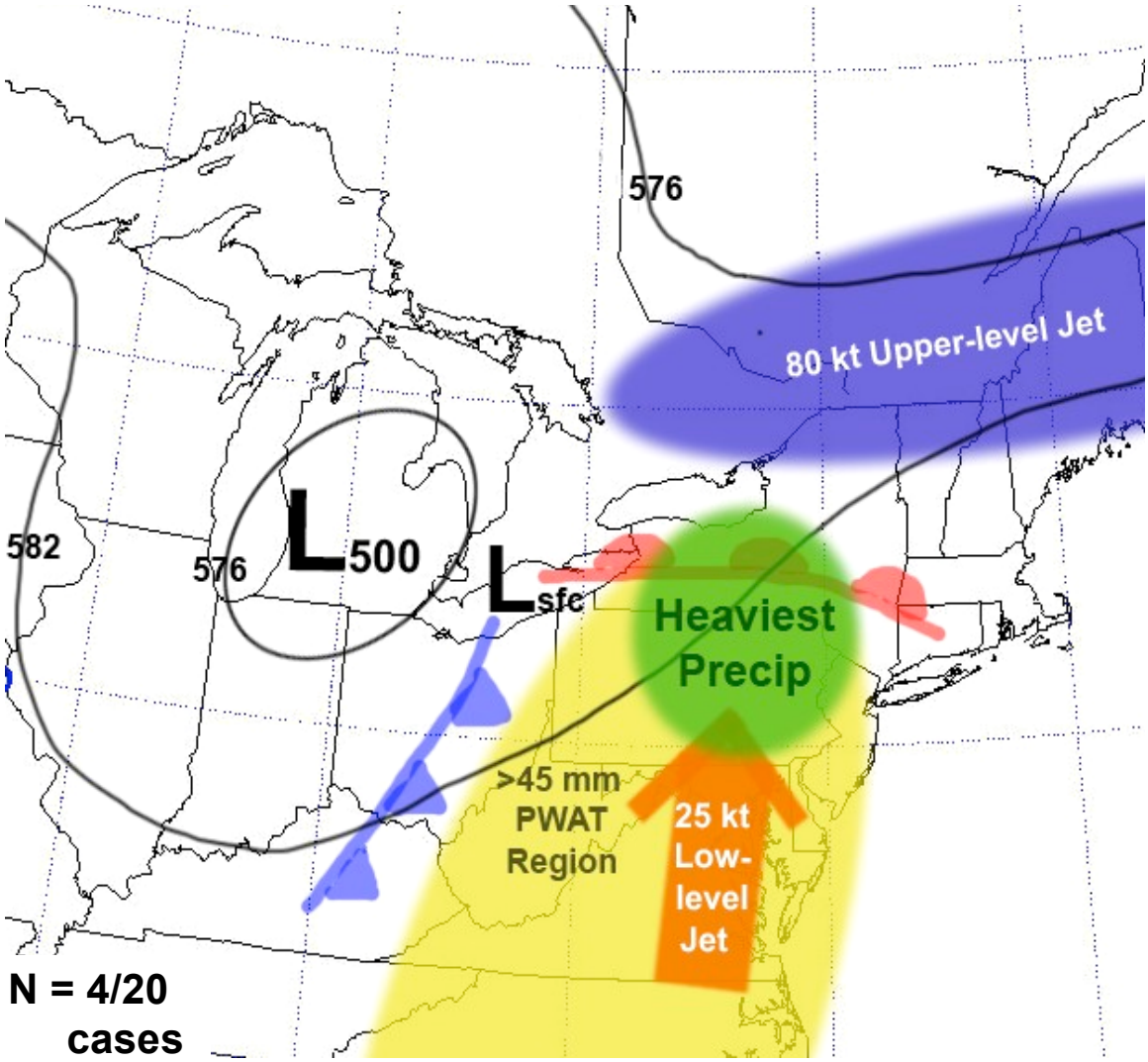

Fig. 4.3. Schematic for the positive tilt “type A” pattern.

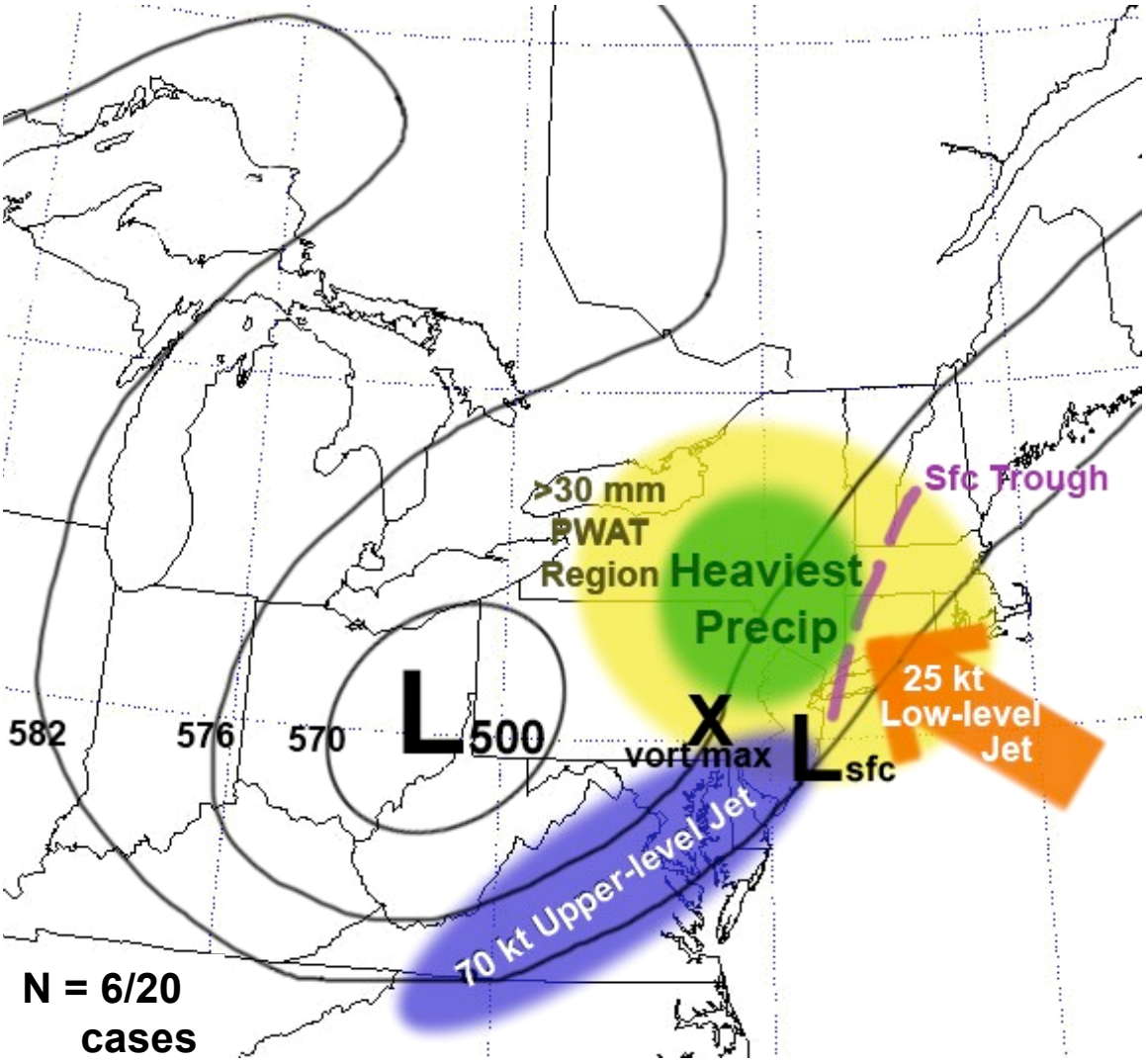

Fig. 4.4. Schematic for the positive tilt “type B” pattern.

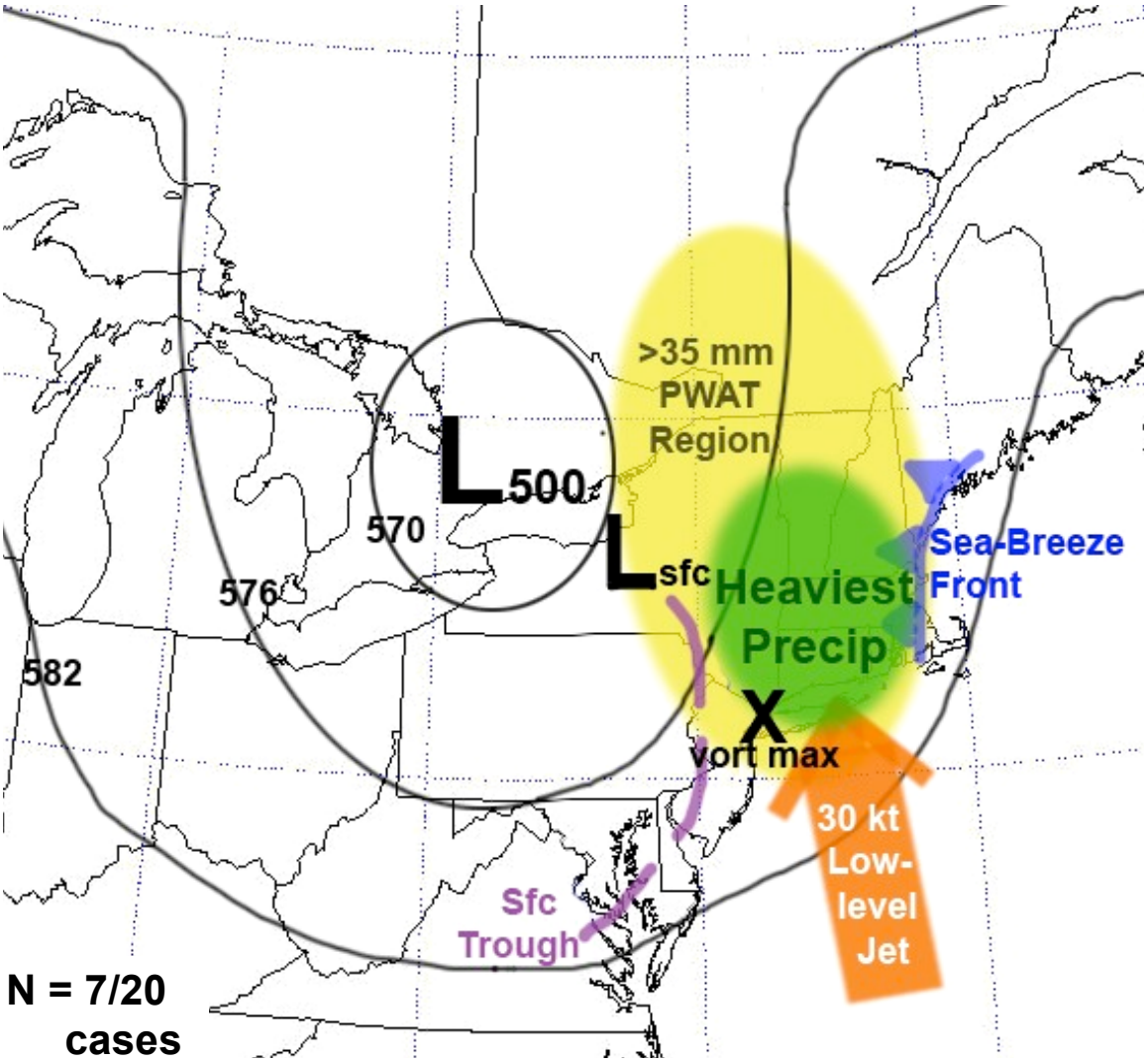

Fig. 4.5. Schematic for the neutral tilt “type A” pattern.

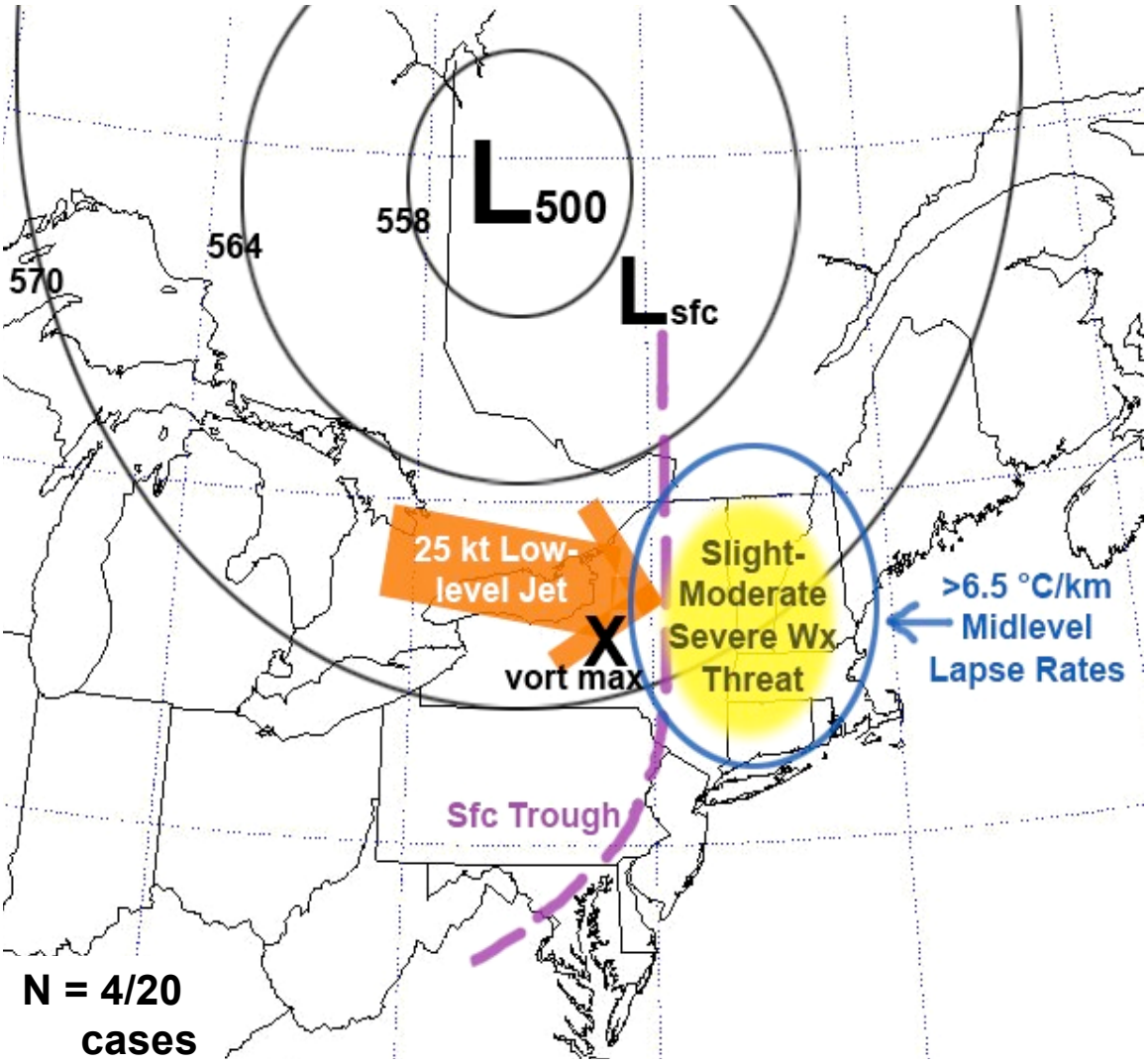

Fig. 4.6. Schematic for the neutral tilt “type B” pattern.

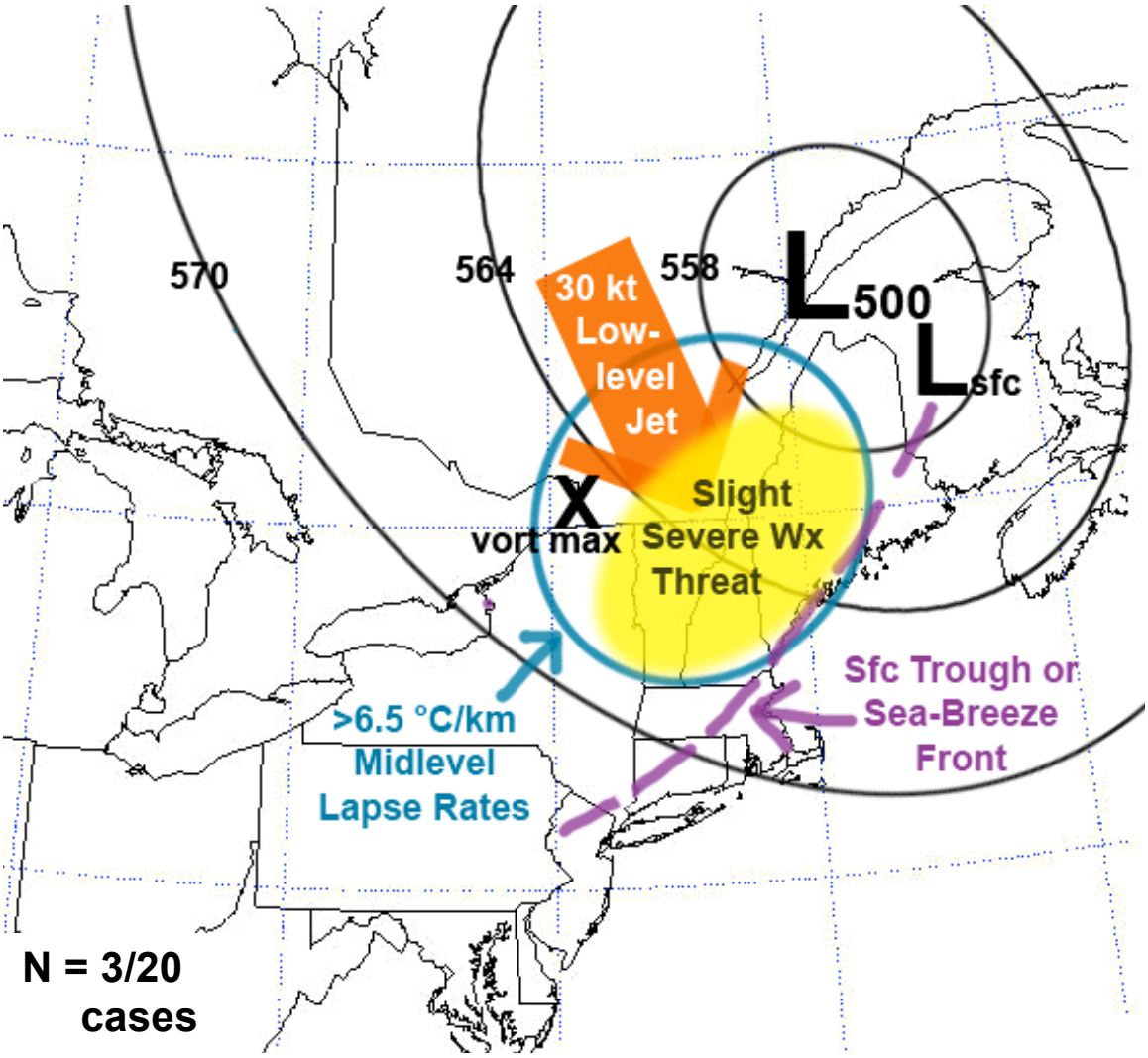

Fig. 4.7. Schematic for the negative tilt pattern.

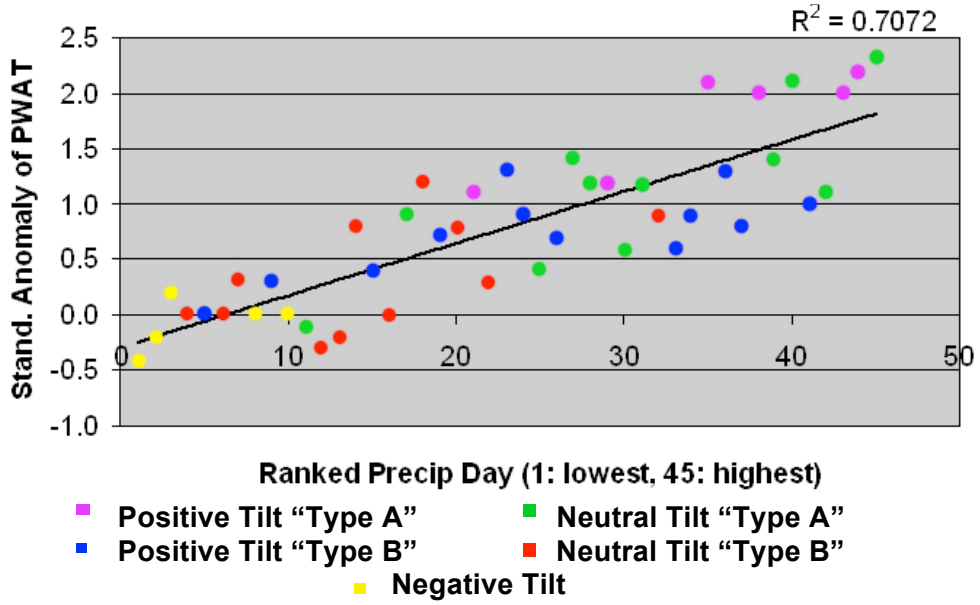

Fig. 4.8. Plot of standardized anomalies of PWAT for each ranked precipitation day.

5. Results: Analyses of Two 2008 Case Studies

5.1 Overview of Two Case Studies

Two cases of 500-hPa cutoff cyclones that tracked through the CSTAR domain were selected for diagnostic analysis. These cases were difficult to forecast and produced high-impact weather conditions across the northeastern U.S. The 16–20 June 2008 cutoff cyclone developed north of the Great Lakes and slowly moved towards northern New York. Over 100 hail reports occurred on 16 June as surface boundaries and midlevel vorticity maxima were interacting with an environment containing very steep lapse rates. Rainfall amounts were generally less than 3 cm as PWAT values were climatologically normal throughout the northeastern U.S. The cutoff cyclone entered a null phase on 17 June that lasted through 20 June, as precipitation amounts were mainly light and severe weather was infrequent. The 23–25 July 2008 cutoff cyclone, on the other hand, was active throughout. Widespread rainfall amounts of 7–9 cm and extensive flooding were associated with severe weather in a very moist environment (PWAT anomalies were 1–2.5 SDs above normal).

A discussion of how the June and July 2008 cases fit into the five distinct flow patterns of cutoff cyclones introduced in chapter 4 will be presented in chapter 6. In addition, an overview of the forecast issues with these cutoff cyclones will appear in chapter 6. The rest of this chapter provides in-depth analyses of the two aforementioned cutoff cyclone cases.

5.2 Case 1: 16–20 June 2008

5.2.1 Cutoff Cyclone Track and Total Precipitation

Figure 5.1 shows the mean 500-hPa geopotential height field over the 4-day period (1200 UTC 16 June–1200 UTC 20 June 2008) that the cutoff cyclone existed over the CSTAR domain. Also shown in Fig. 5.1 is a blue line corresponding to the track of the 500-hPa cutoff cyclone center, with its position at 12-h intervals denoted by red dots. The cutoff cyclone developed from a preexisting neutrally tilted trough north of Lake Superior. It moved southeastward over the next 48 h before stalling over extreme northern New York. The cutoff cyclone then moved northwards and gradually weakened.

Plots of 500-hPa geopotential height and associated standardized anomalies are shown at 24-h intervals in Figs. 5.2a–d. The cutoff cyclone maintained a relatively neutral tilt throughout its life cycle, with a tendency towards a slight negative tilt on 19–20 June. The 500-hPa geopotential heights were more than two standard deviations below normal in many regions to the south of the cutoff cyclone center. Overall, the cutoff cyclone was very broad in areal extent and resulted in anomalously low 500-hPa geopotential heights over much of the eastern U.S.

Figure 5.3 shows storm-total precipitation amounts. Portions of the northeastern U.S., including parts of Pennsylvania, New Jersey, and central New England, did not receive measurable precipitation over the 4-day period. Areas from western New York eastwards to southern New England received 1–3 cm on average. The highest

precipitation amounts occurred along the U.S./Canadian border and especially western Maine, where some areas received greater than 8 cm of precipitation.

5.2.2 Active Phase: 1200 UTC 16 June–1200 UTC 17 June 2008

5.2.2a Precipitation Distribution and Severe Weather

This section covers the precipitation distributions and accompanying atmospheric conditions from 1200 UTC 16 June through 1200 UTC 17 June. Figure 5.4 shows 1-day precipitation amounts ending at 1200 UTC 17 June. Highest precipitation amounts were 3–5 cm and occurred over parts of southeastern New York and southern New England. Portions of Pennsylvania, New York, and Maine received greater than 1 cm of precipitation.

SPC severe storm reports for 16 June 2008 are shown in Fig. 5.5. There were a total of 217 storm reports over the northeastern U.S. The majority of these storm reports (165) were hail reports. Hail damage was widespread across New York and there were even some large hail (>5 cm diameter) reports. The majority of the wind reports occurred across Pennsylvania and eastwards to Long Island, New York. Note that 16 June 2008 had the most hail and total severe storm reports out of all the 45 storm days studied over the 2000–2008 warm seasons.

Figures 5.6a–c show three NEXRAD base reflectivity images to illustrate differences in precipitation mode associated with the cutoff cyclone. Figure 5.6a (1220 UTC 16 June) shows a small area of showers across eastern New York that are in the

process of weakening as they move into drier air to their east. About 6 h later at 1819 UTC (Fig. 5.6b), widespread deep convection has developed throughout New York and Pennsylvania. Deep convection was mainly in the form of multicells and supercells but was organizing and transitioning towards line segments. Figure 5.6c (0017 UTC 17 June) shows a well-defined squall line across Connecticut with a large trailing stratiform region. By this time, severe weather associated with the aforementioned squall line had ended as the line of storms was approaching a low-level stable marine layer. Farther to the west, some isolated multicells and stratiform-rain regions were occurring closer to the cold pool coinciding with the 500-hPa cutoff cyclone.

5.2.2b Atmospheric Conditions

Maps for the lower, middle, and upper levels of the troposphere will be presented to examine the synoptic-scale and mesoscale conditions present for this case study. Two times, 1800 UTC 16 June and 0000 UTC 17 June, will be analyzed throughout this section in conjunction with the radar images found in Figs. 5.6b–c. Figures 5.7a–b show 500-hPa geopotential height, absolute vorticity, and wind at these times. At 1800 UTC 16 June, the 500-hPa cutoff cyclone is centered just northeast of Lake Superior. Important vorticity maxima are seen across southern Michigan and northwestern Pennsylvania. The convection across Pennsylvania and central New York at 1800 UTC (Fig. 5.6b) occurred in conjunction with DCVA associated with the vorticity maximum over northwestern Pennsylvania. The cutoff cyclone and two aforementioned vorticity

maxima move eastwards over the next 6 h with the vorticity maximum in northwestern Pennsylvania growing stronger.

Figures 5.8a–b show sea level pressure (SLP), 1000–500-hPa thickness, and 300-hPa wind speed at 1800 UTC 16 June and 0000 UTC 17 June. The 300-hPa wind speeds across the northeastern U.S. are generally 25–35 m s^{-1}, with an upper-level jet streak found to the west. The SLP field at 1800 UTC 16 June shows a large area of low pressure centered over western Quebec. An elongated cold front extends from extreme southeastern Ontario through the Ohio Valley, while an apparent prefrontal lee trough is located from southeastern Pennsylvania south through extreme eastern Virginia. A regional surface weather map is shown in Fig. 5.9 to more closely examine the prefrontal lee trough. This trough is evident near Binghamton, New York, southward through the Chesapeake Bay. The warmest temperatures across the northeastern U.S. are found near this trough. Surface temperatures across eastern Pennsylvania are 27–29°C. Figure 5.9 also clearly depicts the cold front near Lake Erie. The cold front and prefrontal lee trough push eastwards over the next 6 h (Figs. 5.8a–b).

Figures 5.10a–b show 1000–500-hPa wind shear and CAPE at 1800 UTC 16 June and 0000 UTC 17 June. The 1000–500-hPa wind shear is greater than 40 kt over portions of Pennsylvania and New York at 1800 UTC where convection developed (Fig. 5.6b). Widespread CAPE values of at least 1,000–1,500 J kg^{-1} along with strong shear led to the development of multicells and isolated supercells. The high shear also helped to maintain the eastward-moving deep convection through the evening.

Figures 5.11a–b show 850-hPa wind and θ_e at 1800 UTC 16 June and 0000 UTC 17 June. At 1800 UTC 16 June, a 20–25 kt westerly low-level jet across Pennsylvania

and southern New York advected high θ_e air eastwards. A θ_e ridge with a core value of greater than 327 K θ_e provided warm and moist low-level air that aided in the development of deep convection. By 0000 UTC 17 June, a corridor of high θ_e air with values greater than 324 K was found in the vicinity of the squall line moving through southern New England (Fig. 5.6c).

A cross section of absolute vorticity, θ, and ω at 1800 UTC 16 June from Erie, Pennsylvania, to Williamsport, Pennsylvania, is shown in Fig. 5.12. The cross section, chosen to sample the severe convection, shows the upper-level vorticity maximum over northwestern Pennsylvania seen in Fig. 5.7a. On the basis of the wind and absolute vorticity patterns shown in Fig. 5.12, DCVA is indicated east of the absolute vorticity maximum, which includes the areas where precipitation is occurring in Fig. 5.6b. The inferred upward vertical motion associated with the DCVA is evident in the cross section. Also note that isentropes are vertically farther apart in some areas downstream of the absolute vorticity maximum, indicative of reduced static stability and less resistance to vertical motion.

Figure 5.13a shows 700-hPa geopotential height, PWAT, and standardized PWAT anomalies at 1800 UTC 16 June. The 700-hPa flow over the northeastern U.S. was fairly dry and from the west and northwest. The PWAT values were climatologically normal and ranged from 20 to 30 mm over most of the region. This likely contributed to the lack of flooding reports on 16 June. The convection that led to numerous hail reports over Pennsylvania, New York, and New Jersey occurred in an area of very steep lapse rates. Figure 5.13b shows that 850–500-hPa lapse rates were greater than 7.0 °C km^{-1} over much of Pennsylvania at 1800 UTC 16 June and exceeded 7.5 °C km^{-1} in some locations.

This translates to lapse rate anomalies of 2–3.5 SDs above normal. Thermodynamic ingredients for hail occurrence, such as large CAPE and steep lapse rates, were in place for any convection that could develop across Pennsylvania, New York, and New Jersey.

Figure 5.14 shows a sounding for Albany, New York (ALB), at 1800 UTC 16 June. The sounding shows a veering low-level vertical wind profile and 0–6 km speed shear of about 40 kt. The CAPE is greater than 1,000 J kg^{-1} and no capping inversions are evident in the lower troposphere. These parameters are conducive to the formation of the observed multicells and isolated supercells that developed throughout eastern New York on 16 June (Fig. 5.6b).

5.2.3 Null Phase: 1200 UTC 17 June–1200 UTC 20 June 2008

5.2.3a Precipitation Distribution and Severe Weather

This section covers the precipitation distributions and accompanying atmospheric conditions from 1200 UTC 17 June through 1200 UTC 20 June. Figures 5.15a–c show 1-day precipitation amounts ending at (a) 1200 UTC 18 June, (b) 1200 UTC 19 June, and (c) 1200 UTC 20 June. Precipitation areal coverage and amounts were less on these three days than on the previously discussed first day of the cutoff cyclone (Fig. 5.4). Precipitation was mainly in the convective mode and diurnal in nature. Highest precipitation amounts tended to occur close to the 500-hPa cutoff cyclone center across western Maine. Figures 5.15d–f show that severe weather was not nearly as widespread as the first day and storm reports were mostly hail.

5.2.3b Atmospheric Conditions

Maps for the lower, middle, and upper levels of the troposphere will now be presented to examine the atmospheric conditions during the null phase of the cutoff cyclone. Two times, 0000 UTC 18 June and 0000 UTC 19 June, will be analyzed throughout the remainder of this section. Figures 5.16a–b show 500-hPa geopotential height, absolute vorticity, and wind at these two times. At 0000 UTC 18 June, the 500-hPa cutoff cyclone is centered east of Georgian Bay and several vorticity maxima are rotating around the cutoff cyclone. DCVA associated with one vorticity lobe over eastern New York and western New England led to an area of deep convection across eastern New England that produced some hail reports (Fig. 5.15d). The cutoff cyclone moved slowly east over the next 24 h while vorticity maxima continued to rotate around it.

Figures 5.17a–b show SLP, 1000–500-hPa thickness, and 300-hPa wind speeds at 0000 UTC 18 June and 0000 UTC 19 June. The SLP field at 0000 UTC 18 June shows a negatively tilted 1004-hPa surface cyclone over southern Quebec. Much of the northeastern U.S. was in an area of negative thickness advection. Upper-level jet dynamics were not conducive to large areas of upper-level divergence, as the strongest upper-level winds were to the south. By 0000 UTC 19 June, the surface cyclone weakened to 1006 hPa.

Figures 5.18a–b show 1000–500-hPa wind shear and CAPE at 0000 UTC 18 June and 0000 UTC 19 June. The 1000–500-hPa wind shear was 10–20 kt over most of the northeastern U.S., making it very difficult for any convection to become organized and

propagate. CAPE values were generally small, though some areas had CAPEs greater than 1,000 J kg^{-1}. Figures 5.19a–b show 700-hPa geopotential height, PWAT, and standardized PWAT anomalies at 0000 UTC 18 June and 0000 UTC 19 June. Midlevel flow was generally light over the northeastern U.S. and no moisture sources were being tapped. PWAT was about 20 mm on average, slightly below climatological normal. Thunderstorms that developed were short lived and slow moving.

Figure 5.20a shows a sounding for ALB at 0000 UTC 18 June. The sounding shows backing winds in low levels, indicative of cold-air advection. In addition, 0–3 km speed shear is 0 km, CAPE is 17 J kg^{-1}, and PWAT is only 17 mm. These parameters are not conducive to severe weather or heavy precipitation. Another sounding (Fig. 5.20b) for ALB at 0000 UTC 19 June again shows low-level backing of winds. The vertical profile is a little moister than it was the previous day (PWAT is 5 mm higher), but there is still a lack of significant CAPE and shear. Any convective storms that did develop were of the pulse type, short-lived, and generally produced less than 2.5 cm of precipitation.

5.3 Case 2: 23–25 July 2008

5.3.1 Cutoff Cyclone Track and Total Precipitation

Figure 5.21 shows the mean 500-hPa geopotential height field over the 3-day period (1200 UTC 22 July–1200 UTC 25 July 2008) that the cutoff cyclone existed over the CSTAR domain. The cutoff cyclone developed from a preexisting positively tilted

trough over eastern Canada. The first phase comprised the formation of its center southeast of James Bay at 1200 UTC 22 July and the slow southwestward movement of the center over the next 12–18 h. The precipitation distributions and atmospheric conditions on 22 July are not discussed because the precipitation over the northeastern U.S. on this day was mainly light and attributable to surface boundaries present prior to cutoff cyclogenesis. The second phase of the cutoff cyclone consisted of the redevelopment of its center over Lake Huron at 1200 UTC 23 July. The center drifted eastwards over the next 24 h before retreating to the north and east (third phase).

Plots of 500-hPa geopotential height and associated standardized anomalies are shown at 12-h intervals in Figs. 5.22a–d. The cutoff cyclone pivoted from a slight positive to slight negative tilt over its life cycle, but overall exhibited a relatively neutral tilt throughout the life cycle. The 500-hPa geopotential heights were more than two standard deviations below normal in the southern part of the cutoff cyclone core from 1200 UTC 23 July through 1200 UTC 24 July. The cutoff cyclone started to weaken by 0000 UTC 25 July as it moved to the north and east. Also evident during 24–25 July is a strong downstream ridge to the east and northeast of the cutoff cyclone where 500-hPa geopotential heights were more than two standard deviations above normal.

Figure 5.23 shows storm-total precipitation amounts. The vast majority of the northeastern U.S. with the exception of parts of northeastern Maine received measurable precipitation during the cutoff cyclone life cycle. Widespread rain amounts of 7–9 cm occurred over eastern New York and central Massachusetts. There were also some clear orographic signals of enhanced precipitation (e.g., Pocono, Catskill, Green, and southeast

Adirondack Mountains). Highest precipitation amounts were greater than 13 cm and occurred near Springfield, Massachusetts, and over parts of the Catskills.

5.3.2 Day 1: 1200 UTC 23 July–1200 UTC 24 July 2008

5.3.2a Precipitation Distribution and Severe Weather

This section covers the precipitation distributions and accompanying atmospheric conditions from 1200 UTC 23 July through 1200 UTC 24 July. Figure 5.24 shows 1-day precipitation amounts ending at 1200 UTC 24 July. The heaviest precipitation occurred along north–south-oriented bands, especially across eastern New York where much of the region received at least 5 cm of precipitation. Some orographic signals of enhanced precipitation amounts over the 24-h period are apparent (e.g., Pocono and Catskill Mountains).

SPC severe storm reports for 23 July 2008 are shown in Fig. 5.25. For the northeastern U.S., the majority of severe storm reports were wind reports stretching from southern New England southwestward. More isolated wind and hail reports occurred farther west near the cold pool coinciding with the 500-hPa cutoff cyclone core. An EF1 tornado occurred over Swansea, Rhode Island.

Figures 5.26a–c show three NEXRAD base reflectivity images. Figure 5.26a (1218 UTC 23 July) shows a mesoscale convective system (MCS) that originated over West Virginia and Virginia now decaying across eastern New York. About 6 h later at 1804 UTC (Fig. 5.26b), there are three areas of precipitation that will be discussed in

detail in the next section. The first area is a narrow broken squall over western Pennsylvania and New York. Farther to east across eastern Pennsylvania and New York, a large band of stratiform precipitation with substantial embedded convection can be seen. Finally, a few multicells and heavy-precipitation (HP) supercells are developing across southern New England. About 7 h later at 0121 UTC 24 July (Fig. 5.26c), several areas across the northeastern U.S. continue to receive heavy precipitation. The squall line over western Pennsylvania and New York has decreased in intensity as it enters an area of clouds remaining from the stratiform band to the east, and due to a loss of daytime heating. The aforementioned large stratiform band has remained relatively stationary and now has stronger embedded convection within it, including line echo wave patterns and bow echoes. Farther to the north there is widespread stratiform precipitation falling in a cool air mass. Finally, convection continues to form over southern New England.

5.3.2b Atmospheric Conditions

Maps for the lower, middle, and upper levels of the troposphere will be presented to examine the synoptic-scale and mesoscale conditions present for this case study. Two times, 1800 UTC 23 July and 0000 UTC 24 July, will be analyzed throughout the remainder of this section in conjunction with the radar images found in Figs. 5.26b–c. Figures 5.27a–b show 500-hPa geopotential height, absolute vorticity, and wind at these times. At 1800 UTC 23 July, the 500-hPa cutoff cyclone is centered between Lakes Huron and Ontario, with its strongest lobe of vorticity stretching southward through Ohio. The broken squall line over western Pennsylvania and New York (Fig. 5.26b)

strengthened due to DCVA associated with the aforementioned vorticity lobe. Farther east over eastern Pennsylvania, a vorticity maximum and associated DCVA likely produced ascent that enhanced the rainband across eastern Pennsylvania, eastern New York, and New Jersey. The cutoff cyclone pivots from a slight positive tilt to a neutral tilt during the 6-h period ending 0000 UTC 24 July.

Figures 5.28a–b show SLP, 1000–500-hPa thickness, and 250-hPa wind speed at 1800 UTC 23 July and 0000 UTC 24 July. The SLP field shows a large area of disorganized low pressure starting to develop a center over eastern Lake Ontario and a cold front extending to the south by 0000 UTC 24 July. The SLP and thickness patterns also suggest the existence of a warm/stationary front to the east-northeast of New Jersey at 1800 UTC 23 July moving northward during the next 6 h. The orientation of the isobars and thickness contours over southern New England is indicative of strong warm-air advection over the region. The cold front, warm/stationary front, and warm-air advection served as lifting mechanisms acting on a moist air mass and leading to heavy precipitation. The 250-hPa wind speed field displays an upper-level jet streak extending across western New York northeastward into southwestern Quebec. This jet streak had v-winds in excess of 2 SDs above normal at 250 hPa (not shown). The location of the jet streak placed portions of Pennsylvania and New York in its equatorward-entrance region, a position known to be favorable for upper-level divergence and associated upward vertical motion.

Figure 5.29 shows a surface weather map for southern New England and vicinity with temperature contoured at 0100 UTC 24 July. A surface boundary over southern New England is depicted, both by a wind shift and relatively large thermal gradient.

Temperatures across this boundary ranged from 24°C at Hartford, Connecticut, to 18°C at Manchester, New Hampshire. The combination of surface easterlies north of the boundary and southerlies at 500 hPa (Fig. 5.27b) indicates a veering wind profile in the vertical, which aided in HP supercell development and the spinup of an EF1 tornado in Rhode Island.

Figures 5.30a–b show 1000–700-hPa wind shear and CAPE at 1800 UTC 23 July and 0000 UTC 24 July. The 1000–700-hPa wind shear was greater than 40 kt across eastern Pennsylvania, northern New Jersey, and southeastern New York at 1800 UTC 23 July. This relatively high shear helped to generate and maintain convection along the large rainband across these aforementioned regions. In addition, the alignment of the shear with the rainband (relatively parallel to each other) led to training echoes along the rainband, as well as some convectively driven backbuilding cells within the rainband. Note also that shear values of about 35 kt were found over southern New England. CAPE values at 1800 UTC 23 July were largest (at least 1,500–2,000 J kg^{-1}) over southeastern Pennsylvania and southern New Jersey. This provided sufficient instability for deep convection to develop along and to the south of the aforementioned rainband. The highest CAPE values were found over Long Island, New York, and southern New England at 0000 UTC 24 July, coinciding with the location of the surface boundary there (Fig. 5.29).

Figures 5.31a–b show 850-hPa wind and θ_e at 1800 UTC 23 July and 0000 UTC 24 July. A 30 kt low-level jet is surging northwards along the northeastern U.S. coast. A θ_e ridge is also evident over the tri-state area of New York, New Jersey, and Connecticut at 1800 UTC 23 July and eastern New York and New England at 0000 UTC 24 July.

This θ_e ridge signifies the presence of warm and moist low-level air conducive to the development of thunderstorms. The high θ_e air also enabled thunderstorms to develop along the frontal boundary across southern New England at 0000 UTC 24 July. As high θ_e air was advected northwards over the 6-h period ending at 0000 UTC 24 July, precipitation started to develop across central New England (Figs. 5.26b–c).

PWAT and 700-hPa geopotential height and wind at 1800 UTC 23 July are shown in Fig. 5.32. PWAT values were greater than 55 mm across the Gulf of Mexico and southeastern U.S. coasts. This high PWAT was being advected to the east and northeast by the midlevel flow. A combination of a 309-dam 700-hPa cyclone and strong downstream anticyclone contributed to a strong northward surge of the aforementioned high PWAT. In addition, moisture from the western North Atlantic was being advected northwards at 1800 UTC 23 July. The convergence of the two moisture streams into the northeastern U.S. led to heavy precipitation.

A cross section of frontogenesis, θ, and ω at 1800 UTC 23 July from Harrisburg, Pennsylvania, to Belmar/Farmdale, New Jersey, is found in Fig. 5.33. These endpoints were selected because the large rainband previously mentioned was located between them at this time (Fig. 5.26b). The cross section shows low-level frontogenesis across its horizontal extent. The associated ascent is evident as a large area of -9×10^{-3} hPa s^{-1} vertical motion. Also note the veering low-level wind profile, indicating warm-air advection and additional forcing for ascent.

5.3.3 Day 2: 1200 UTC 24 July–1200 UTC 25 July 2008

5.3.3a Precipitation Distribution and Severe Weather

This section covers the precipitation distributions and atmospheric conditions from 1200 UTC 24 July through 1200 UTC 25 July. Figure 5.34 shows 1-day precipitation amounts ending at 1200 UTC 25 July. Heavy precipitation was widespread across New England, with highest amounts occurring over eastern New England where much of the region received at least 4 cm of precipitation. Note that as a whole precipitation amounts were lower this day than on the previous day (Fig. 5.24), as the 500-hPa cutoff cyclone and upper-level jet streak started to move to the north and east.

SPC severe storm reports for 24 July 2008 are shown in Fig. 5.35. A significant band of severe weather reports, most of which were wind reports, appears over southeastern New Hampshire and southwestern Maine. There was also an EF2 tornado that touched down in Epsom, New Hampshire, and had the longest path of any New England tornado on record. More isolated storm reports and an area of numerous hail reports in central Pennsylvania occurred farther west close to the cold pool coinciding with the 500-hPa cutoff cyclone.

Figures 5.36a–c show three NEXRAD base reflectivity images. Figure 5.36a (1218 UTC 24 July) shows a large stratiform rainband with embedded convection throughout eastern New York and southern New England. More isolated precipitation is apparent to the west across northwestern Pennsylvania. A few hours later at 1549 UTC (Fig. 5.36b), a well-defined MCS in the form of a long convective line with embedded bow echoes occurred over eastern New England. This MCS contained the EF2 tornado (shown at the tip of the arrow in Fig. 5.36b) previously mentioned and will be a focus of

discussion in the following section. To the west of the aforementioned convective line are other north–south-oriented bands starting to develop even before afternoon heating has set in. Numerous convective lines and bow echoes occur throughout New England at 1818 UTC (Fig. 5.36c). Also evident are areas of multicells over central New York and Pennsylvania that produced large hail.

5.3.3b Atmospheric Conditions

The 1200 UTC 24 July and 1800 UTC 24 July analyses times will be investigated throughout this section in conjunction with the radar images found in Figs. 5.36a–c to better establish the character of the precipitation systems. Figures 5.37a–b show 500-hPa geopotential height, absolute vorticity, and wind at these times. By 1200 UTC 24 July, the 500-hPa cutoff cyclone is centered over western Lake Ontario. The strongest vorticity maximum is located over central Pennsylvania at 1200 UTC 24 July and it pivots around the southeast side of the cutoff cyclone during the next 6 h. DCVA associated with the aforementioned vorticity maximum helped generate ascent that resulted in the occurrence of severe convection across upstate New York (Figs. 5.36b–c). Note also that the cutoff cyclone shows signs of slight weakening over the 6-h period ending 1800 UTC 24 July as the area enclosed by the 570-dam contour decreases slightly. In addition, the cutoff–trough system tilt starts to become slightly negative as the cutoff cyclone retreats to the north and east.

Figures 5.38a–b show SLP, 1000–500-hPa thickness, and 250-hPa wind speed at 1200 UTC and 1800 UTC 24 July. The SLP field shows a well-defined surface cyclone

north of Lake Ontario and cold front stretching southward. Warm-air advection has subsided over New England by 1800 UTC 24 July as thickness contours are relatively parallel to the isobars. The loss of the warm-air advection lifting mechanism may be partially responsible for precipitation amounts being lighter on the present day than on the previous day. The 1000–500-hPa thickness pattern also shows the cold pool coinciding with the cutoff cyclone centered over northwestern Pennsylvania with a closed 558-dam contour at 1800 UTC. Finally, the location of a 50 m s^{-1} 250-hPa jet streak placed portions of southern New England in its equatorward-entrance region, a position favorable for midlevel upward vertical motion.

Figure 5.39 shows a surface weather map centered on southern New Hampshire at 1500 UTC 24 July. The surface boundary that was over southern New England at 0100 UTC 24 July (Fig. 5.29) has moved northwards into central New England as a warm front by 1500 UTC. Surface frontogenesis was occurring along the eastern New England coast in conjunction with a developing sea-breeze boundary. Significant baroclinicity is present at the surface as shown by temperatures ranging from 27°C at Boston, Massachusetts, to 18°C in central New Hampshire. Note that winds at the surface throughout much of eastern New England were almost due southerly, while in Portsmouth and Concord, New Hampshire, these winds were backed to southeasterly. These backed winds at the surface and southerlies aloft, as shown in a Gray, Maine (GYX) sounding taken at 1800 UTC 24 July (Fig. 5.40), introduced a directional shear component to the vertical wind profile. This directional shear likely contributed to localized enhanced rotation within the bow echo feature seen at the tip of the red arrow in Fig. 5.36b. The GYX sounding also shows strong speed shear of 45 kt in the lowest 3 km

above the surface, rendering the environment very conducive to convective line or bow echo development. Figure 5.36c shows several bow echoes developing across eastern New Hampshire and southwestern Maine. The GYX sounding is very moist (PWAT is about 43 mm) and is saturated near the surface. The moderate CAPE values of about 800 J kg^{-1} and low lifted condensation level of 974 hPa indicate a tropical-like environment in which warm rain processes are likely important.

Figures 5.41a–b show 850-hPa wind and θ_e at 1200 UTC and 1800 UTC 24 July. A corridor of θ_e values greater than 332 K is found through the Connecticut River Valley at 1200 UTC, collocated with the stratiform rainband there (Fig. 5.36a). At 1800 UTC, a large area of θ_e values greater than 335 K is found across eastern New England and the Gulf of Maine. The θ_e increased from 328 K to 336 K near Boston, Massachusetts, during the 6-h period ending at 1800 UTC. The highest positive θ_e advection was over northern New England at 1800 UTC, a region where the heaviest precipitation advanced into later in the day (not shown).

Figures 5.42a–b show 850-hPa geopotential height, wind, and standardized anomalies of 850-hPa v-wind at 1200 UTC and 1800 UTC 24 July. The 850-hPa winds show a low-level jet over New England in which winds increase from 30 kt at 1200 UTC to 45–50 kt at 1800 UTC as the pressure gradient strengthens. The 850-hPa southerly v-winds in excess of 45 kt within the low-level jet at 1800 UTC were extremely anomalous, at 5 SDs above normal. This strong low-level jet helped to draw in moisture from the south and lead to wind damage associated with convective lines and bow echoes.

Figures 5.43a–b show 700-hPa geopotential height, PWAT, and standardized PWAT anomalies at 1200 UTC and 1800 UTC 24 July. The flow at 700 hPa was

strongly cyclonic over the northeastern U.S. as seen at 850 hPa (Figs. 5.42a–b). PWAT values ranged from 40 to 50 mm (1–2.5 SDs above normal) over most of New England. Isolated areas of New England, including eastern Massachusetts, had PWAT values greater than 50 mm at 1800 UTC. Lower PWAT values (1–2.5 SDs below normal) were being advected eastward to the south of the 700-hPa cyclone.

The convection that led to numerous hail reports over central Pennsylvania (Fig. 5.35) occurred in an area of very cold 500-hPa temperatures and steep midlevel lapse rates. Figure 5.44a shows that at 1200 UTC 24 July the 500-hPa temperatures were below –16°C across portions of central Pennsylvania (less than –3 SDs from normal). The 700–500-hPa lapse rates exceeded 6.5 °C km^{-1} throughout much of Pennsylvania and 7.0 °C km^{-1} over south-central Pennsylvania (Fig. 5.44b). This translates to lapse rate anomalies of 2–3.5 SDs above normal. Farther to the northeast across New England, lapse rates were climatologically normal at around 5.5 °C km^{-1}, leading to stratiform precipitation (as seen in the rainband in Fig. 5.36a) and no hail reports.

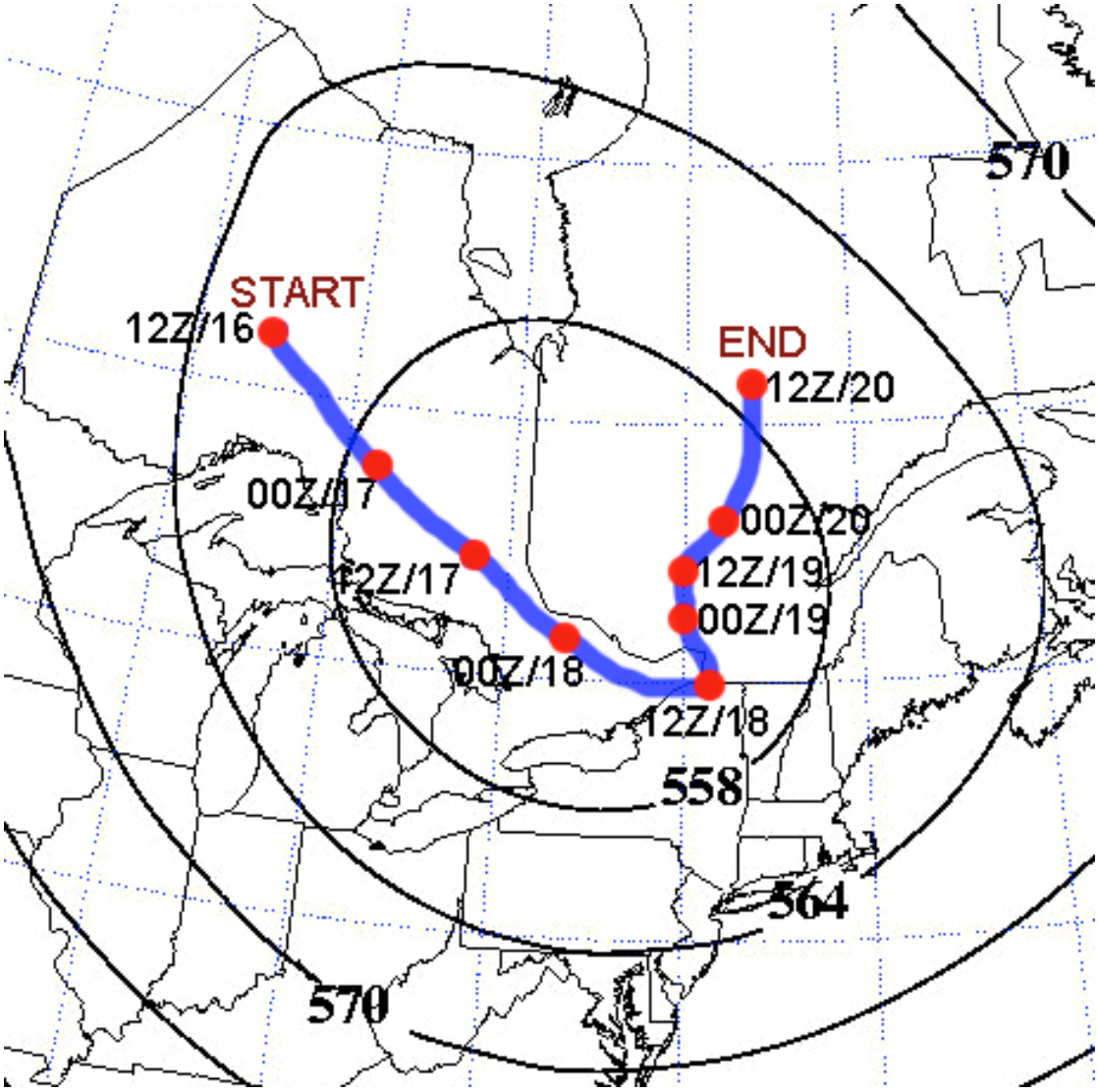

Fig. 5.1. Mean 500-hPa geopotential height (dam) and track of 500-hPa cutoff cyclone center for 1200 UTC 16 June–1200 UTC 20 June 2008.

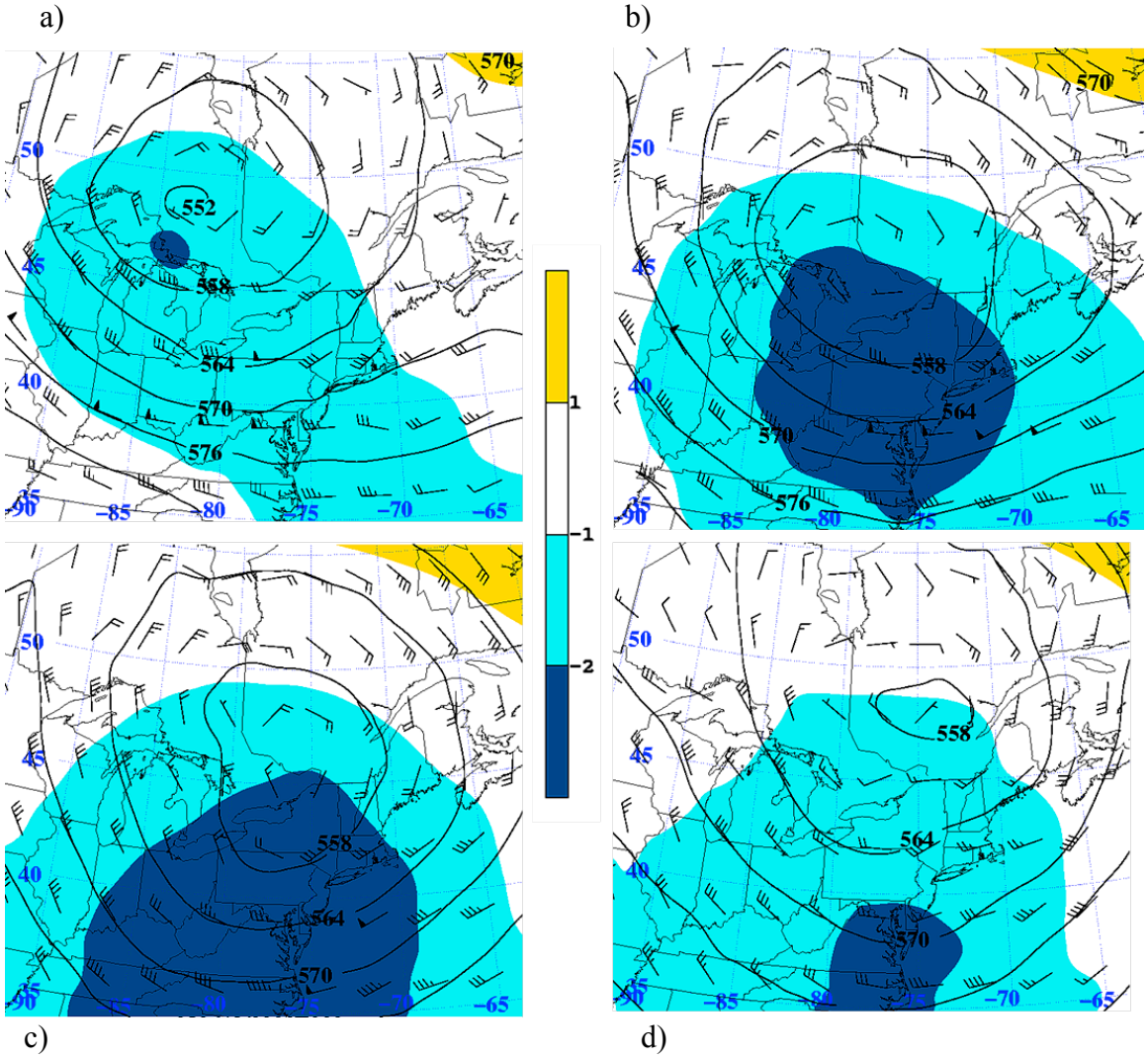

Fig. 5.2. 500-hPa geopotential height contoured every 6 dam, wind (kt), and standardized anomalies of 500-hPa geopotential height shaded according to the color bar every 1 SD at (a) 0000 UTC 17 June 2008, (b) 0000 UTC 18 June 2008, (c) 0000 UTC 19 June 2008, and (d) 0000 UTC 20 June 2008.

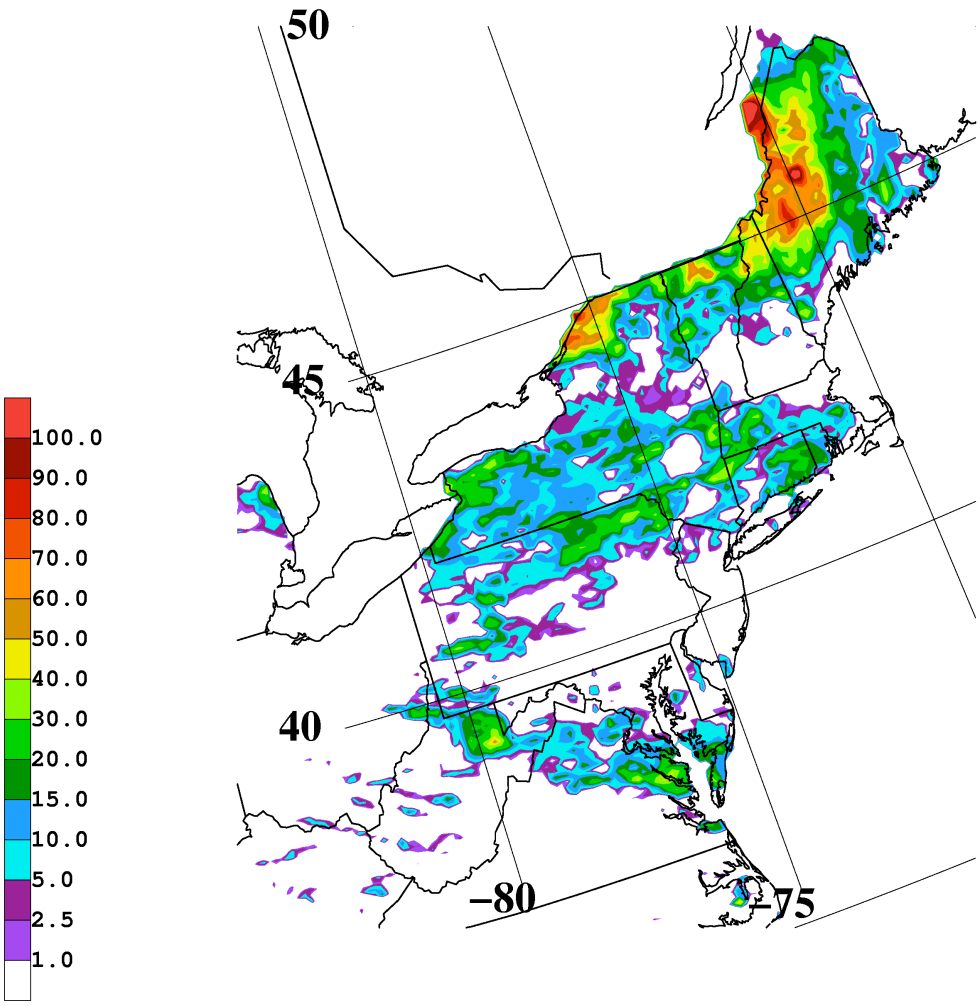

Fig. 5.3. National Precipitation Verification Unit 4-day Quantitative Precipitation Estimates (mm) ending at 1200 UTC 20 June 2008.

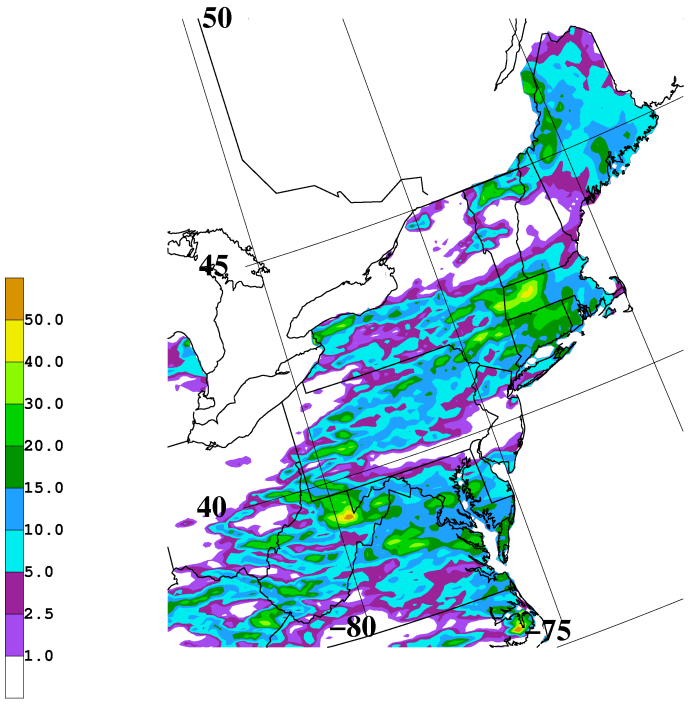

Fig. 5.4. National Precipitation Verification Unit 1-day Quantitative Precipitation Estimates (mm) ending at 1200 UTC 17 June 2008.

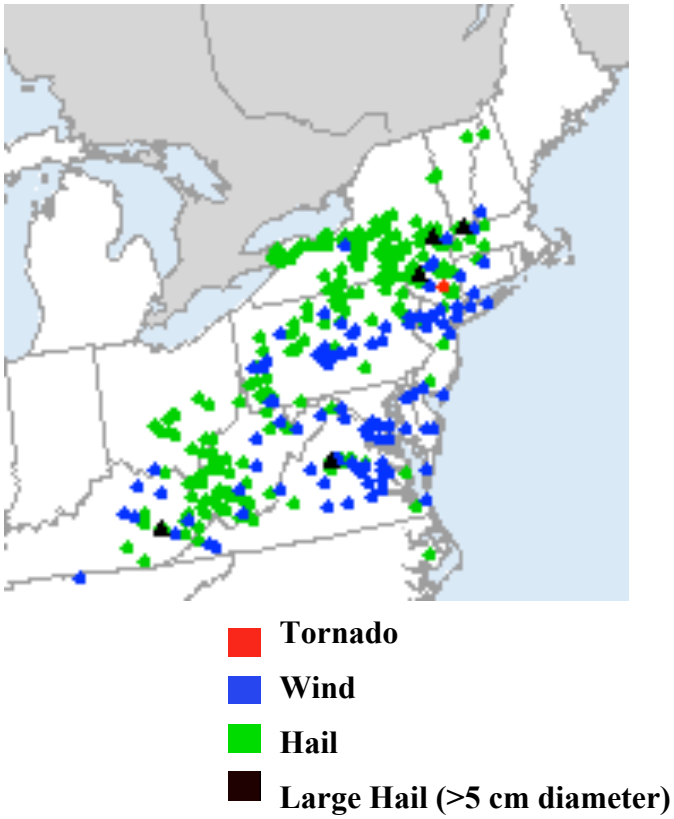

Fig. 5.5. SPC severe storm reports for 16 June 2008.

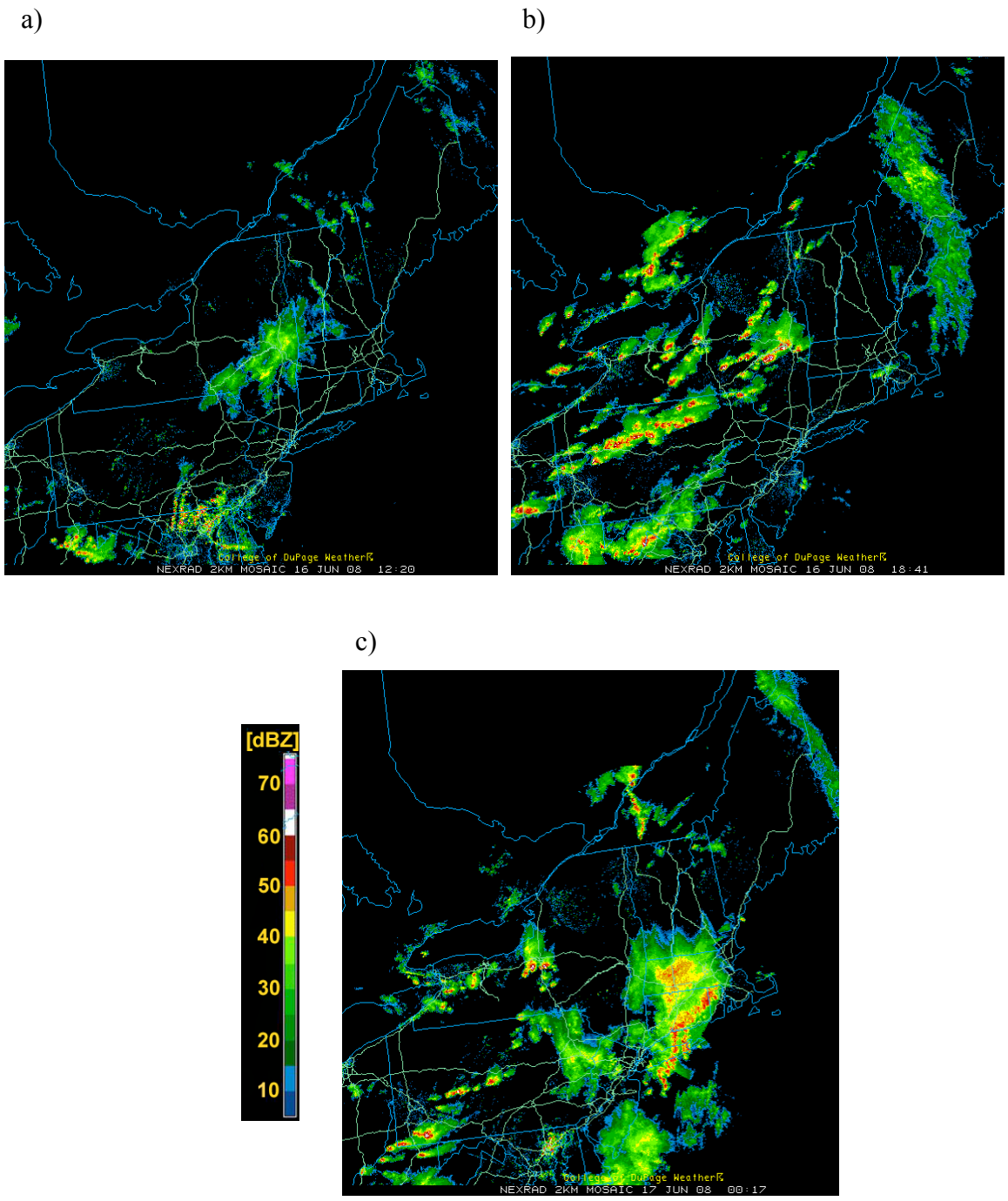

Fig. 5.6. NEXRAD base reflectivity shaded according to the color bar every 5 dB*Z* at (a) 1220 UTC 16 June 2008, (b) 1819 UTC 16 June 2008, and (c) 0017 UTC 17 June 2008.

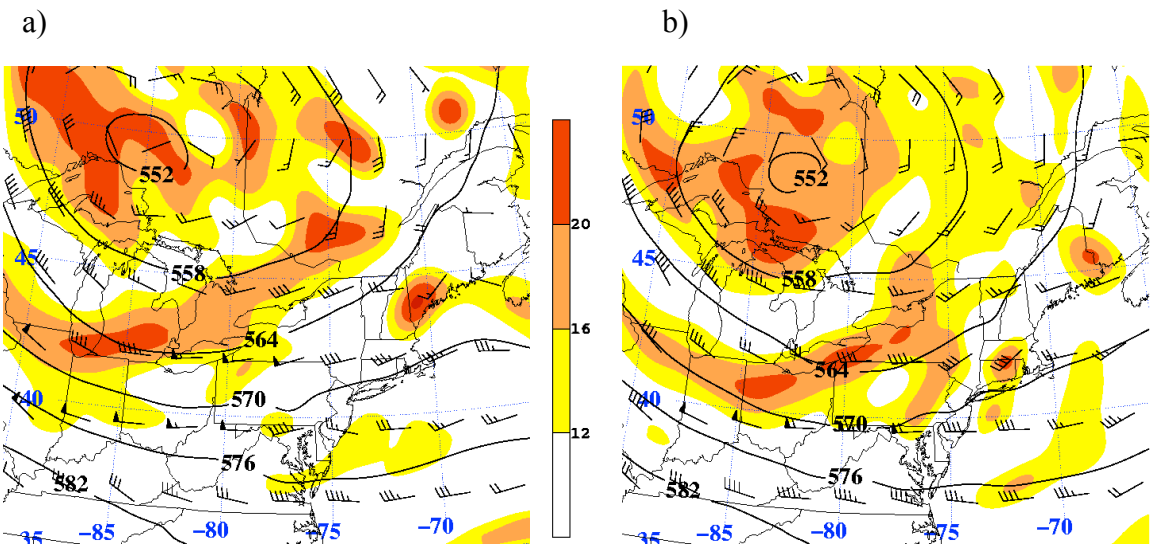

Fig. 5.7. 500-hPa geopotential height contoured every 6 dam, wind (kt), and absolute vorticity shaded according to the color bar every 4×10^{-5} s^{-1} for values above 12×10^{-5} s^{-1} at (a) 1800 UTC 16 June 2008 and (b) 0000 UTC 17 June 2008.

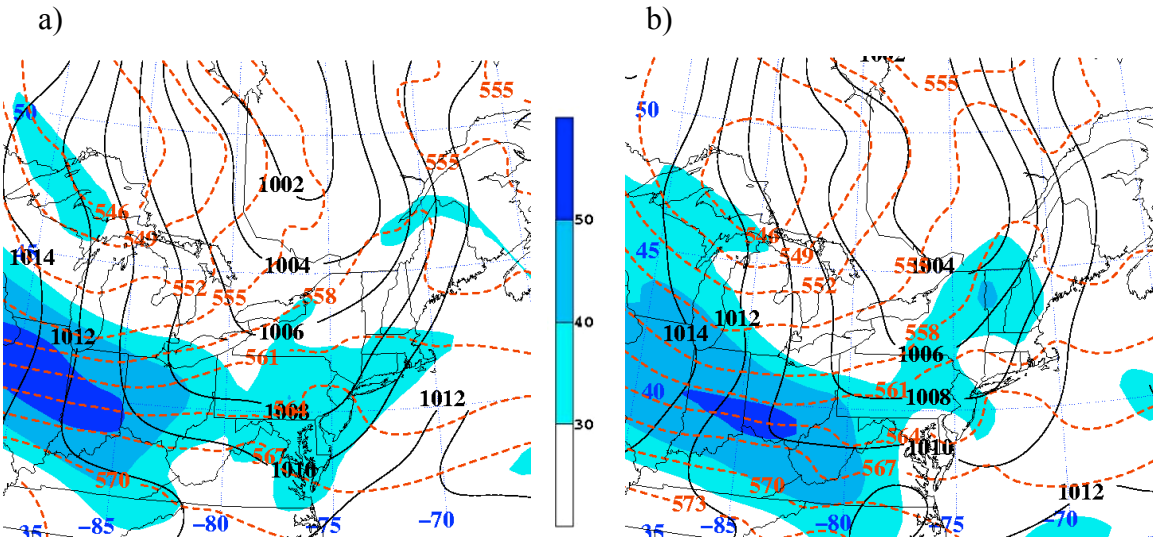

Fig. 5.8. SLP contoured every 2 hPa in black, 1000–500-hPa thickness contoured every 3 dam in dashed orange, and 300-hPa wind speed shaded according to the color bar every 10 m s^{-1} for values above 30 m s^{-1} at (a) 1800 UTC 16 June 2008 and (b) 0000 UTC 17 June 2008.

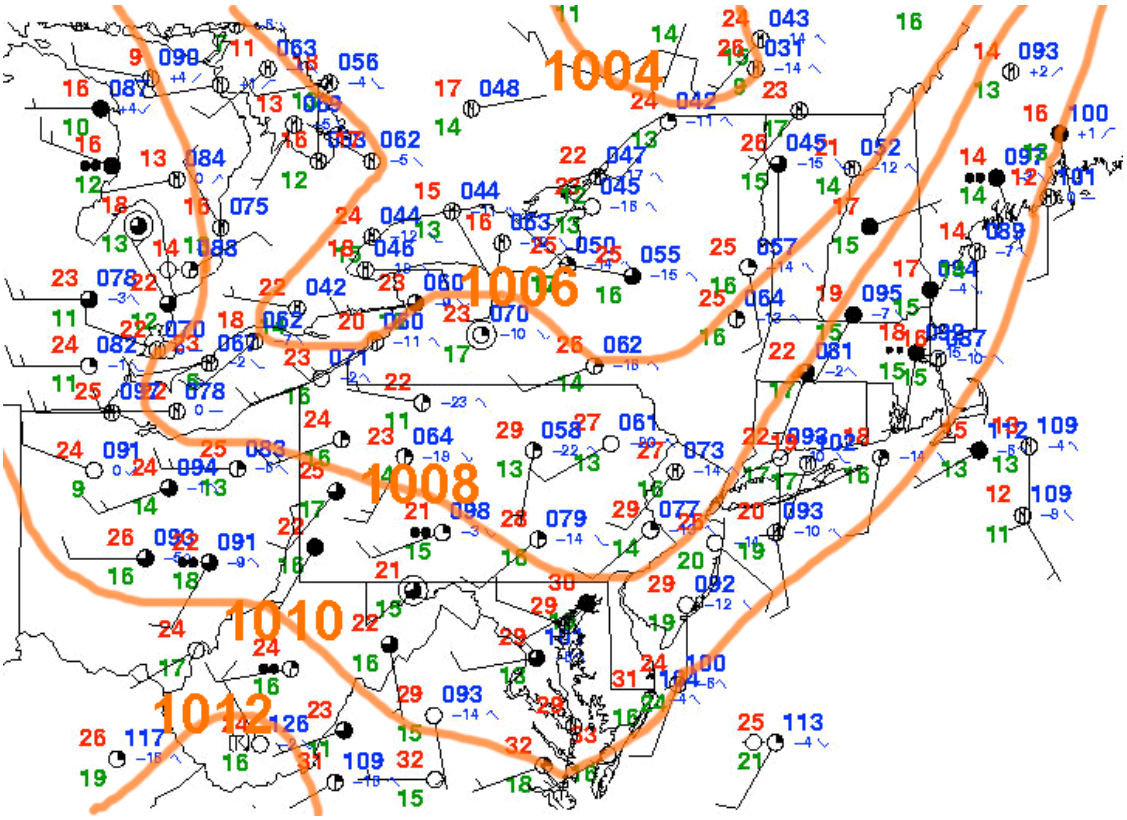

Fig. 5.9. Surface station plot with SLP contoured in orange every 2 hPa at 1800 UTC 16 June 2008.

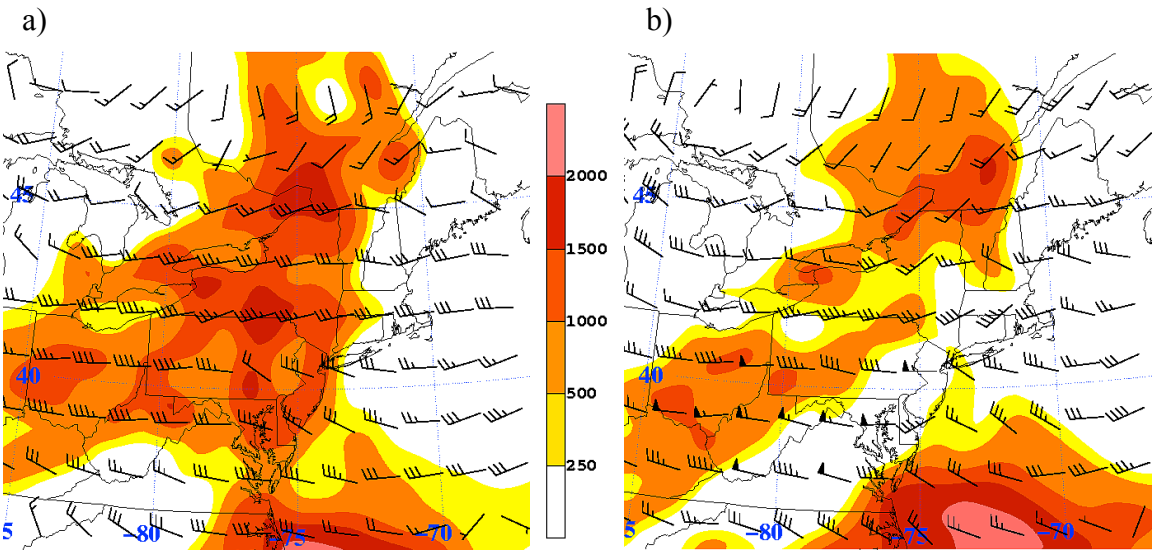

Fig. 5.10. 1000–500-hPa wind shear (barbs) and CAPE (J kg^{-1}) shaded according to the color bar every 250 J kg^{-1} for values below 500 J kg^{-1} and every 500 J kg^{-1} for values above 500 J kg^{-1} at (a) 1800 UTC 16 June 2008 and (b) 0000 UTC 17 June 2008.

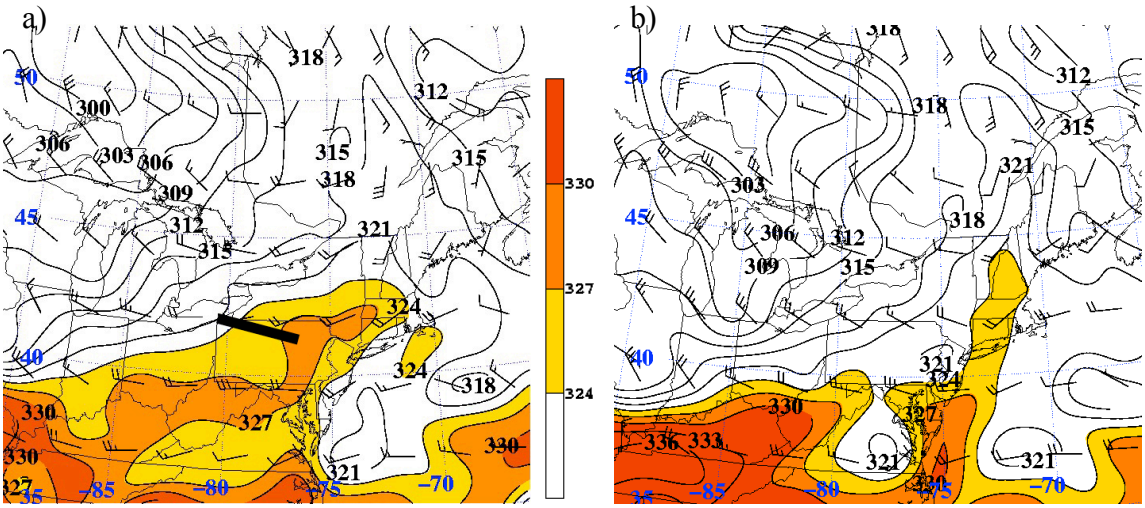

Fig. 5.11. 850-hPa wind (kt) and θ_e contoured every 3 K and shaded according to the color bar every 3 K for values above 324 K at (a) 1800 UTC 16 June 2008 and (b) 0000 UTC 17 June 2008. Dark solid line in (a) shows orientation of cross section in Fig. 5.12.

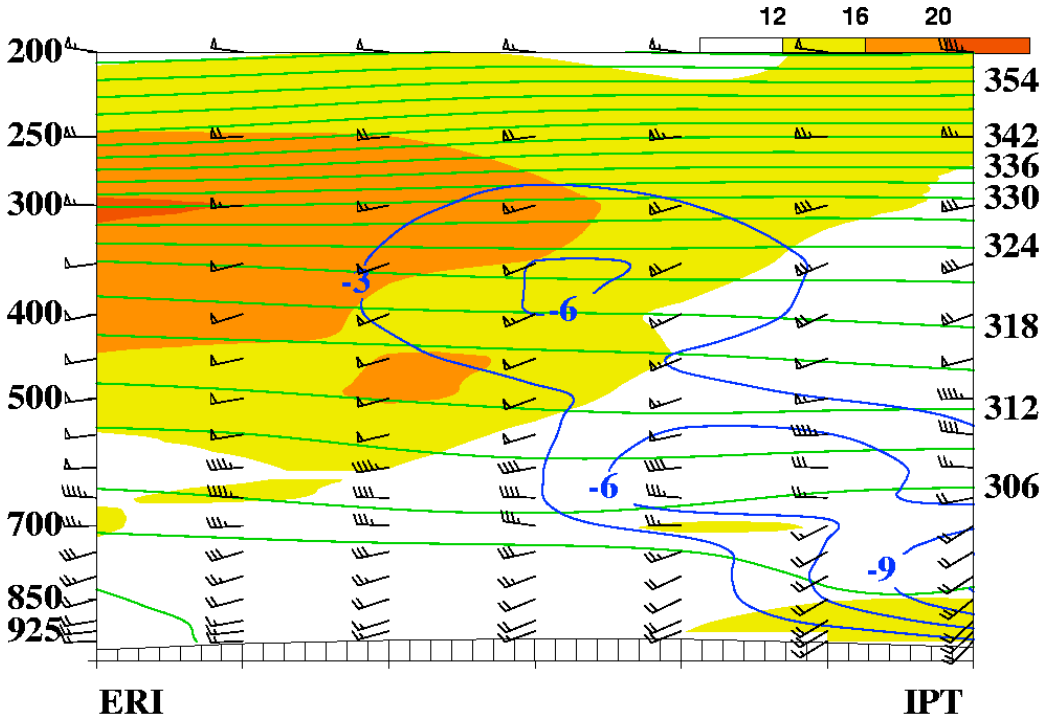

Fig. 5.12. Cross section at 1800 UTC 16 June 2008 from Erie, Pennsylvania (ERI), to Williamsport, Pennsylvania (IPT) (dark solid line in Fig. 5.11a), showing absolute vorticity (shaded according to the color bar every 4×10^{-5} s^{-1} for values above 12×10^{-5} s^{-1}), θ (green lines, contoured every 3 K), ω (blue lines, contoured every 3×10^{-3} hPa s^{-1}), and wind (barbs).

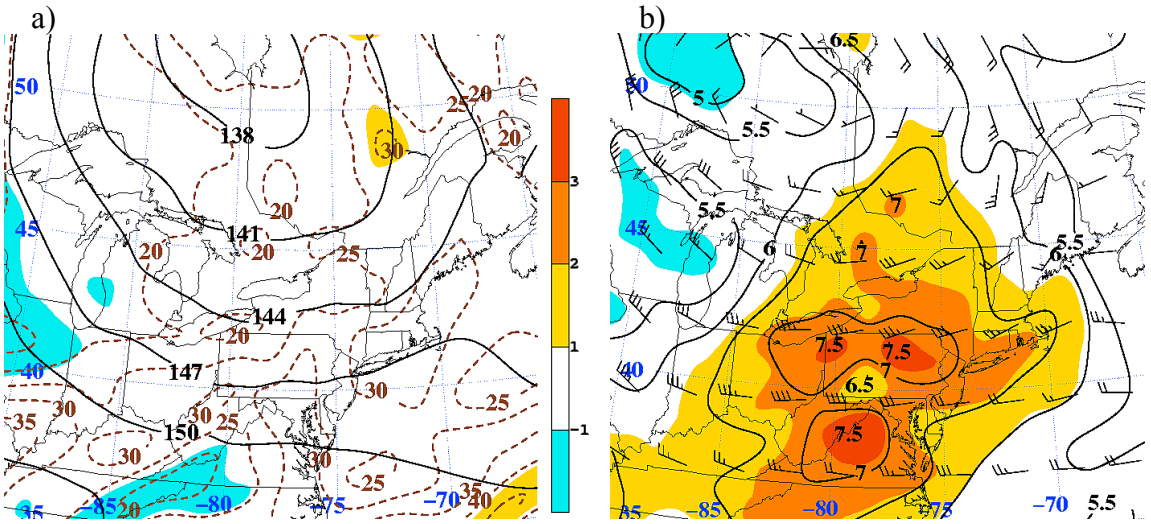

Fig. 5.13. (a) 700-hPa geopotential height contoured every 3 dam in black, PWAT contoured in dashed brown every 5 mm, and standardized PWAT anomalies shaded every 1 SD according to the color bar at 1800 UTC 16 June 2008. (b) 850–500-hPa lapse rate contoured every 0.5 °C km^{-1} in black and standardized anomalies of 850–500-hPa lapse rate shaded every 1 SD according to the color bar at 1800 UTC 16 June 2008.

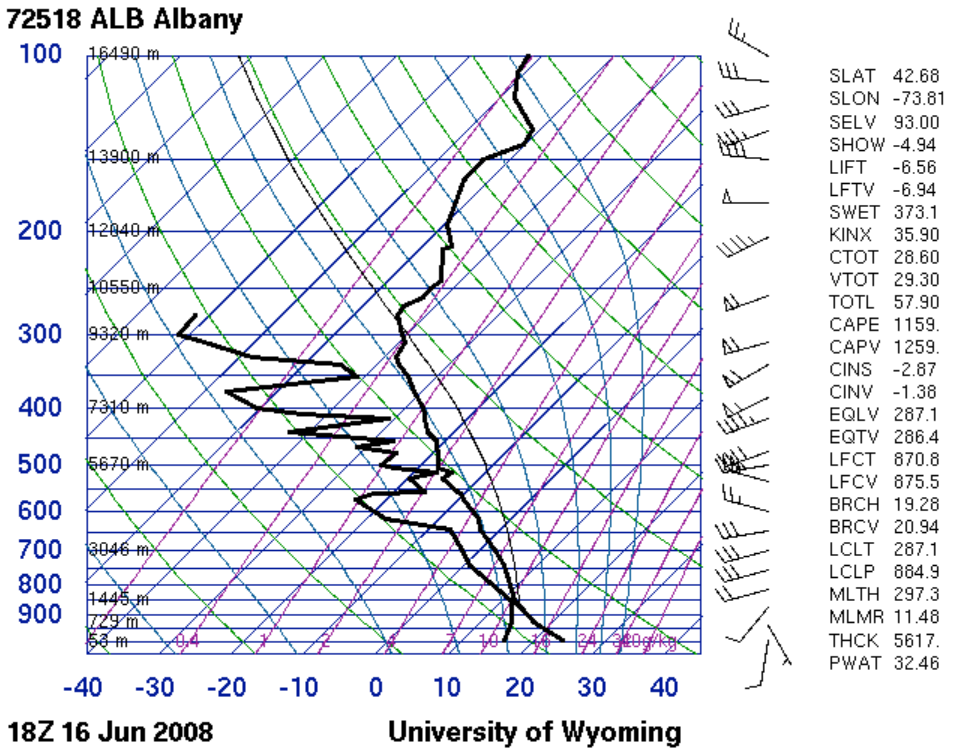

Fig. 5.14. Sounding for ALB at 1800 UTC 16 June 2008.

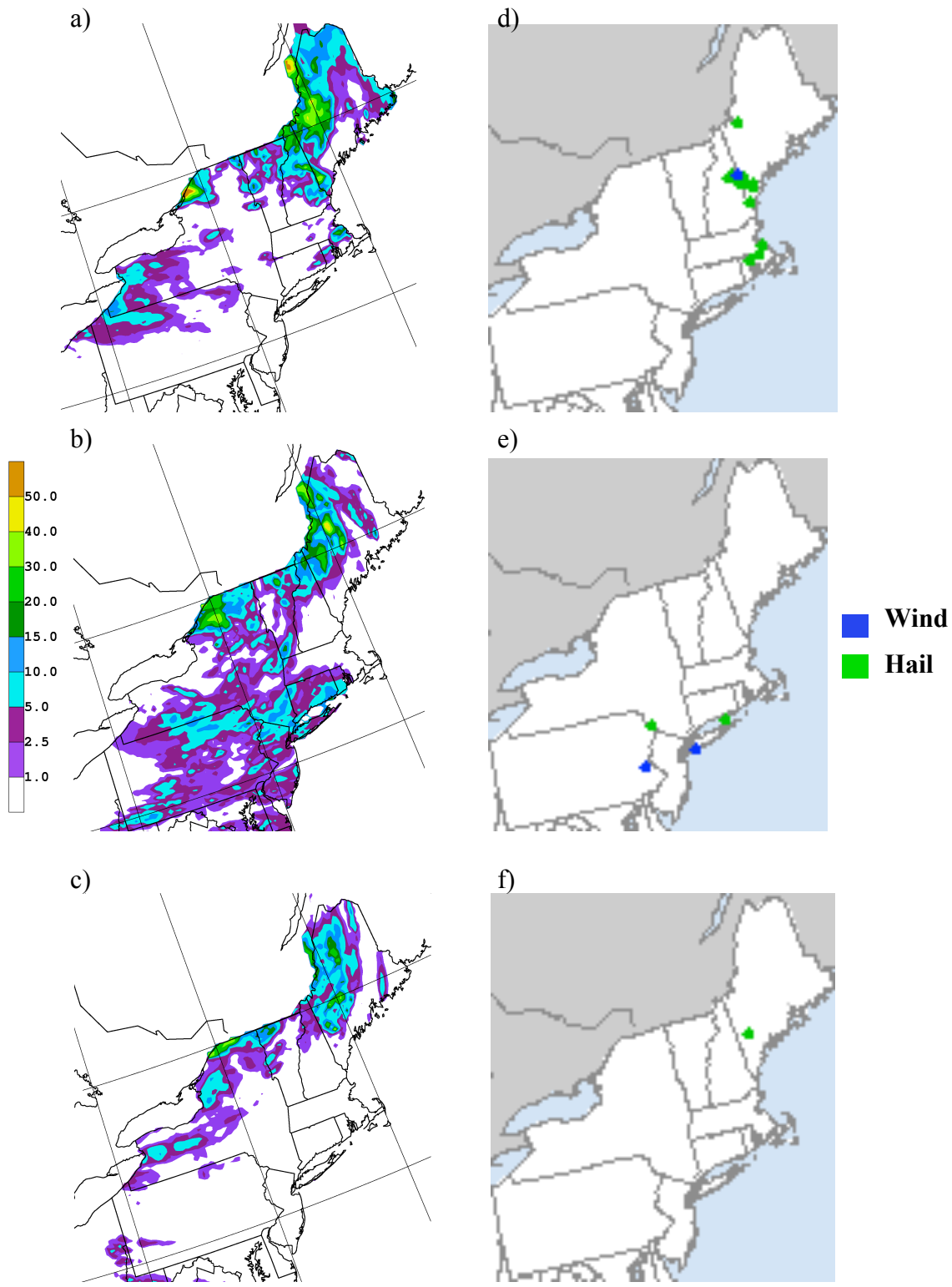

Fig. 5.15. National Precipitation Verification Unit 1-day Quantitative Precipitation Estimates (mm) ending at (a) 1200 UTC 18 June 2008, (b) 1200 UTC 19 June 2008, and (c) 1200 UTC 20 June 2008. SPC severe storm reports for (d) 17 June 2008, (e) 18 June 2008, and (f) 19 June 2008.

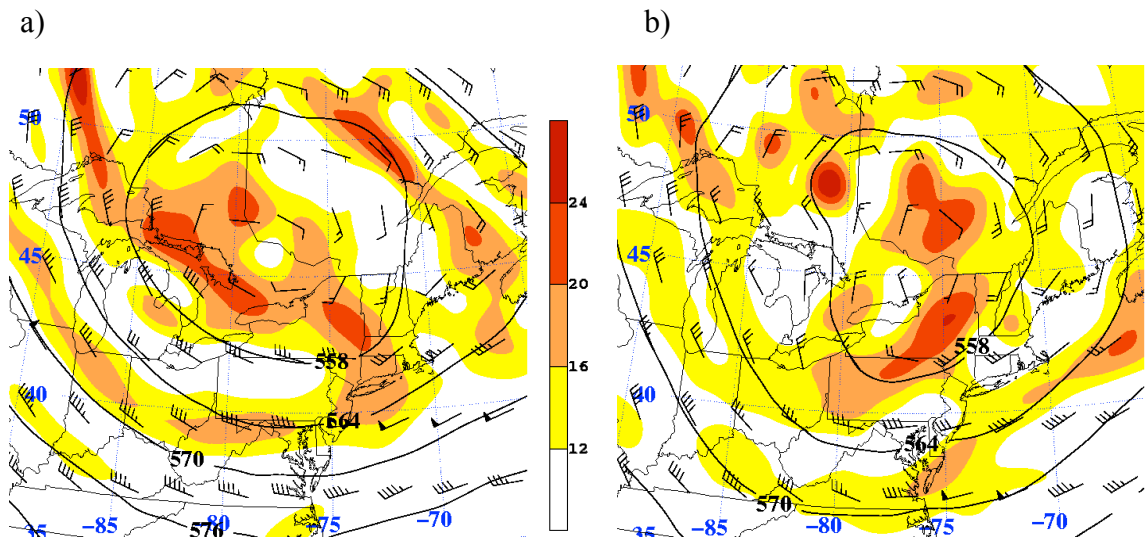

Fig. 5.16. As in Fig. 5.7 but at (a) 0000 UTC 18 June 2008 and (b) 0000 UTC 19 June 2008.

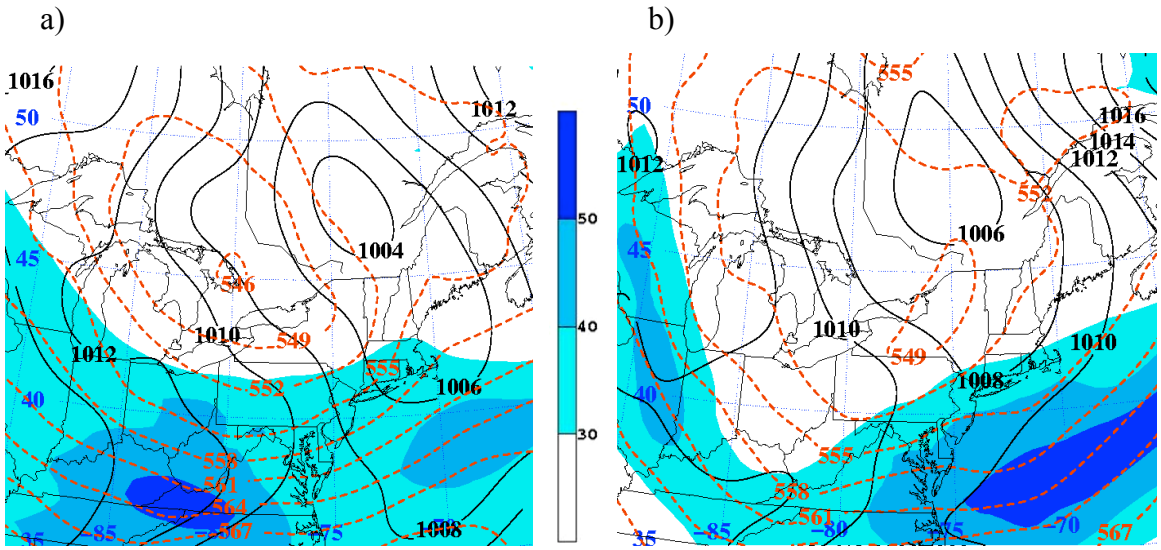

Fig. 5.17. As in Fig. 5.8 but at (a) 0000 UTC 18 June 2008 and (b) 0000 UTC 19 June 2008.

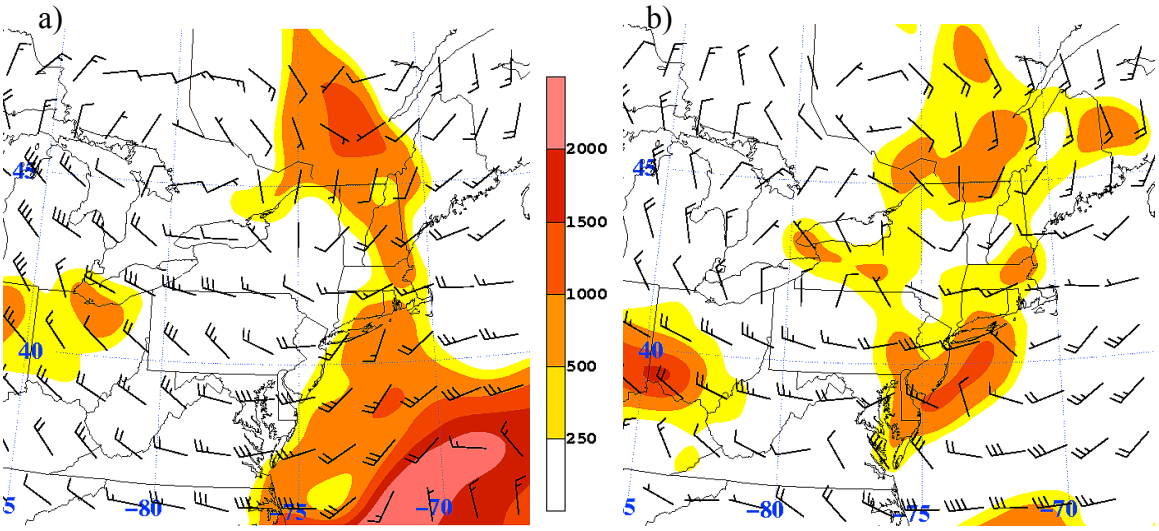

Fig. 5.18. As in Fig. 5.10 but at (a) 0000 UTC 18 June 2008 and (b) 0000 UTC 19 June 2008.

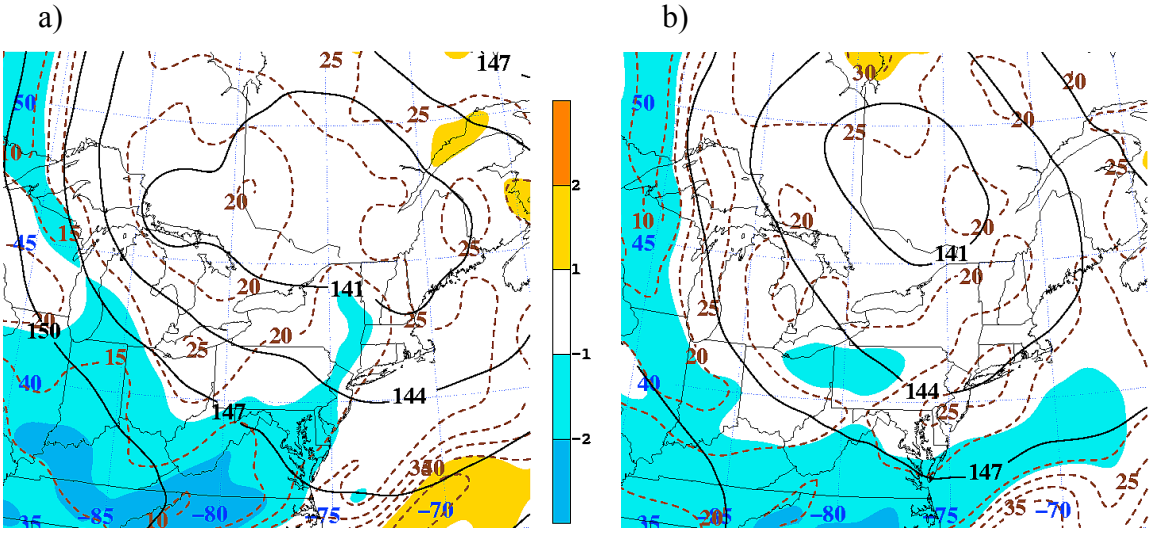

Fig. 5.19. As in Fig. 5.13a but at (a) 0000 UTC 18 June 2008 and (b) 0000 UTC 19 June 2008.

a)

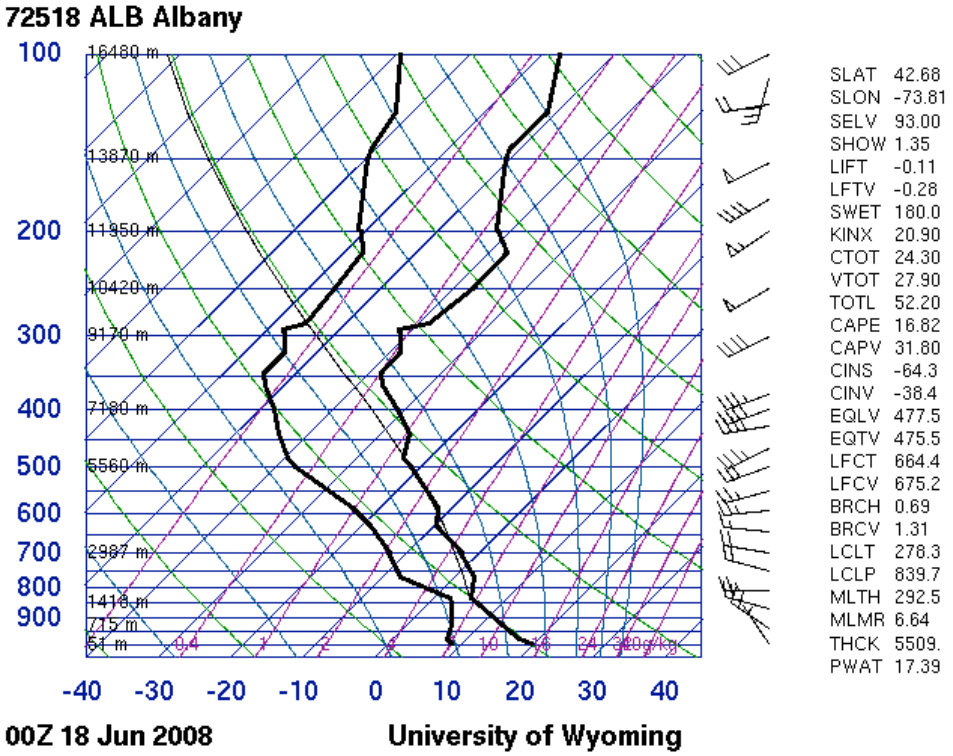

b)

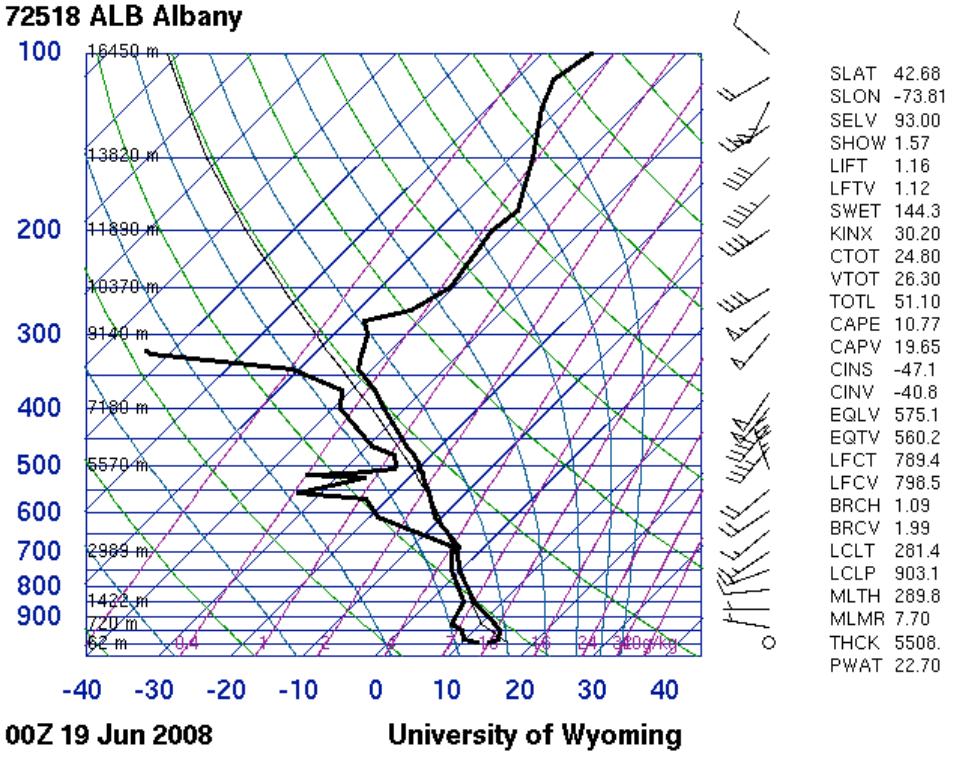

Figs. 5.20a–b. Soundings for ALB at (a) 0000 UTC 18 June 2008 and (b) 0000 UTC 19 June 2008.

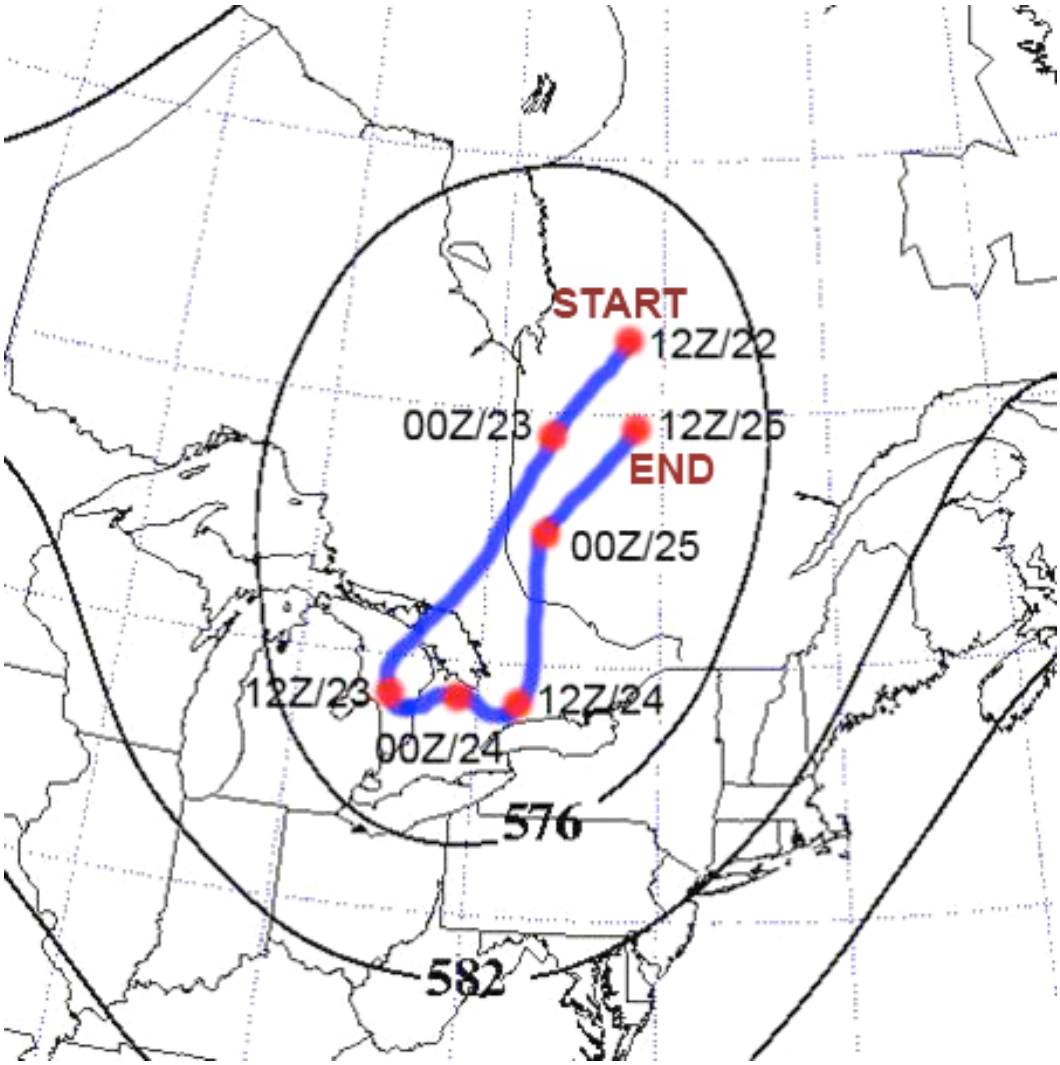

Fig. 5.21. Mean 500-hPa geopotential height (dam) and track of 500-hPa cutoff cyclone center for 1200 UTC 22 July–1200 UTC 25 July 2008.

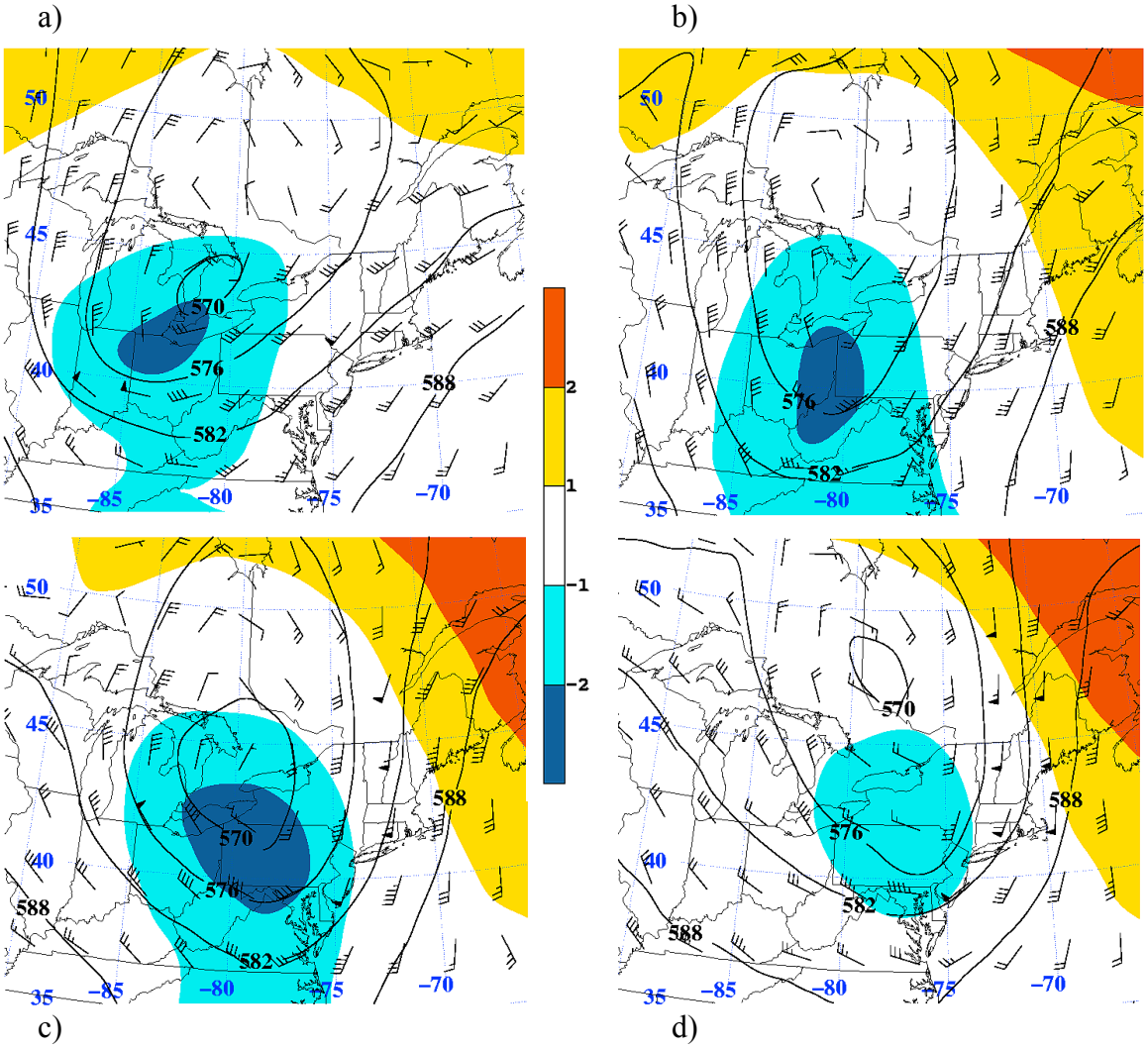

Fig. 5.22. As in Fig. 5.2 but at (a) 1200 UTC 23 July 2008, (b) 0000 UTC 24 July 2008, (c) 1200 UTC 24 July 2008, and (d) 0000 UTC 25 July 2008.

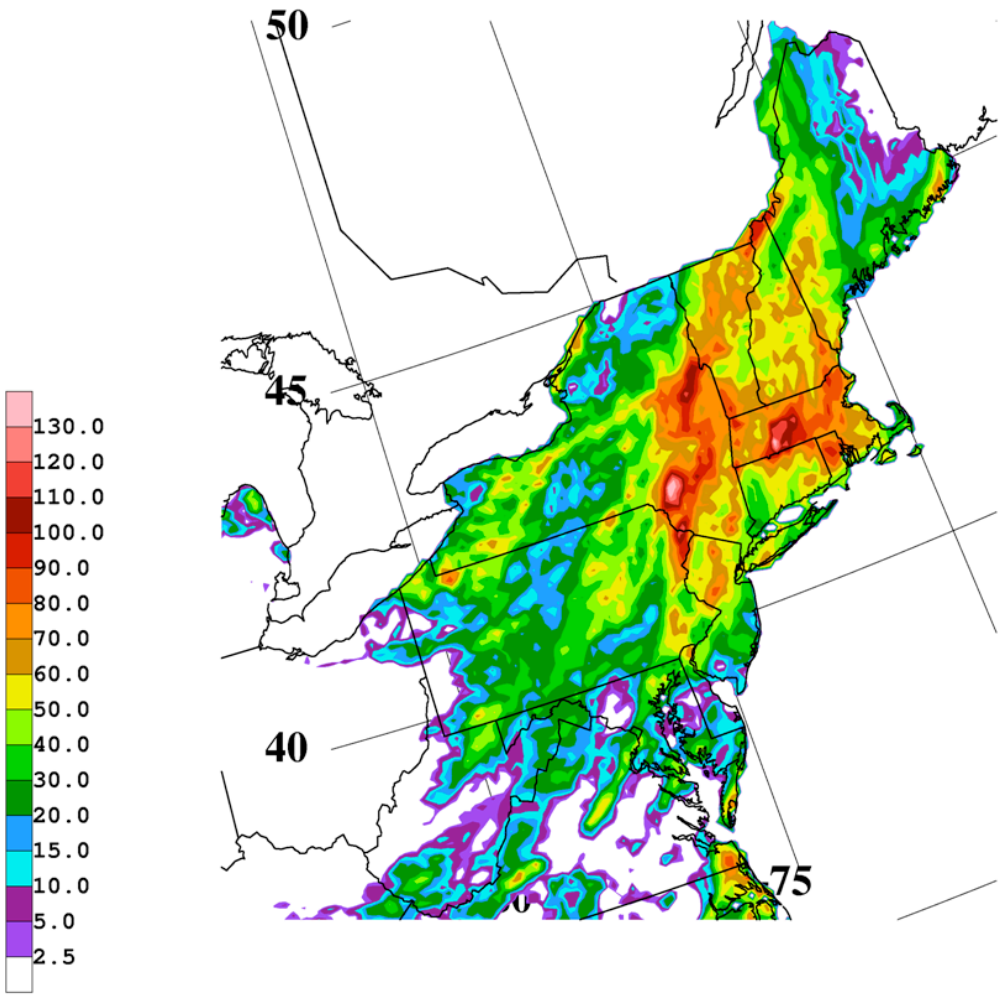

Fig. 5.23. National Precipitation Verification Unit 3-day Quantitative Precipitation Estimates (mm) ending at 1200 UTC 25 July 2008.

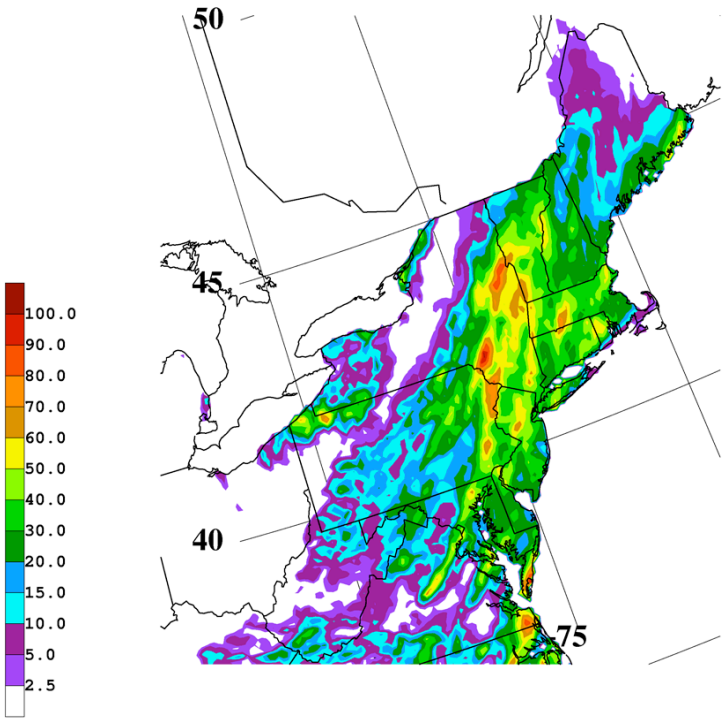

Fig. 5.24. National Precipitation Verification Unit 1-day Quantitative Precipitation Estimates (mm) ending at 1200 UTC 24 July 2008.

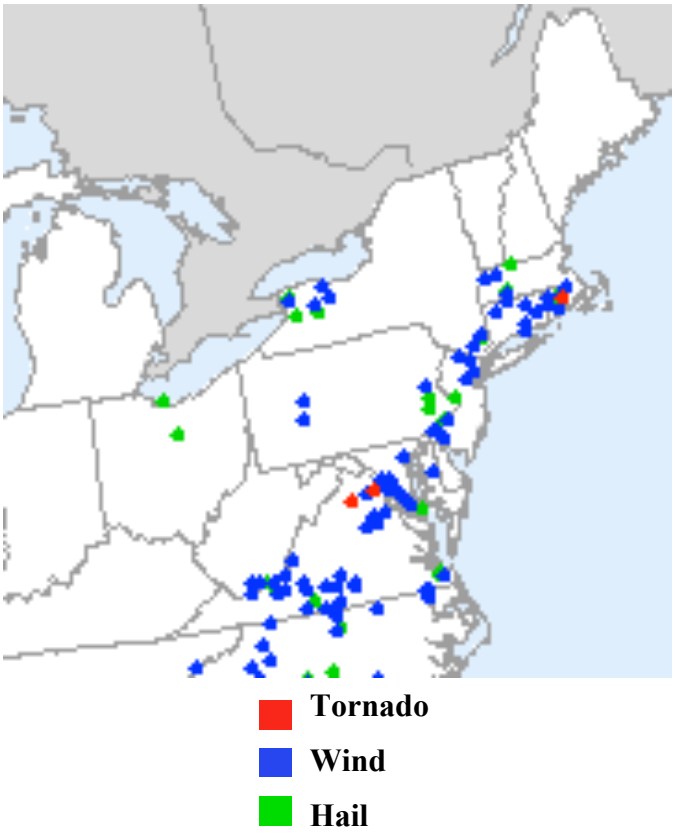

Fig. 5.25. SPC severe storm reports for 23 July 2008.

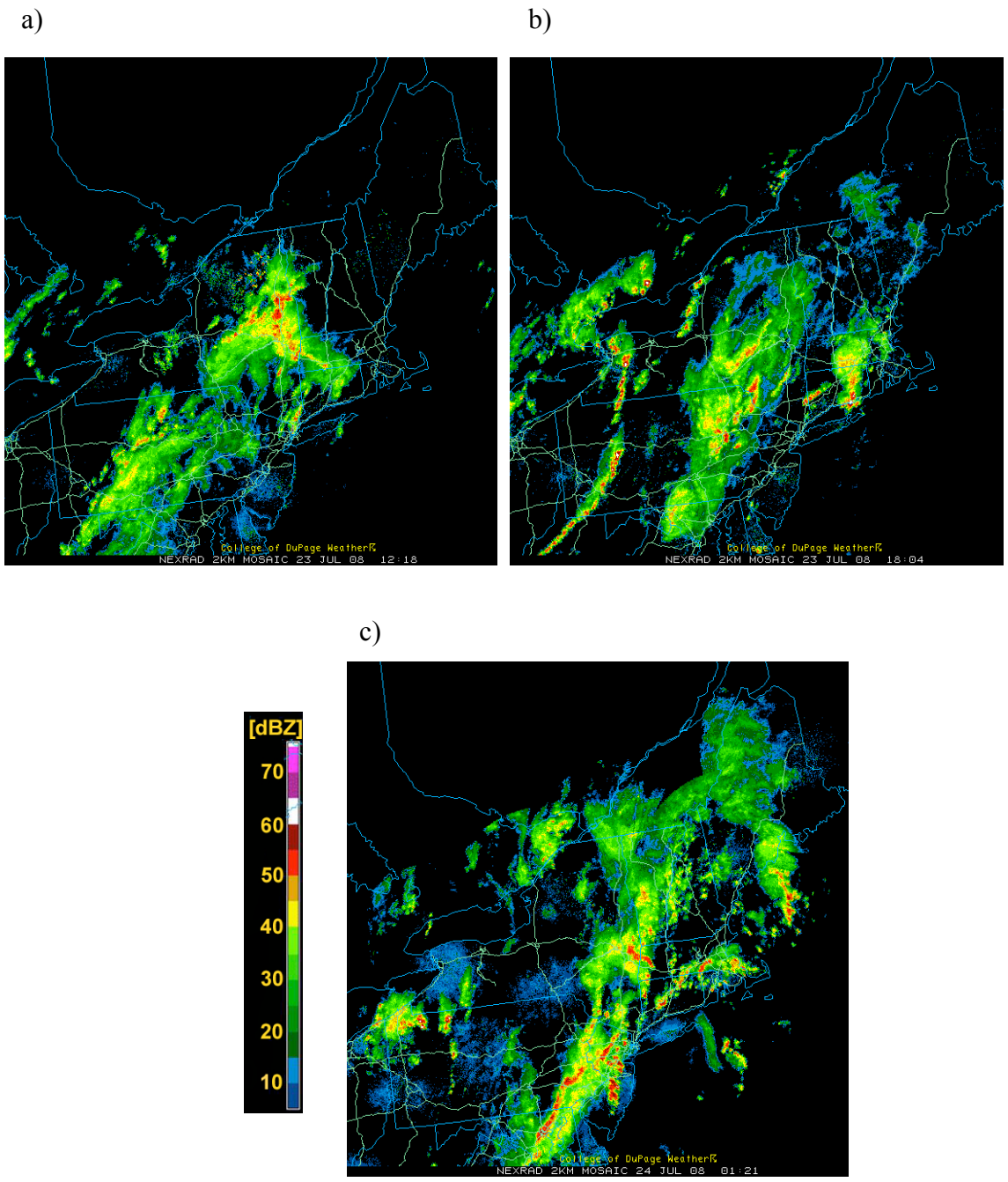

Fig. 5.26. NEXRAD base reflectivity shaded according to the color bar every 5 dB*Z* at (a) 1218 UTC 23 July 2008, (b) 1804 UTC 23 July 2008, and (c) 0121 UTC 24 July 2008.

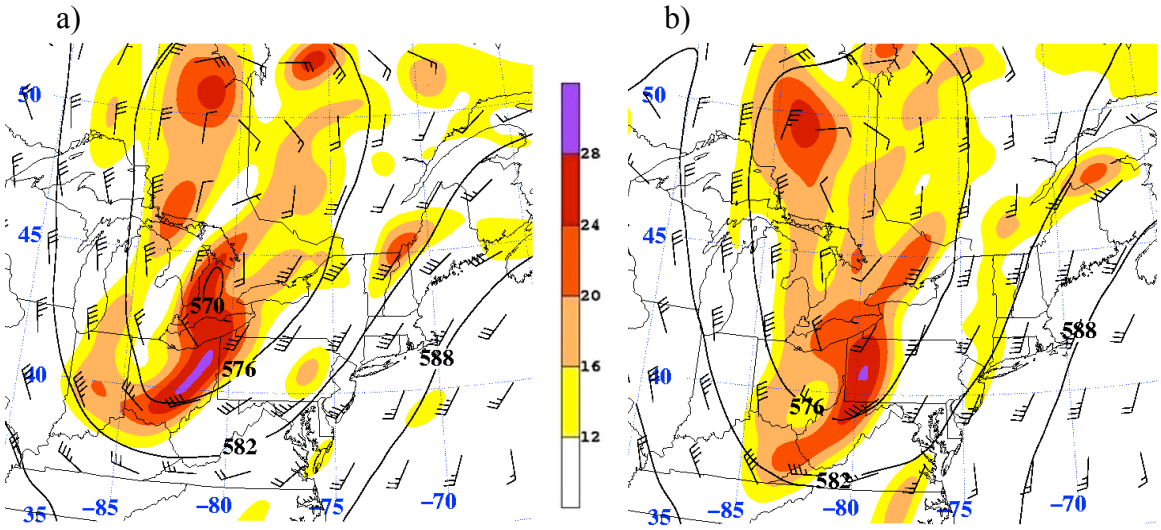

Fig. 5.27. As in Fig. 5.7 but at (a) 1800 UTC 23 July 2008 and (b) 0000 UTC 24 July 2008.

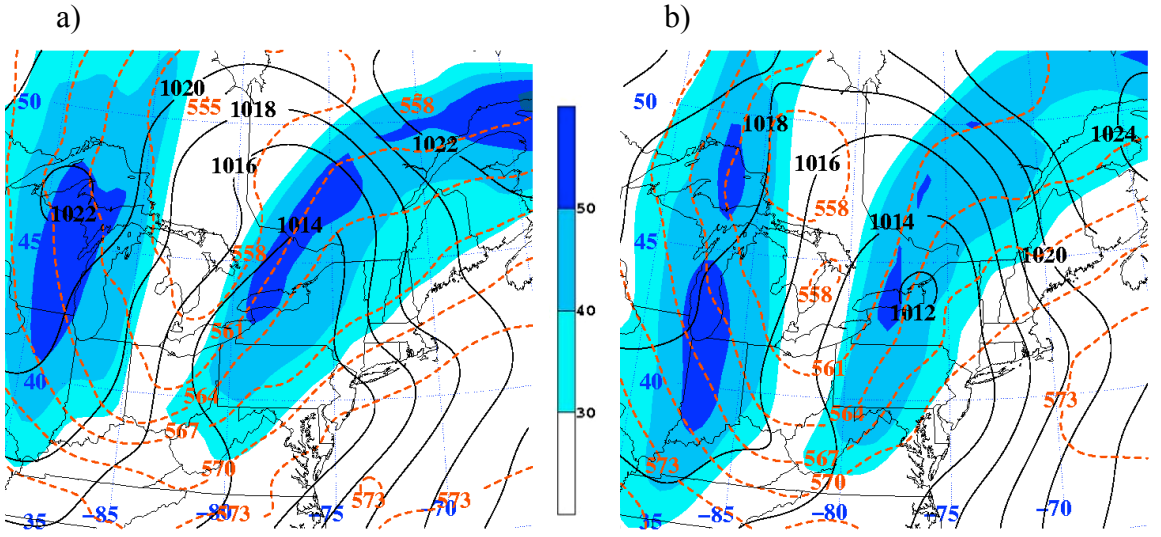

Fig. 5.28. SLP contoured every 2 hPa in black, 1000–500-hPa thickness contoured every 3 dam in dashed orange, and 250-hPa wind speed shaded according to the color bar every 10 m s^{-1} for values above 30 m s^{-1} at (a) 1800 UTC 23 July 2008 and (b) 0000 UTC 24 July 2008.

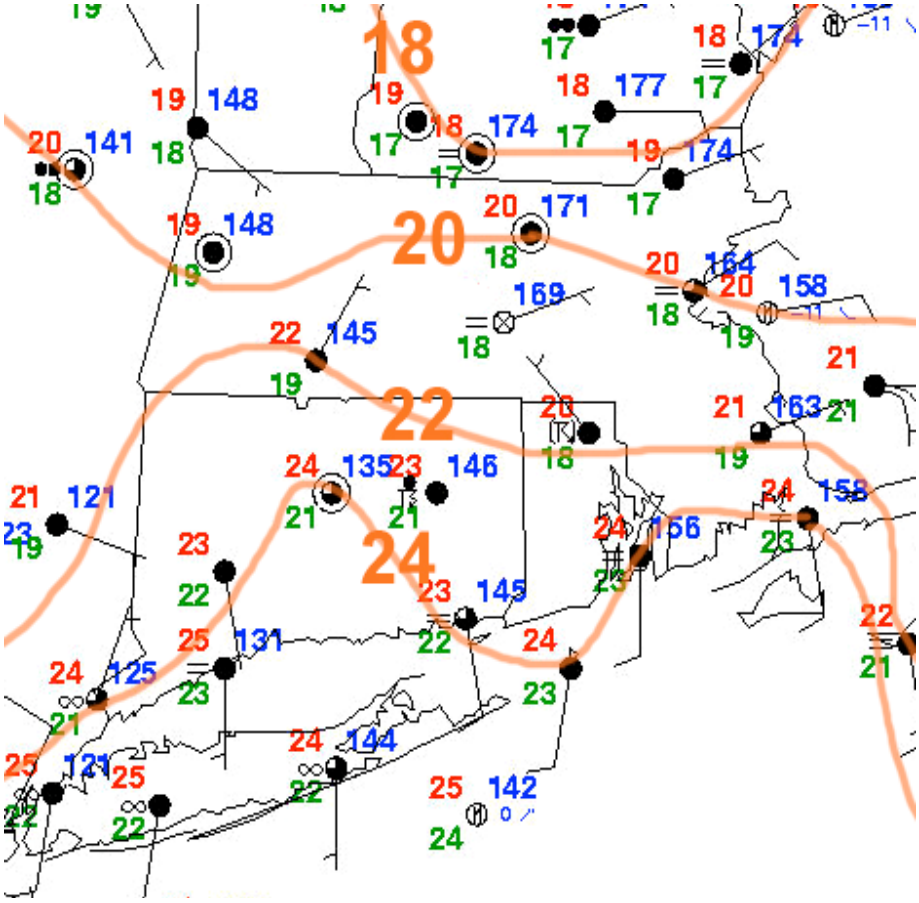

Fig. 5.29. Surface station plot with temperature contoured in orange every 2°C at 0100 UTC 24 July 2008.

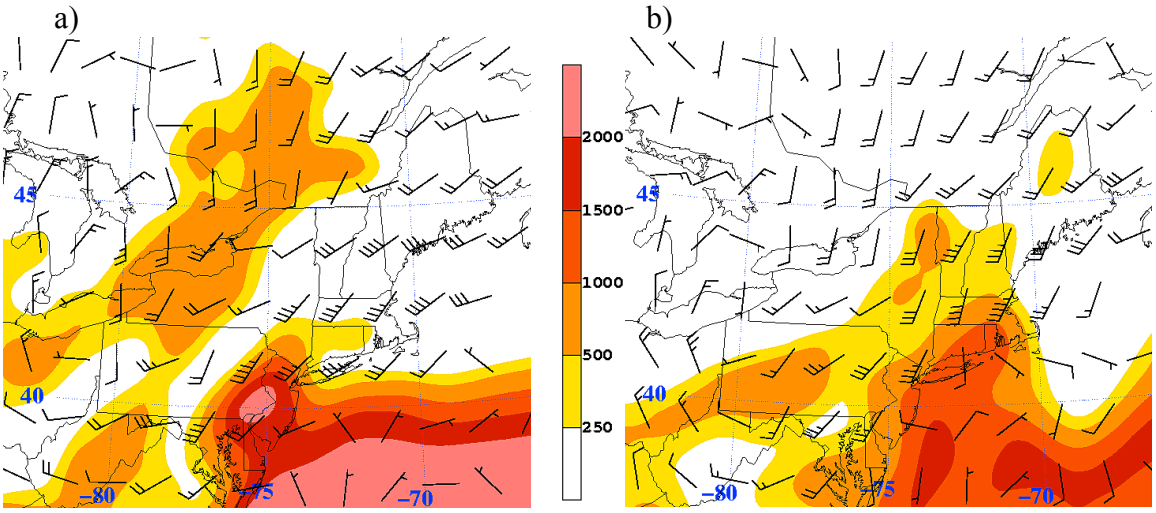

Fig. 5.30. 1000–700-hPa wind shear (barbs) and CAPE (J kg^{-1}) shaded according to the color bar every 250 J kg^{-1} for values below 500 J kg^{-1} and every 500 J kg^{-1} for values above 500 J kg^{-1} at (a) 1800 UTC 23 July 2008 and (b) 0000 UTC 24 July 2008.

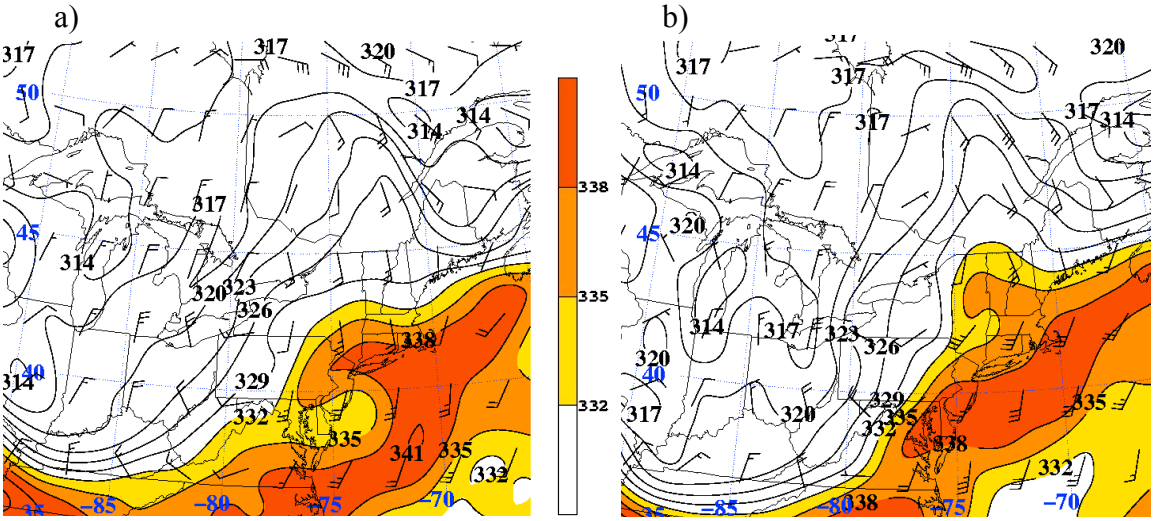

Fig. 5.31. 850-hPa wind (kt) and θ_e contoured every 3 K and shaded according to the color bar every 3 K for values above 332 K at (a) 1800 UTC 23 July 2008 and (b) 0000 UTC 24 July 2008.

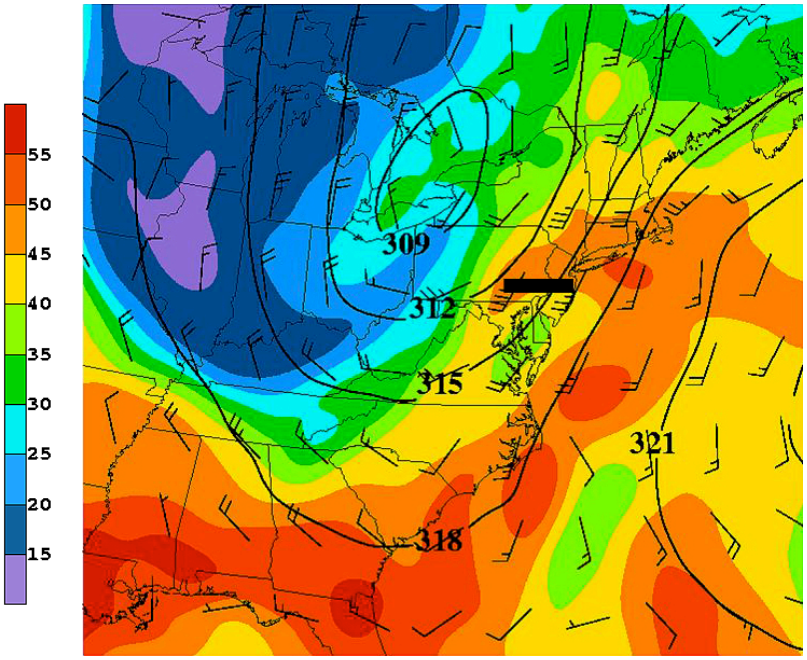

Fig. 5.32. 700-hPa geopotential height contoured every 3 dam, wind (kt), and PWAT shaded according to the color bar every 5 mm for values above 15 mm at 1800 UTC 23 July 2008. Dark solid line shows orientation of cross section in Fig. 5.33.

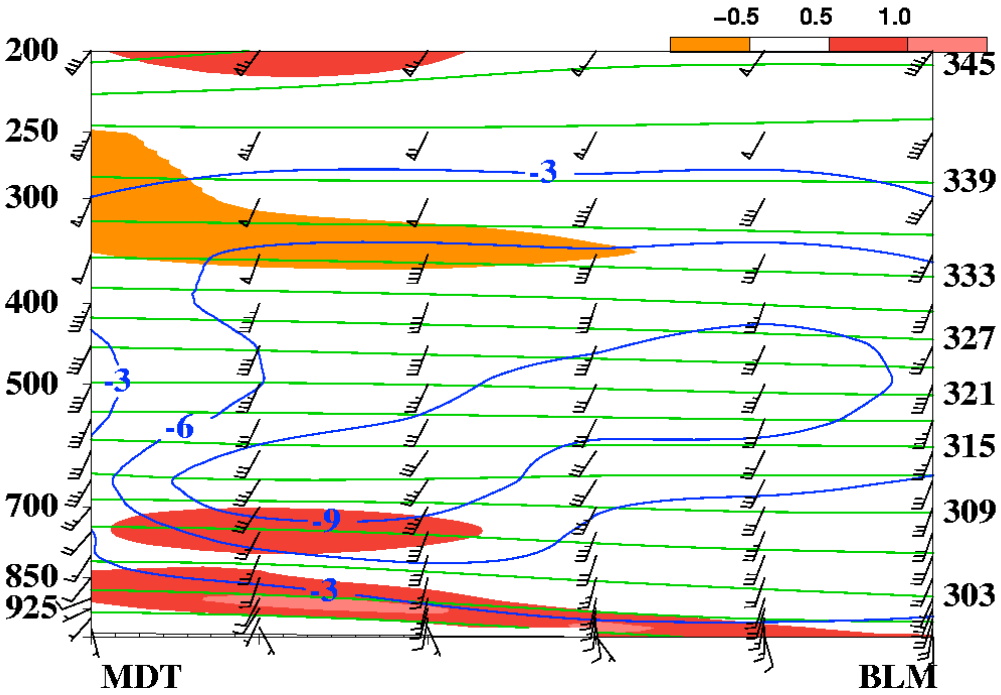

Fig. 5.33. Cross section at 1800 UTC 23 July 2008 from Harrisburg, Pennsylvania (MDT), to Belmar/Farmdale, New Jersey (BLM) (dark solid line in Fig. 5.32), showing frontogenesis [shaded according to the color bar every 0.5 K (100 km)$^{-1}$ (3 h)$^{-1}$], potential temperature (green lines, contoured every 3 K), vertical velocity (blue lines, contoured every 3 × 10^{-3} hPa s^{-1}), and wind (barbs).

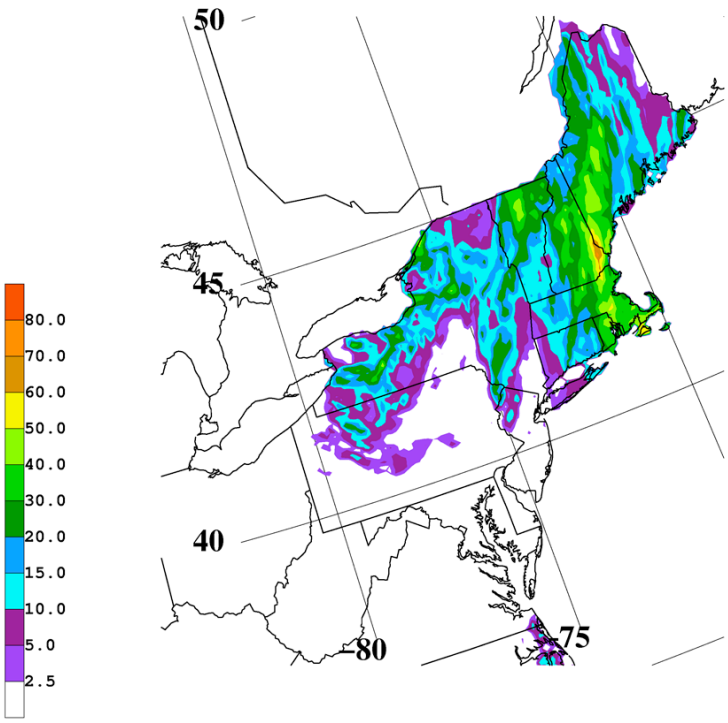

Fig. 5.34. National Precipitation Verification Unit 1-day Quantitative Precipitation Estimates (mm) ending at 1200 UTC 25 July 2008.

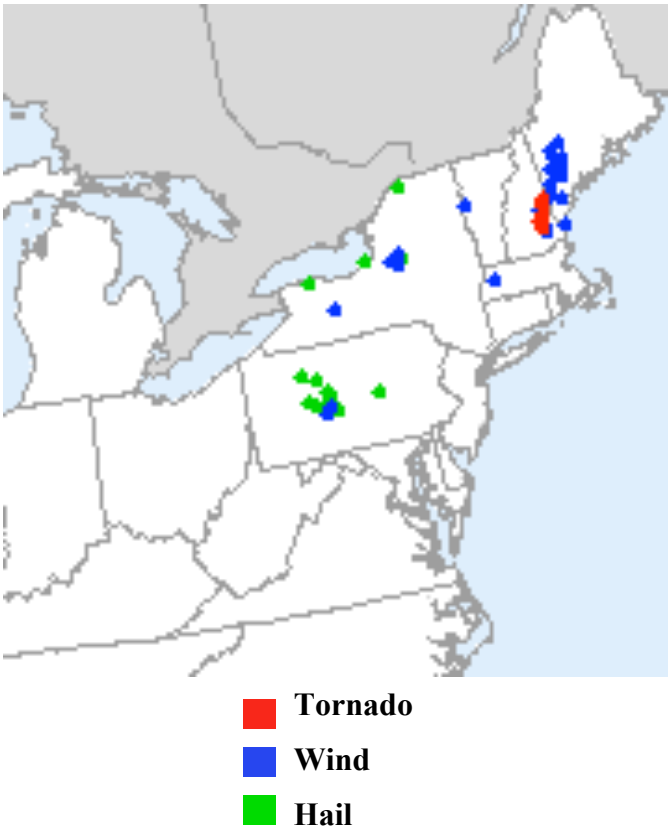

Fig. 5.35. SPC severe storm reports for 24 July 2008.

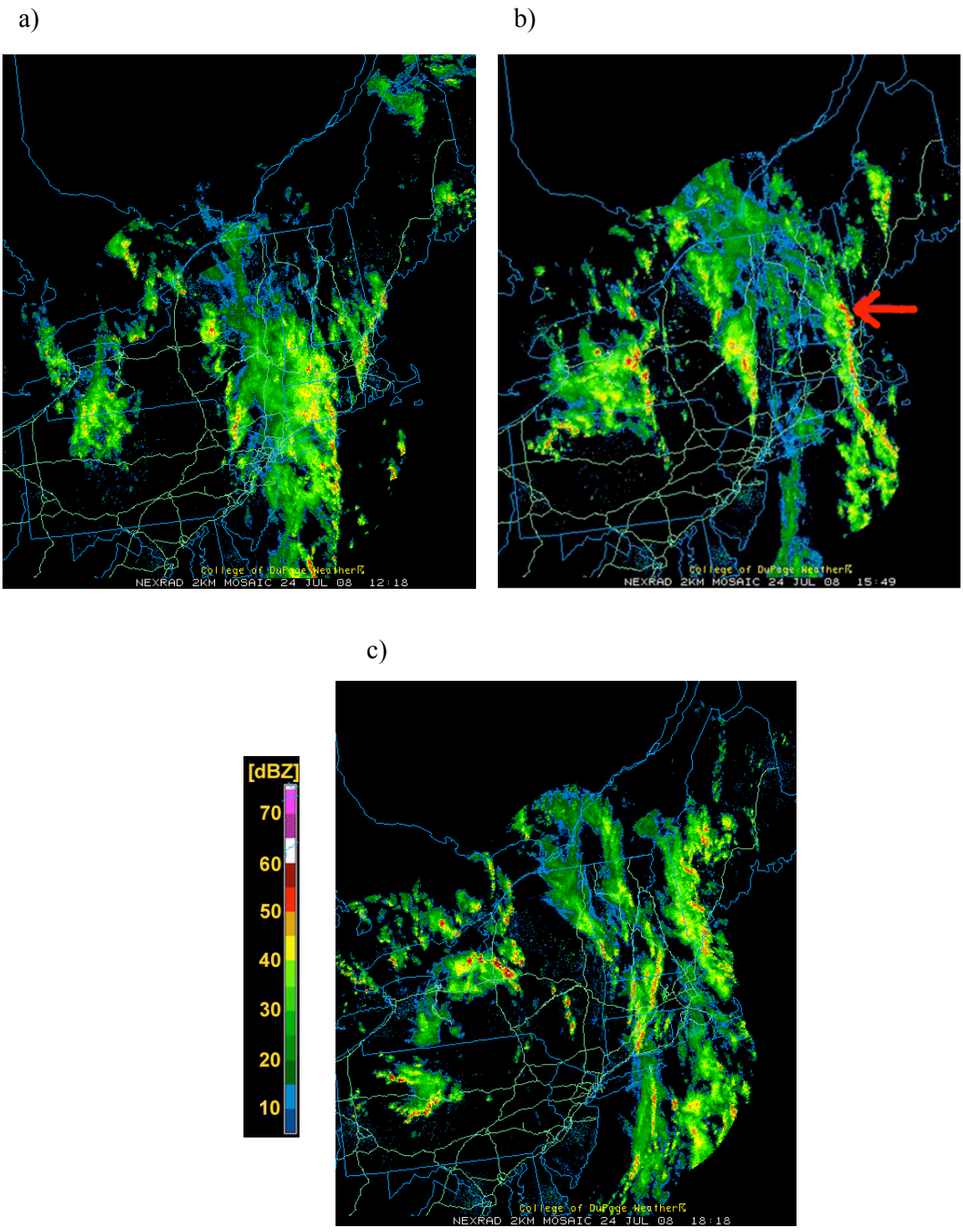

Fig. 5.36. NEXRAD base reflectivity shaded according to the color bar every 5 dB*Z* at (a) 1218 UTC 24 July 2008, (b) 1549 UTC 23 July 2008, and (c) 1818 UTC 24 July 2008. In (b), location of tornado corresponds to tip of red arrow.

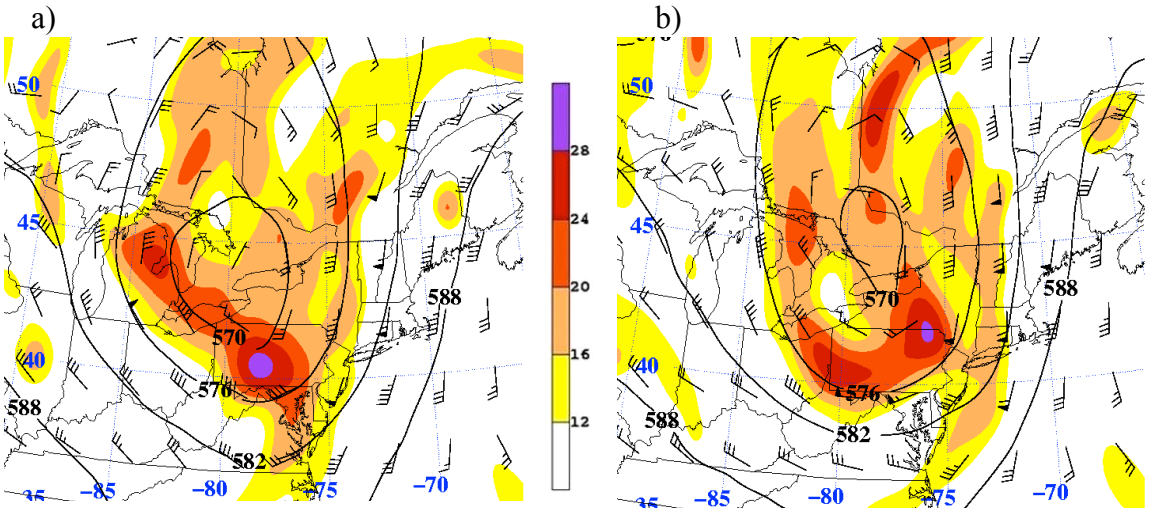

Fig. 5.37. As in Fig. 5.7 but at (a) 1200 UTC 24 July 2008 and (b) 1800 UTC 24 July 2008.

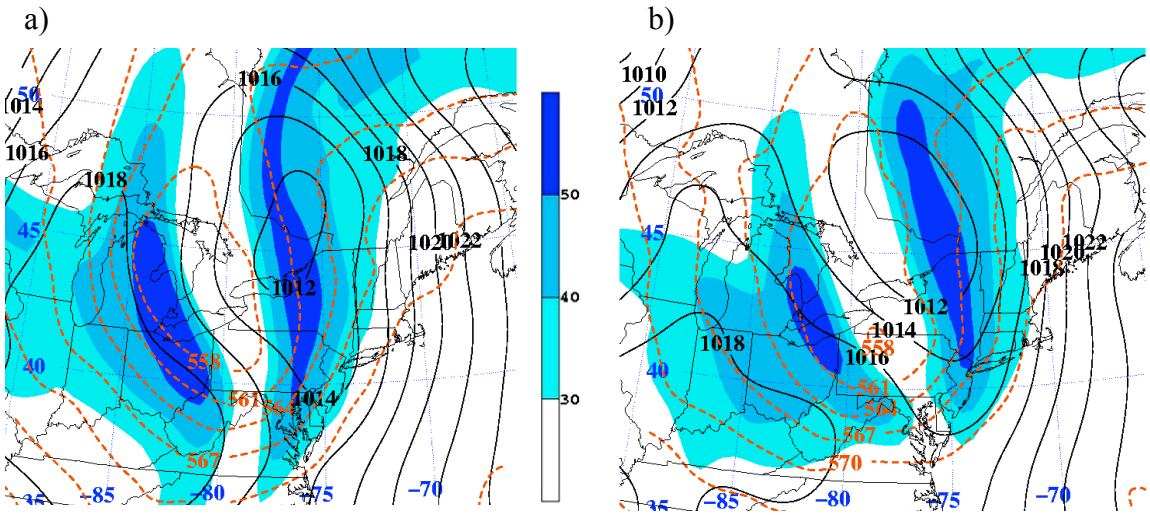

Fig. 5.38. As in Fig. 5.28 but at (a) 1200 UTC 24 July 2008 and (b) 1800 UTC 24 July 2008.

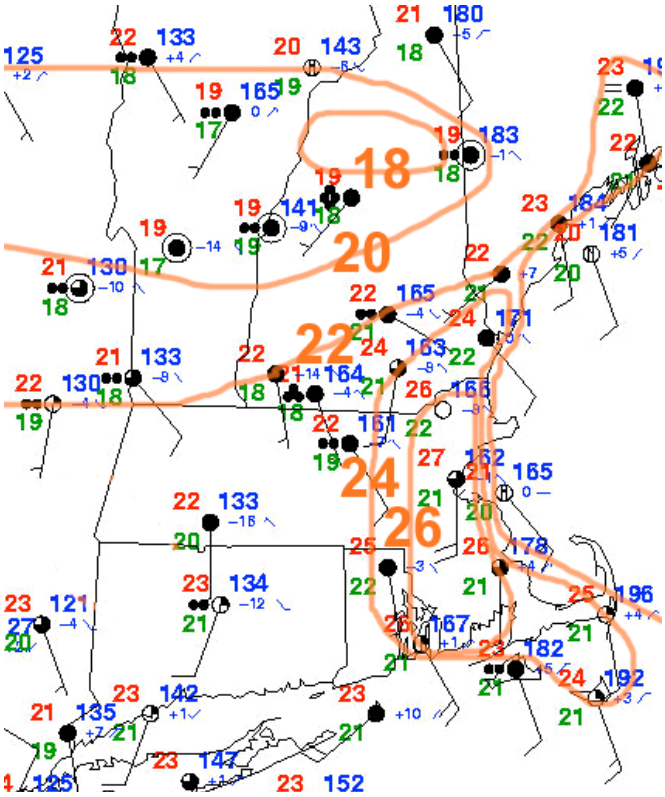

Fig. 5.39. Surface station plot with temperature contoured in orange every 2°C at 1500 UTC 24 July 2008.

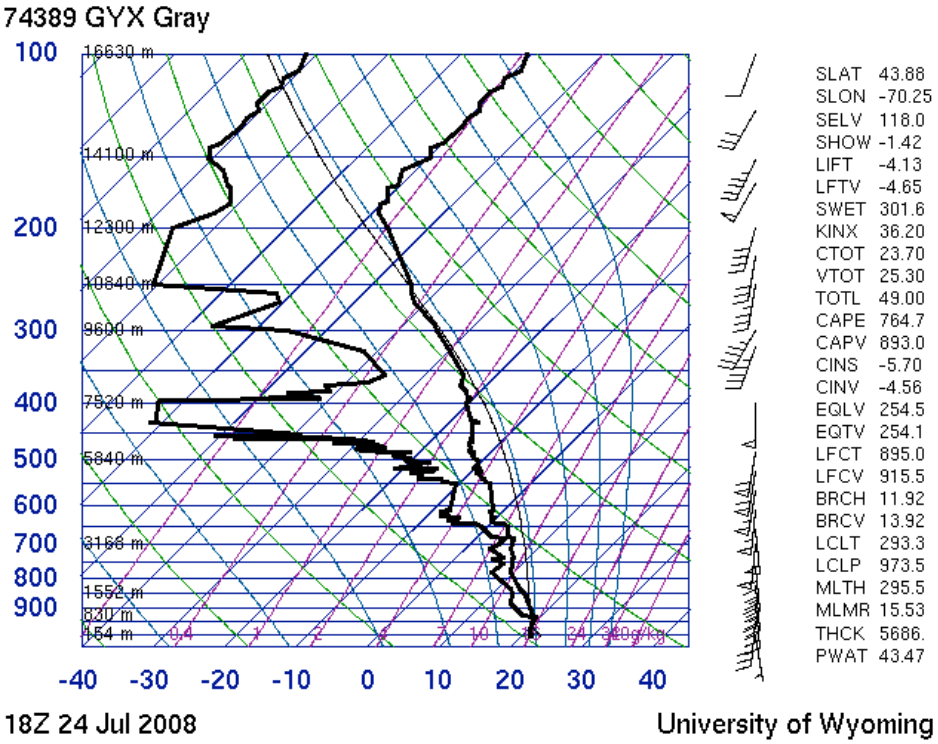

Fig. 5.40. Sounding taken for GYX at 1800 UTC 24 July 2008.

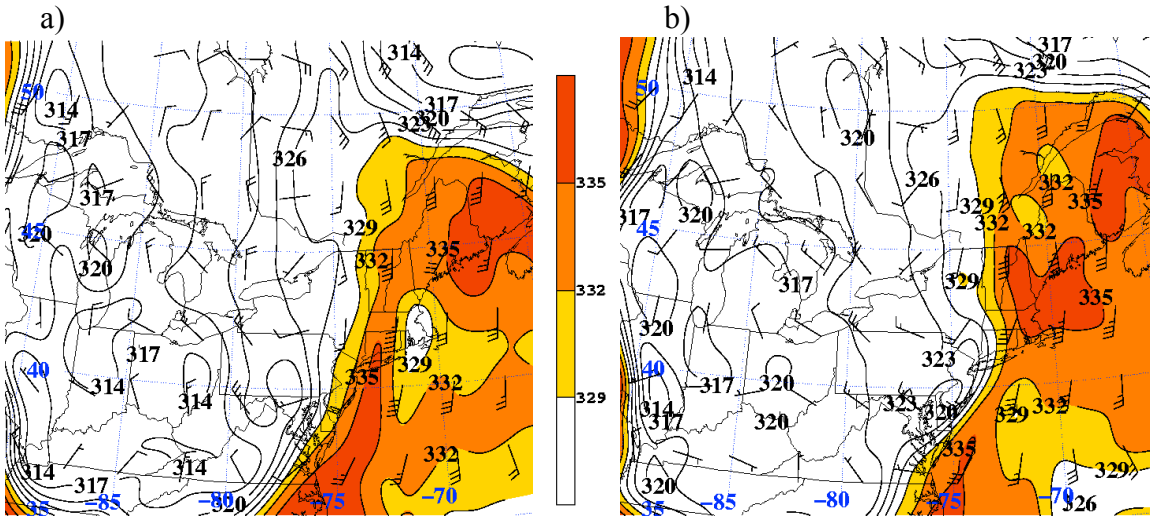

Fig. 5.41. 850-hPa wind (kt) and θ_e contoured every 3 K and shaded according to the color bar every 3 K for values above 329 K at (a) 1200 UTC 24 July 2008 and (b) 1800 UTC 24 July 2008.

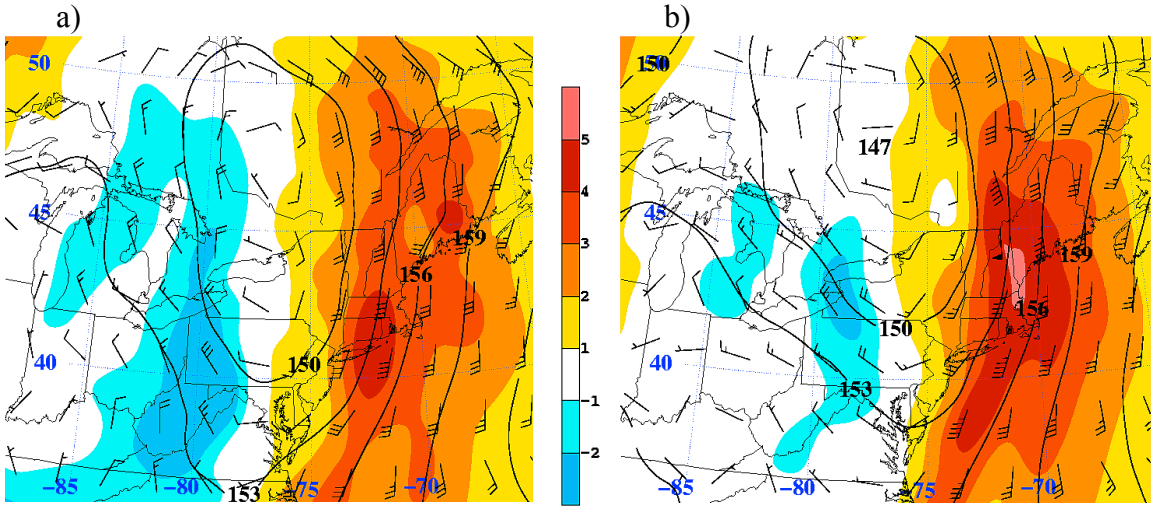

Fig. 5.42. 850-hPa geopotential height contoured every 3 dam, wind (kt), and standardized anomalies of 850-hPa v-wind shaded every 1 SD according to the color bar at (a) 1200 UTC 24 July 2008 and (b) 1800 UTC 24 July 2008.

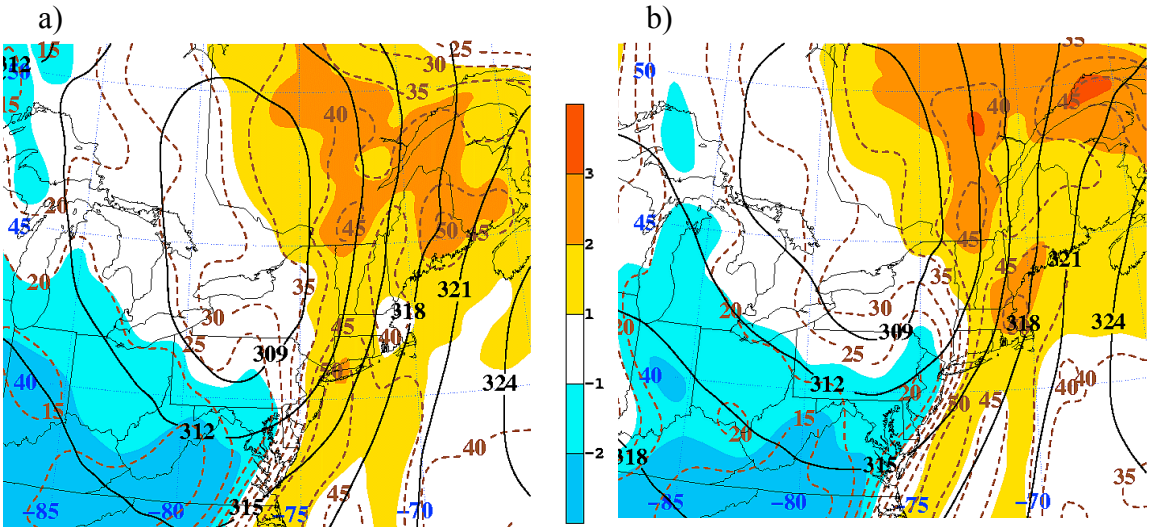

Fig. 5.43. As in Fig. 5.13a but at (a) 1200 UTC 24 July 2008 and (b) 1800 UTC 24 July 2008.

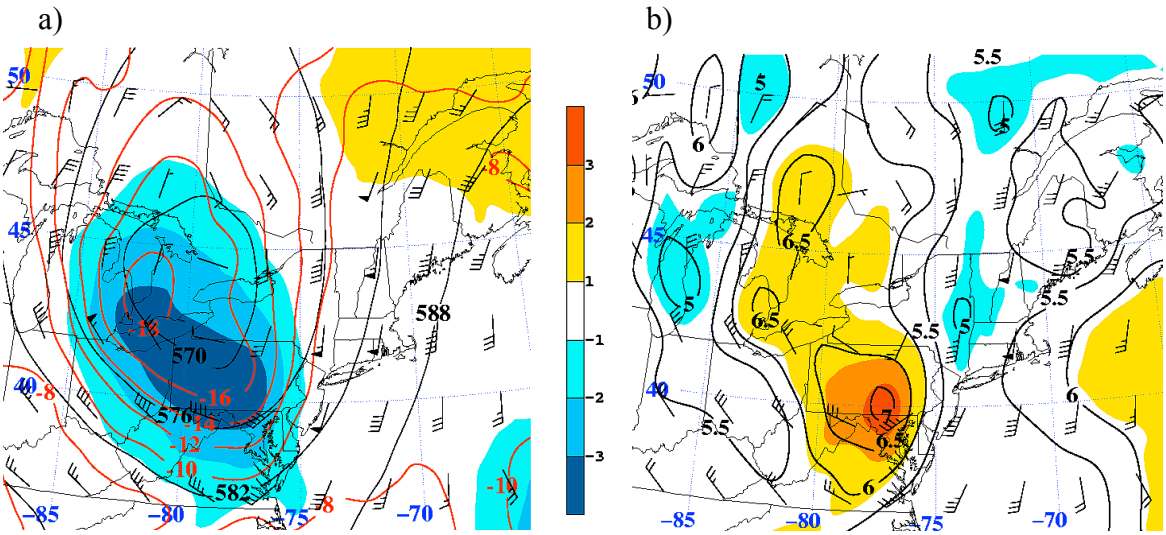

Fig. 5.44. (a) 500-hPa geopotential height contoured every 6 dam in black, 500-hPa temperature contoured every 2°C in red, and standardized anomalies of 500-hPa temperature shaded every 1 SD according to the color bar at 1200 UTC 24 July 2008. (b) 700–500-hPa lapse rate contoured every 0.5 °C km^{-1} in black and standardized anomalies of 700–500-hPa lapse rate shaded every 1 SD according to the color bar at 1200 UTC 24 July 2008.

6. Discussion

6.1 Climatology

The methodology used to identify 500-hPa cutoff cyclones in this study is similar to that used in Smith (2003) (hereafter SM). The difference is that a longer time period for the NCEP–NCAR reanalysis is utilized in the current study (61 years vice 54 years). Note that as an initial accuracy check, the algorithms used in SM were run against those used in BB and PHCM for the same time period, and the results (not shown) were consistent.

6.1.1 Northern Hemisphere

6.1.1a Comparison to Previous Work

The results shown in chapter 3 are consistent with those in SM. Figure 1.8, taken from Fig. 3.2 of SM, shows the total number of cutoff cyclone events per grid point for the NH for 1948–2001. Comparing Fig. 1.8 with Fig. 3.2 of the current study, it is evident that the most favored regions for 500-hPa cutoff cyclones are similar: across the North Pacific, Hudson Bay region, Canadian Maritimes, and southeast of Greenland. There are also weaker maxima in cutoff cyclone activity over the southwestern U.S., near the Iberian Peninsula, and over the Mediterranean Basin.

Figure 6.1, taken from Fig. 3.5 of SM, shows the total number of cutoff cyclone events per grid point for the NH fall for 1948–2001. Comparing Fig. 6.1 with Fig. 3.3, it is apparent that the most favored regions for cutoff cyclone occurrence during the fall are similar; these being the North Pacific, Hudson Bay region, southeast of Greenland, and southern Europe. Comparisons between SM and the current study concerning other seasons (not shown) yield similar results as well. Figure 3.4 shows that the maxima in cutoff cyclone frequency during the winter over the North Pacific and U.S./Canadian Maritimes are shifted slightly equatorwards from their positions in the fall months, which is likely a reflection of the equatorward shift of the mean westerlies into the winter months. Cutoff cyclone activity increases from winter into spring (Fig. 3.5) throughout the majority of NH, especially over the Gulf of Alaska, southwestern U.S., and Turkish Plateau. Parker et al. (1989) noted that cutoff cyclones over the southwestern U.S. frequently occur during the fall, winter, and spring. This high frequency was attributed to strong diffluent upper-level flow across the eastern North Pacific and western North America. The cutoff cyclone freeway from the southwestern U.S. northeastward through the U.S./Canadian Maritimes is most active during the spring. The frequencies of cutoff cyclones for the NH summer (Fig. 3.6) show high levels of activity over the Gulf of Alaska, Hudson Bay, and southeast of Greenland. Cutoff cyclones occur least frequently over the U.S. during the summer than in any other season, as the mean westerlies are positioned farther poleward than in other seasons. Another area with a high frequency of cutoff cyclones is over the Bay of Bengal and eastern Indian subcontinent (Fig. 3.16). Cutoff cyclones here occur primarily during the Asian summer monsoon and are associated with strong sensible and latent heating.

Preferred regions of 500-hPa cutoff cyclone activity over the NH were chosen for further study by SM and in the current research. Fig. 6.2, taken from Fig. 3.11 of SM, shows regional analysis boxes chosen to represent selected areas over the NH where cutoff cyclones are common. Several of these regional analysis boxes, specifically those in and around North America, were redrawn with altered geographic dimensions (Fig. 3.7) to better account for the new frequencies found in the current study. Figure 6.3a, taken from Fig. 3.12c of SM, and Fig. 3.8a represent Gulf of Alaska cutoff cyclone activity. Cutoff cyclones occur more (less) frequently during the warm (cool) season. Qausi-stationary cutoff cyclones also appear to be common throughout the summer. Figure 6.3b, taken from Fig. 3.12d of SM, and Fig. 3.8b represent southwestern U.S. cutoff cyclone activity. A stronger seasonal dependence occurs in this region than in any other area in and around North America. Cutoff cyclones occur most frequently in mid-spring and sharply decline in frequency into the summer, before increasing with the onset of fall. Consistencies between cutoff cyclone frequencies over the Hudson Bay area and U.S./Canadian Maritimes regions between SM and the current study were also evident (not shown).

6.1.1b Discussion of Selected Areas

This section will explain why 500-hPa cutoff cyclone activity is favored more in certain regions of the NH than in others. As mentioned in sec. 3.1, cutoff cyclones frequently occur over the northeastern Asia/Northwest Pacific and Hudson Bay regions, especially during the winter. Figure 6.4 shows a climatological 500-hPa temperature

analysis averaged over December, January, and February, 1968–1996, for the NH. The two aforementioned regions contain some of the coldest 500-hPa temperatures across the NH during the winter, and with the ideas presented in PN (e.g., that cutoff cyclones are isolated pools of cold air with distinct cyclonic motion), it is reasonable to assume that such cold air pools would favorably occur across these two areas.

The Gulf of Alaska is another prominent area of cutoff cyclone activity. The semipermanent Aleutian Low renders this region conducive to storm tracks and cutoff cyclone occurrences. Figure 6.5 shows 250-hPa wind speed averaged for 1968–1996 for the NH. The Gulf of Alaska is located within the poleward-exit region of the mean upper-level jet found across the North Pacific. Thorncroft et al. (1993) noted that the poleward exit region of the mean jet is an area favorable for cutoff cyclone development associated with the LC2 life cycle. The LC2 life cycle involves cyclonic wrapping of PV and may lead to the formation of bombs, as seen, e.g., in Sanders and Gyakum (1980) and Konrad and Colucci (1998). Other areas where cutoff cyclones frequently occur, including near the Canadian Maritimes and southeast of Greenland, are also poleward of a mean upper-level jet (Fig. 6.5) and exhibit cutoff cyclone development through the LC2 life cycle.

Figure 3.8b shows that cutoff cyclones across the southwestern U.S. commonly occur during the fall, winter, and spring. The cutoff cyclones in this area are generally associated with the LC1 life cycle as described in Thorncroft et al. (1993). The LC1 life cycle is associated with anticyclonic wave breaking and the formation of a high-PV tail (Hoskins et al. 1985) that can stretch well southward and may lead to cutoff cyclone development. Cutoff cyclone formation over the southwestern U.S. is favored in

response to LC1 anticyclonic wave breaking events over the eastern North Pacific that result in deep troughs digging southward over western North America. Bell and Bosart (1994) noted that strong amplification of an upstream upper-level ridge occurred one-to-two days prior to cutoff cyclone development over the southwestern U.S. Subsequently, these southwestern U.S. cutoff cyclones typically move northeastward along the cutoff cyclone freeway shown in Fig. 3.17. During the NH summer (Fig. 3.6), the southwestern U.S. maximum and cutoff cyclone freeway are absent as ridges dominate aloft and storm tracks are confined to the north. The LC1 life cycle and associated cutoff cyclone development also occurs near the Iberian Peninsula (Thorncroft et al. 1993). Figure 6.5 shows that the southwestern U.S. and Iberian Peninsula regions are in locations between the exit and entrance regions of two mean jets, which may favor large-scale deformation flow and associated cutoff cyclone development.

As discussed in sec. 1.2, orography influences cutoff cyclone distributions. For example, a cutoff cyclone frequency minimum is found just north of and over the Alps, while a maximum exists to the south over Italy (Fig. 3.2). A midlevel cyclone can develop and possibly become a cutoff cyclone south of the Alps due to vortex stretching and associated generation of a cyclonic circulation. Cutoff cyclone formation south of the Alps also was noted by Bell and Bosart (1994) to occur in association with upstream ridge amplification. Additional areas across the NH where terrain-induced cutoff cyclogenesis may occur include the Gulf of Alaska and southeast of Greenland. The Gulf of Alaska is separated from the mainlands to the north and east by mountain ranges, which keep deep cold pools trapped over the Gulf of Alaska. The idealized model simulations performed by Doyle and Shapiro (1999) showed that cutoff cyclones develop

near the southern tip of Greenland in response to an orographically induced jet. Klein and Heinemann (2002) found that cyclones can form near the southeastern coast of Greenland due to cyclonic vorticity generation through vortex stretching as katabatic flow descends towards the Atlantic Ocean.

6.1.2 Southern Hemisphere

6.1.2a Comparison to Previous Work

The results presented in chapter 3 regarding 500-hPa cutoff cyclone frequencies for the SH are consistent with those in SM. Figure 6.6, taken from Fig. 3.24 of SM, shows the total number of cutoff cyclone events per grid point for the SH for 1948–2001. Comparing Fig. 6.6 with Fig. 3.10, it is evident that the most favored regions for cutoff cyclones are similar: near the Lars Christensen Coast (65°E) and along a 15°-latitude-wide band surrounding Antarctica from 20°W through 120°E longitude. Weaker maxima are found near the Mawson Peninsula (155°E) and the Ross Sea (170°W). Comparisons between SM and the current study concerning seasonal cutoff cyclone frequencies (not shown) display similar results as well.

6.1.2b Discussion of Selected Areas

As mentioned in sec. 3.2, 500-hPa cutoff cyclones frequently occur along a wide ring surrounding the Antarctic mainland, especially from 20°W through 120°E longitude.

Figure 6.7 shows the climatological 250-hPa wind speed for 1968–1996 for the SH. Jet entrance regions are found east of Argentina, southwest of South Africa, and just east of Australia. The frequencies revealed in Fig. 3.10 show that cutoff cyclones occur preferentially poleward of mean jet entrance regions in the SH. These areas include the Bellingshausen and Weddell Seas, directly south of Africa and just north of Antarctica, and between Australia and New Zealand. Cutoff cyclones over eastern Australia and New Zealand commonly form in association with a blocking regime (e.g., Kerr 1953; van Loon 1956). The high level of cutoff cyclone frequency stretching eastwards from New Zealand to 140°W (Fig. 3.10) occurs in conjunction with an active South Pacific storm track. This storm track was noted in Hoskins and Hodges (2005), who applied a feature-tracking technique to the European Centre for Medium-Range Weather Forecasts (ECMWF) Re-Analysis (ERA-40). Trenberth (1991) also noted the importance of the SH upper-level polar jet position on storm track tendencies. Figure 6.7 shows that jet exit regions are located northeast of New Zealand and well southwest of Australia. As in jet entrance regions, cutoff cyclones occur preferentially poleward of jet exit regions. Jet exit development can be associated with the LC2 life cycle of cyclonic wrapping of PV (Thorncroft et al. 1993).

Not all cutoff cyclone formation across the SH is entirely related to upper-level jets. Several maxima in cutoff cyclone activity over the higher latitudes of the SH are generally found over the ocean and close to coasts. Cutoff cyclone frequency maxima are found both southwest and southeast of the South American and African mainlands. Thermal gradients between the ocean and land and associated baroclinicity may favor coastal cyclogenesis events, some of which may result in cutoff cyclone development.

Terrain also plays a role on cutoff cyclone frequency distributions over the SH. Tennant and Van Heerden (1994) found that topography was at least partially responsible for cutoff cyclone formation over southern Africa, and this may explain the frequency maxima seen there (Fig 3.10). Cutoff cyclones tend to occur on both sides of the southern Andes Mountains (Fig. 3.15), as shown in Hoskins and Hodges (2005), but not directly over the mountains. It is possible that cutoff cyclones approaching the Andes from the west within mean westerly flow break up upon reaching the high terrain. A midlevel cyclone can redevelop and possibly become a cutoff cyclone east of the Andes due to vortex stretching and associated regeneration of a cyclonic circulation. This may also be the case near the Antarctic Peninsula. Cutoff cyclones frequently occur over the Bellingshausen and Weddell Seas to the west and east of the Antarctic Peninsula, respectively, but not over the Antarctic Peninsula due to its high terrain. Other areas over the Antarctic coast and mainland are favored for cutoff cyclone activity where ice shelves are lower in elevation (e.g., the Amery Ice Shelf near the Lars Christensen Coast).

6.2 Overview of 20 Case Studies

The analysis of 20 warm-season cases of 500-hPa cutoff cyclones that tracked through the CSTAR domain led to the identification of five distinct patterns of lower-, middle-, and upper-level features based on 500-hPa cutoff–trough system tilt (two positive tilts: types “A” and “B,” two neutral tilts: types “A” and “B,” and one negative tilt). Of the five patterns, the positive tilt “type A” scenario (Fig. 4.3) has the most defined frontal structures associated with a surface cyclone. A surface warm front and/or

prefrontal trough often act as a focus for critical lifting mechanisms. Large southerly 850-hPa v-wind anomalies associated with a warm conveyor belt east of the surface cyclone lead to strong isentropic lifting as the flow ascends the warm front and towards the equatorward-entrance region of an upper-level jet streak. Although pivoting midlevel vorticity maxima and associated DCVA may contribute to ascent and heavy precipitation over the northeastern U.S., warm-air advection and the aforementioned surface boundaries tend to be the main forcing mechanisms that lead to heavy precipitation.

The positive tilt "type B" pattern (Fig. 4.4) includes a surface cyclone that develops off the Northeast or mid-Atlantic coasts. The southeasterly low-level flow to the northeast of the surface cyclone draws in moisture from the western North Atlantic and enhances instability. The magnitude of the low-level moisture flux within the aforementioned southeasterly flow was found to be directly correlated to precipitation amounts in the positive tilt "type B" pattern. Moisture flux convergence has been shown to be a good indicator of the intensity of precipitation (e.g., Banacos and Schultz 2005). The three highest ranked precipitation days out of all 12 days of the positive tilt "type B" pattern had 850-hPa moisture fluxes greater than 1 SD above normal. This strong moisture flux and the associated lifting mechanisms discussed in sec. 4.1.2 lead to stratiform bands with embedded convection rotating around the north side of the surface cyclone.

The neutral tilt "type A" pattern (Fig. 4.5) also involves strong low-level flow off the western North Atlantic. A surface trough and sea-breeze front approach New England from the west and east, respectively. Moisture is advected northwards by a low-level jet and can lead to heavy precipitation in conjunction with the aforementioned

lifting mechanisms. Severe wind reports are common in the heaviest precipitation areas. Farther to the west near the cold pool coinciding with the 500-hPa cutoff cyclone, thermodynamic parameters are generally conducive to large hail in conjunction with deep convection. The three highest ranked precipitation days out of all the neutral tilt days fit into the "type A" pattern.

The westerly-to-northwesterly low-level flow occurring with the neutral tilt "type B" pattern (Fig. 4.6) leads to drier conditions over the northeastern U.S. than for the previous three flow patterns discussed in the current section. Localized heavy precipitation still can result from slow-moving deep convection occurring in conjunction with ascent driven by DCVA associated with midlevel vorticity maxima pivoting around the cutoff cyclone. Vorticity maxima that are elongated in shape and oriented perpendicular to the midlevel flow are likely to generate large convective bands that can produce severe weather. Geopotential height falls at 500 hPa can be significant as the 500-hPa cutoff cyclone approaches the northeastern U.S. from the north and west. Several studies (e.g., David 1976; Johns 1984) have noted that hail commonly occurs during the warm season when 500-hPa geopotential height falls are significant. More hail reports occurred with the neutral tilt "type B" pattern than in any other flow pattern.

The negative pattern (Fig. 4.7) exhibits several similarities to the neutral tilt "type B" pattern, including dry low-level flow, an elongated surface trough, and favorable thermodynamic ingredients for severe weather. The terrain over the northeastern U.S. can aid in development of convection, as differential heating between the ground over elevated terrain and the adjacent free atmosphere at the same height can lead to convergent upslope flow (e.g., Pielke and Segal 1986). The presence of a sea-breeze

front over the eastern New England coast may also increase the threat for severe weather (e.g., Wilson 2008).

Figure 4.8 shows a direct relationship between standardized anomalies of PWAT and ranked precipitation days. The positive tilt "type A" pattern features the highest ranked precipitation days on average and over half of the days experiencing PWAT anomalies greater than 2 SDs above normal. This high PWAT is a result of the synoptic-scale southerly flow east of the 500-hPa cutoff cyclone advecting moisture from the Gulf of Mexico and western North Atlantic. Precipitation in the neutral tilt "type A" pattern is usually heavy over a larger area than in the positive tilt "type B" pattern. This difference may be due to the tendency for stronger low-level moisture fluxes and warm-air advection associated with the neutral tilt "type A" scenario. The neutral tilt "type B" and negative tilt patterns involve westerly-to-northwesterly dry flow and are low in the precipitation day ranking scheme. The tendency for the 500-hPa cutoff cyclones in these two flow patterns to be located north of the northeastern U.S. and follow Northwest tracks (Novak et al. 2002) inhibits the development of moist flow from off the western North Atlantic.

6.3 Analyses of Two 2008 Case Studies

6.3.1 16–20 June 2008

The 16–20 June 2008 cutoff cyclone followed a Northwest track (Fig. 5.1) and can be classified as a neutral tilt "type B" cutoff cyclone. Severe weather was

widespread across the northeastern U.S. on 16 June (183 severe storm reports total) as northwesterly flow associated with the cutoff cyclone led to a northwesterly flow severe weather event (Johns 1982, 1984; Fritsch and Giordano 1991). Instability was widespread as midlevel cold-air advection and low-level diurnal heating occurred across Pennsylvania and New York, yielding very steep lapse rates (Fig. 5.13b). In addition, 500-hPa geopotential heights fell significantly on 16 June (e.g., from 571 dam on 0000 UTC 16 June to 564 dam on 0000 UTC 17 June at ALB), which is a favorable ingredient for thunderstorms to produce hail (e.g., David 1976; Johns 1984).

The 0000 UTC 13 June NCEP GFS forecast (not shown) predicted morning precipitation to end midday on 16 June, with no widespread convection forming across Pennsylvania and New York later in the day. The NCEP North American Mesoscale model (NAM) forecast (not shown), on the other hand, correctly predicted widespread precipitation to develop across Pennsylvania and New York during the afternoon. A forecasting issue on 15 June was whether a prefrontal lee trough across eastern Pennsylvania would extend northward into New York during the afternoon of 16 June and if any other mesoscale boundaries would develop. The prefrontal lee trough did verify northwards into New York on 16 June (Fig. 5.13a), and severe weather was widespread across central and eastern New York (Fig. 5.10). The deep convection across Pennsylvania and New York was also driven by ascent occurring in conjunction with DVCA associated with a midlevel vorticity maximum (Figs. 5.7a–b and 5.12). Multicells and isolated supercells occurring across eastern New York and Pennsylvania at 1800 UTC 16 June (Fig. 5.6b) became organized later in the day into an elongated squall line (Fig. 5.6c) as the midlevel flow was strong and shear was unidirectional. Farther to the

north across northeastern New York, convection did not develop because of persistent cloud cover that limited surface heating and instability.

Although precipitation and severe weather across the northeastern U.S. on 16 June was widespread, amounts were generally less than 3 cm as low-level moisture fluxes and PWAT values (Fig. 5.13a) were climatologically normal. This shows the value in using PWAT anomaly forecasts in QPFs. Precipitation amounts were also generally light because of strong midlevel flow yielding relatively fast storm motion. The cutoff cyclone entered a null phase on 17 June that lasted through 20 June, as PWAT values were low (Figs. 5.19a–b) and forcing for ascent was either absent or localized. Severe weather was infrequent and primarily diurnal in nature. The main forecasting issue on 17–20 June was where exactly isolated convection would form due to any surface boundaries or differential heating between elevated terrain and the adjacent free atmosphere at the same altitude.

6.3.2 23–25 July 2008

The 23–25 July 2008 cutoff cyclone can be classified as a neutral tilt "type A" cutoff cyclone. A strengthening downstream ridge over the western North Atlantic (greater than 2 SDs above normal in terms of 500-hPa geopotential height) (Fig. 5.22) led to a blocking pattern and associated upstream amplification of a positively tilted trough over eastern Canada. Bell and Bosart (1994) noted that significant downstream ridge amplification acted as a dynamical precursor leading to cutoff cyclogenesis. As a strong 500-hPa wind speed maximum reached the base of a slight positively tilted trough on 23

July, vorticity was highly concentrated at the trough base, and a resulting closed cyclonic circulation formed just north of Lake Erie at 1200 UTC 23 July, as shown in Fig. 5.22a. The same scenario leading to cutoff cyclogenesis has been studied in Keyser and Shapiro (1986, sec. 2d), Bell and Bosart (1993), and Bell and Keyser (1993).

In the 23–25 July 2008 case, several cyclonic vorticity maxima developed as the 500-hPa cutoff cyclone formed (Figs. 5.27a–b). Severe weather tended to cluster in regions of DCVA near surface boundaries (Figs. 5.29 and 5.39) in regions of strong low-level vertical wind shear (Figs. 5.30 and 5.40). Severe weather on 24 July, including an EF2 tornado, was associated with low-level positive θ_e advection and a southerly 850-hPa jet that had v-wind anomalies of 4–5 standard deviations above normal (Figs. 5.41 and 5.42). The anomalously strong low-level jet and anomalously high PWAT values were symptomatic of the rapid poleward transport of tropical moisture from the Gulf of Mexico and western North Atlantic and the resulting moisture convergence over the northeastern U.S. (Fig. 5.32).

A major forecasting issue with this cutoff cyclone was where the axis of heaviest precipitation would occur during 23–24 July. The NCEP GFS forecast (not shown) in the two days leading up to 23 July was consistently too fast in advancing the largest rainband (Figs. 5.26b–c) eastward and predicted the heaviest precipitation to fall across central New England. The NCEP NAM forecast (not shown) was more accurate than the GFS forecast, and predicted the heaviest precipitation to occur farther to the west. The axis of heaviest precipitation verified to eastern New York (Fig. 5.23), where widespread rain amounts of 7–9 cm occurred along a north–south-oriented band. Areawide storm-total precipitation amounts also were under-forecasted in both models. Forecast challenges

arose from the presence of multiple precipitation modes, including convective lines/bow echoes, HP supercells, and stratiform rain regions. PWAT anomalies of 1–2.5 SDs above normal yielded flash flooding over the northeastern U.S. (Figs. 43a–b).

An upper-level jet streak across western New York and southwestern Quebec was critical in that portions of Pennsylvania and New York were located in its equatorward-entrance region on 23 July (Figs. 5.28a–b). The same jet streak placed southern New England in its equatorward-entrance region on 24 July (Figs. 5.38a–b). The implied upper-level divergence and associated midlevel upward vertical motion in these areas likely maintained and enhanced the north–south-oriented rainbands on 23–24 July (Figs. 5.26b–c and 5.36a–c). The location of upper-level jet streaks associated with 500-hPa cutoff cyclones and the accompanying areas of upper-level divergence were found to be key factors in determining a precipitation distribution with a cutoff cyclone in the current study and several others (e.g., Hsieh 1949; PN, sec. 12.6; Najuch 2004).

6.4 Forecasting Considerations

Forecasting precipitation and severe weather distributions associated with 500-hPa cutoff cyclones can be challenging during the warm season. Accurately forecasting these distributions relies on properly timing short-wave troughs and associated vorticity maxima, along with assessing the thermodynamic environment that these features will encounter. It is hoped that this study can contribute to increased situational awareness concerning cutoff cyclones and lead to improved precipitation forecasts. The following steps can be utilized to improve cutoff cyclone forecasts:

1) Use the five distinct patterns of lower-, middle-, and upper-level features based on 500-hPa cutoff–trough system tilt as a means of pattern recognition.
2) Survey the large-scale upper-level jet pattern. As previously stated, areas of upper-level divergence associated with jet streaks are favored for high precipitation amounts.
3) Use guidance from multiple models and ensembles to judge the timing of midlevel vorticity maxima pivoting around the 500-hPa cutoff cyclone.
4) Utilize standardized anomaly forecasts, especially those of PWAT and 850-hPa wind speed, to assess the potential impact and significance of a precipitation event.
5) Locate where surface troughs and midlevel vorticity maxima intersect areas of steep midlevel lapse rates, as thunderstorms and hail are favored in these regions.
6) Pay close attention to surface boundaries, including prefrontal troughs and sea-breeze fronts, which can be critical in the near-term forecast.

This list offers forecasters tools to better predict precipitation and severe weather distributions associated with a 500-hPa cutoff cyclone. Although numerical weather prediction models may help to predict the formation and general movement of a cutoff cyclone, the human forecaster needs to accurately assess multiscale atmospheric conditions and be aware of their potential impacts (e.g., flash flooding and severe weather).

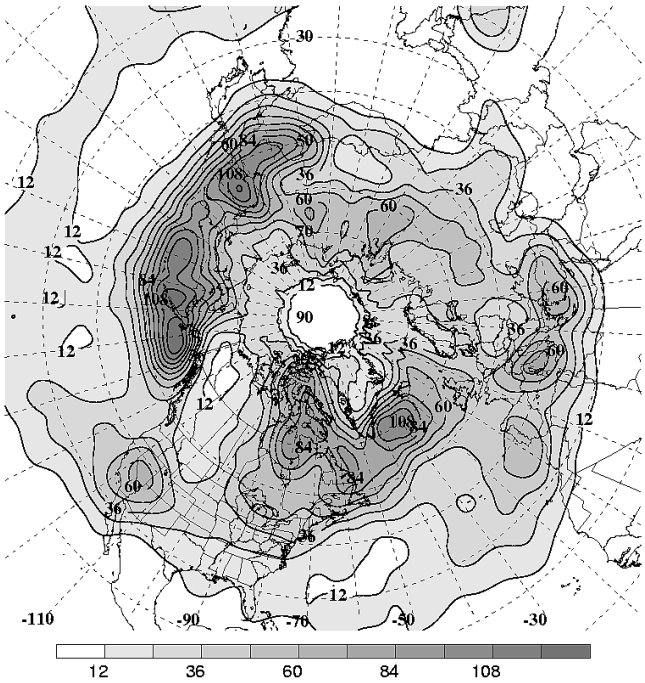

Fig. 6.1. Total number of cutoff cyclone events (shaded and contoured every 12 events) per grid point for the NH fall for 1948–2001. Source: Smith (2003), Fig. 3.5.

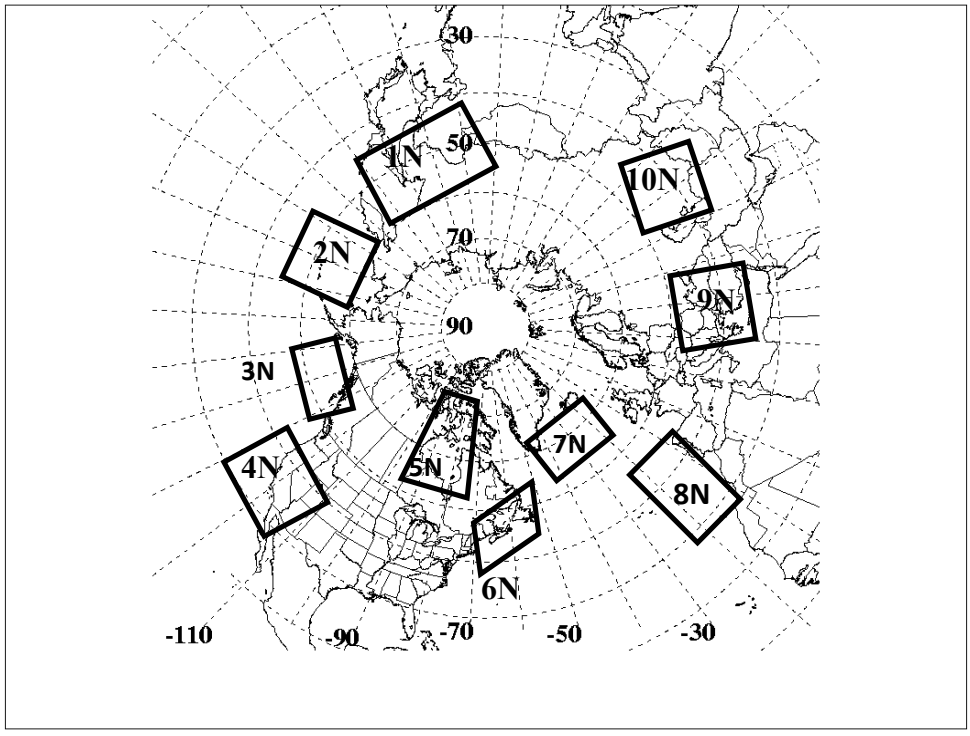

Fig. 6.2. Favored areas of 500-hPa cutoff cyclone activity across the NH. Source: Smith (2003), Fig. 3.11.

a)

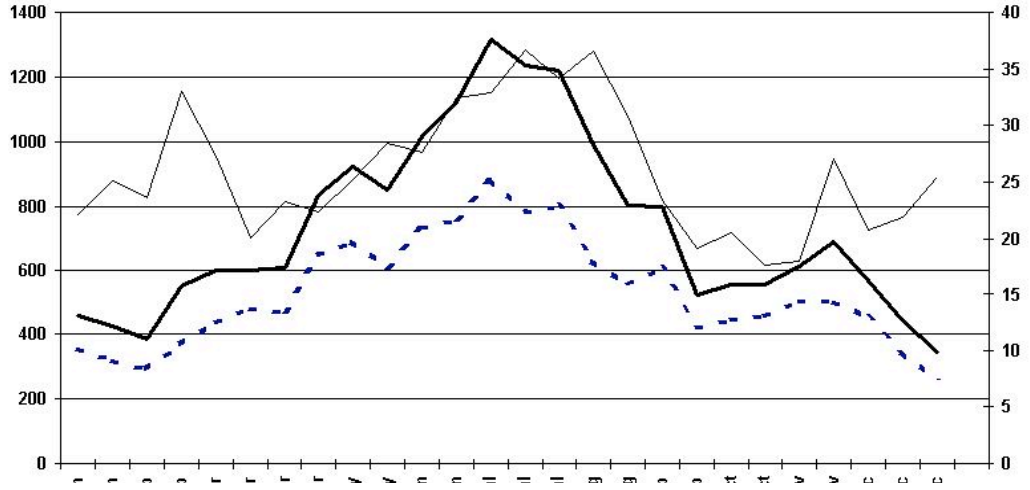

b)

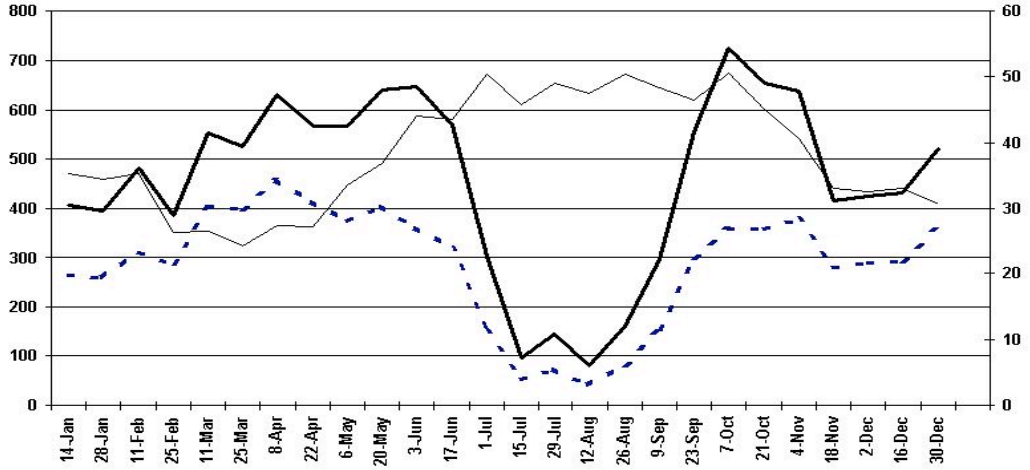

Fig. 6.3. Number of 500-hPa cutoff cyclones (dashed line), 6-h analyses with a cutoff cyclone (thick solid line), and percentage of 6-h analyses that exceed number of events (thin solid line) for (a) box 3N and (b) box 4N, as defined in Fig. 6.2. Source: Smith (2003), Figs. 3.12c–d.

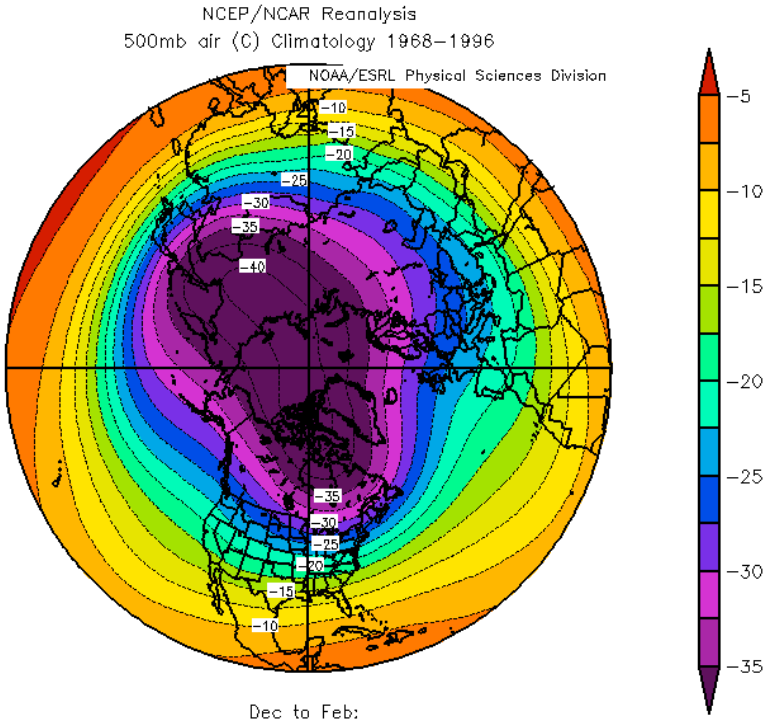

Fig. 6.4. Composite mean 500-hPa temperature (shaded according to the color bar every 5ºC) for December, January, and February, 1968–1996.

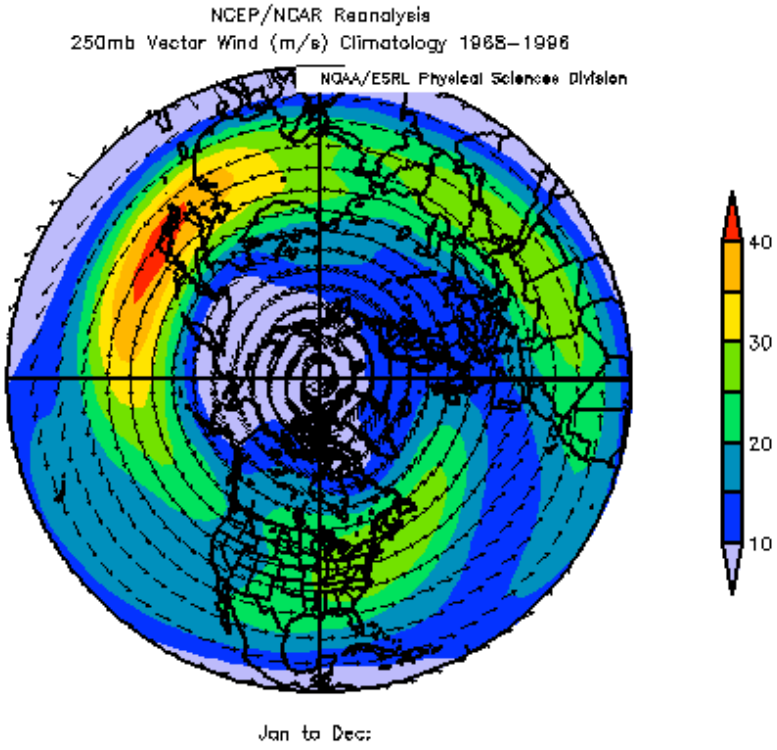

Fig. 6.5. Composite mean 250-hPa wind direction (arrows) and speed (shaded according to the color bar every 5 m s^{-1}) for 1968–1996.

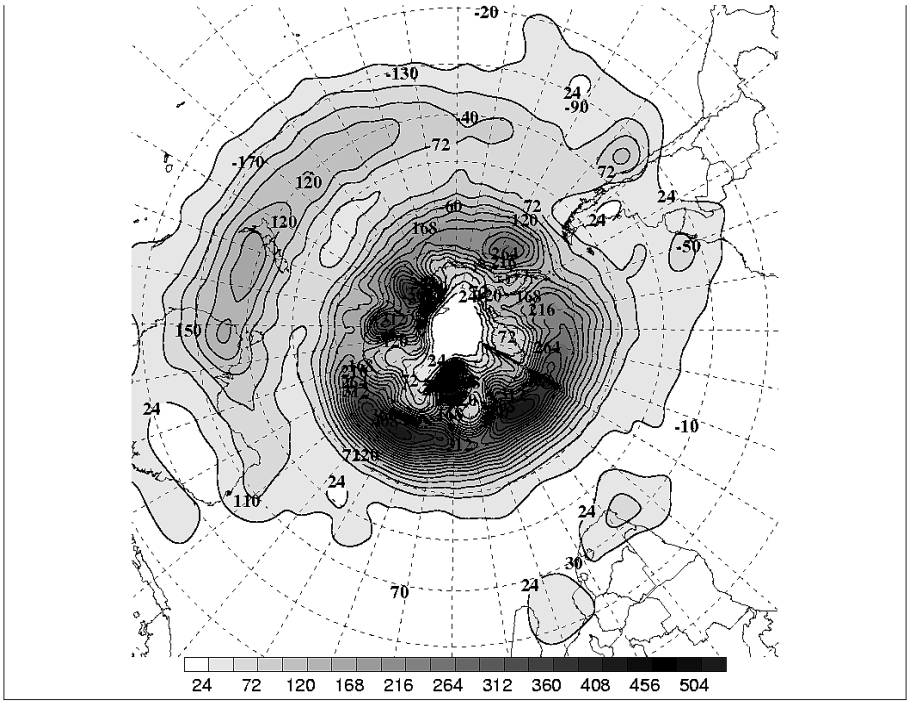

Fig. 6.6. Total number of cutoff cyclone events (shaded and contoured every 24 events) per grid point for the SH for 1948–2001. Source: Smith (2003), Fig. 3.24.

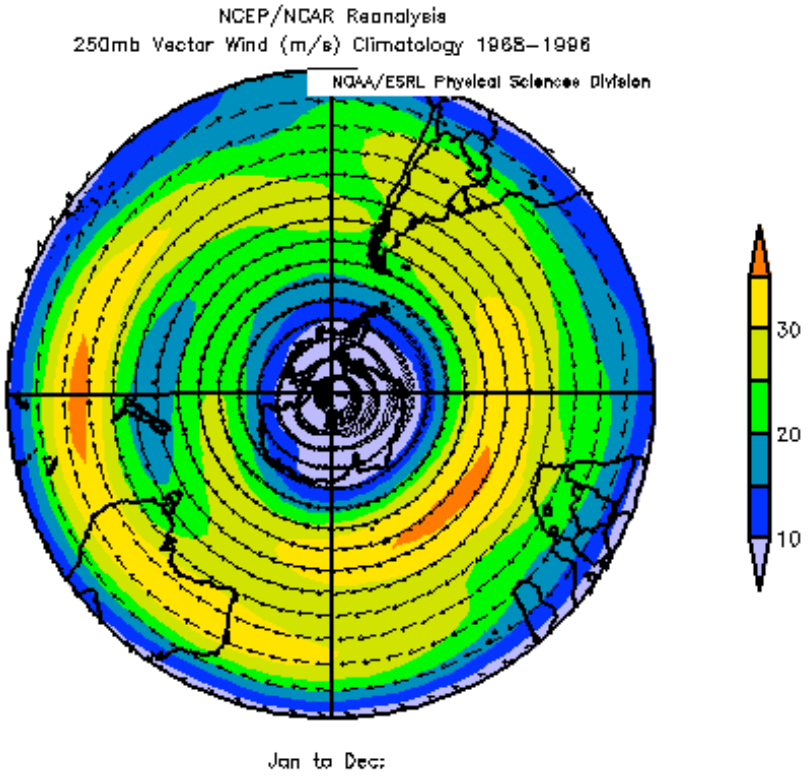

Fig. 6.7. As in Fig. 6.5 but for the SH.

7. Conclusions and Future Work

7.1 Conclusions

A 61-year (1948–2008) global and regional climatology of 500-hPa cutoff cyclones has been presented. Cutoff cyclones were objectively identified using the NCEP–NCAR global gridded reanalysis dataset. A cutoff cyclone was defined as a 500-hPa geopotential height minimum possessing at least a 30-m geopotential height rise in all directions for at least 12 h. Distributions of cutoff cyclone frequencies are shown for the NH, SH, and Tropics. The frequency distributions indicate particular regions favorable for cutoff cyclone occurrence. The most prolific area of frequent cutoff cyclone activity for the NH is over the northern Pacific Ocean. Other notable areas include the southwestern U.S., Hudson Bay region, U.S./Canadian Maritimes, southeast of Greenland, southern Europe eastward through the Turkish Plateau, and eastern India. Minima in cutoff cyclone frequency, found over a large portion of China, Greenland, the Rocky Mountains, and the subtropical central Atlantic and central Pacific, are related to either high terrain or to semipermanent high pressure systems, which produce unfavorable environments for the vorticity production needed for cyclogenesis. The most prominent areas of frequent cutoff cyclone activity over the SH are near the Lars Christensen Coast, Mawson Peninsula, Ross Sea, and along a 15°-latitude-wide band surrounding Antarctica from 20°W through 120°E longitude. Although less common than in polar regions, cutoff cyclones do occur in SH middle latitudes, especially near New Zealand and both southwest and southeast of the South American and African

mainlands. Major influences on cutoff cyclone development include orography, upper-level jets, and baroclinicity along coasts.

The results of an in-depth study of 20 warm-season cases of 500-hPa cutoff cyclones that passed through the CSTAR domain during the 2000–2008 warm seasons have been shown. Cases were chosen that illustrate the various challenges associated with forecasting heavy precipitation and severe weather in conjunction with cutoff cyclones. A total of 45 storm days occurring in conjunction with the 20 cutoff cyclone cases were selected for examination. This examination led to the identification of five distinct patterns of lower-, middle-, and upper-level fields and features, including low-level temperature and moisture, low-level jets, and upper-level jet streaks, based on 500-hPa cutoff–trough system tilt (two positive tilts: types "A" and "B," two neutral tilts: types "A" and "B," and one negative tilt). The positive tilt "type A" and neutral tilt "type A" scenarios tend to produce the most widespread heavy precipitation of the five patterns. The neutral tilt "type B" and negative tilt patterns yield a higher threat of severe weather than flash flooding. These five patterns can be used as a means of pattern recognition when a cutoff cyclone is forecasted to occur over the northeastern U.S.

Two cases of 500-hPa cutoff cyclones from the sample of 20 warm-season cases were selected for detailed diagnostic analysis due to their difficult-to-forecast nature and widespread high-impact weather conditions across the northeastern U.S. One case occurred in June (16–20 June 2008) and the other occurred in July (23–25 July 2008). Both cases had over 100 severe storm reports, while only the July case had widespread flash flooding. Precipitation was lighter in the June case, as moisture fluxes and PWAT values were climatologically normal. Severe weather was widespread across the

northeastern U.S. on 16 June in association with a northwesterly flow severe weather event. The June case entered a null phase on 17 June that lasted through 20 June, as available moisture was consistently low and forcing for ascent was either absent or localized. The 23–25 July 2008 cutoff cyclone, on the other hand, was active throughout its lifetime. Widespread heavy precipitation and severe weather occurred in a very moist environment containing PWAT values of 1–2.5 SDs above normal.

7.2 Future Work

This research was a continuation of the 500-hPa cutoff cyclone research performed by Novak et al. (2002), SM, Fracasso (2004), and Najuch (2004). The current study advances the work on forecasting precipitation distributions associated with warm-season cutoff cyclones. Tasks to be conducted in future research include:

1) Perform the cutoff cyclone climatology with a finer resolution dataset. The ECMWF ERA-40 has a 1.0° latitude–longitude grid. The North American Regional Reanalysis dataset has 32-km resolution and could be utilized to perform a cutoff cyclone climatology over North America.
2) Study cutoff cyclone frequencies and trends with respect to teleconnection indices, including the Arctic Oscillation, North Atlantic Oscillation, Pacific/North American Index, and Antarctic Oscillation.
3) Include additional fields in the schematics of the five synoptic-scale flow patterns, including temperature and height anomalies at various levels.

4) Composite tropospheric fields and features in a similar manner as the current study to create schematics for cool-season cutoff cyclones.
5) Perform detailed diagnostic analysis for several cutoff cyclone cases from all five synoptic-scale flow patterns.

REFERENCES

Alpert, P., B. U. Neeman and Y. Shay-El, 1990: Intermonthly variability of cyclone tracks in the Mediterranean. *J. Climate,* **3**, 1474–1478.

Anthes, R. A., 1983: Regional models of the atmosphere in middle latitudes. *Mon. Wea. Rev.,* **111**, 1306–1335.

Atallah, E. H. and A. R. Aiyyer, 2002: Precipitation associated with 500 hPa closed Cyclones. *4th Northeast Operational Regional Workshop, 5–6 November 2002, Albany, NY.*

———, L. F. Bosart, and A. R. Aiyyer, 2007: Precipitation distribution associated with landfalling tropical cyclones over the eastern United States. *Mon. Wea. Rev.,* **135**, 2185–2206.

Banacos, P. C., and D. M. Schultz, 2005: The use of moisture flux convergence in forecasting convective initiation: Historical and operational perspectives. *Wea. Forecasting,* **20**, 351–366.

Bell, G. D. and L. F. Bosart, 1989: A 15-year climatology of 500 hPa closed cyclone and anticyclone centers. *Mon. Wea. Rev.*, **117**, 2142–2163.

——— and ———, 1993: A case study diagnosis of the formation of an upper-level cutoff cyclonic circulation over the eastern United States. *Mon. Wea. Rev.*, **121**, 1635–1655.

——— and ———, 1994: Mid-tropospheric closed cyclone formation over the southwestern United States, the eastern United States, and the Alps. *Mon. Wea. Rev.*, **122**, 791–813.

——— and D. Keyser, 1993: Shear and curvature vorticity and potential-vorticity interchanges: Interpretation and application to a cutoff cyclone event. *Mon. Wea. Rev.,* **121**, 76–102.

Berggren, R., B. Bolin, and C. G. Rossby 1949: An aerological study of zonal motion, its perturbation and breakdown**.** *Tellus.*, **1**, 14–37.

Blender, R., M. Schubert, 2000: Cyclone tracking in different spatial and temporal resolutions. *Mon. Wea. Rev.*, **128**, 377–384.

Bowie, E. H., and R. H. Weightman, 1914: Types of storms of the United States and their average movement. *Mon. Wea. Rev.,* **42** (Suppl.), 1–37.

Businger, S., T. Birchard, K. Kodama, P. Jendrowski, and J.-J. Wang, 1998: A bow echo and severe weather associated with a Kona low in Hawaii. *Wea. Forecasting,* **13**, 576–591.

Chan, A. C., S. J. Colucci and A. T. DeGaetano, 2003: Predicting East Coast winter storm frequencies from midtropospheric geopotential height patterns. *Weather and Forecasting*, **18**, 1177–1191.

Colucci, S. J., 1985: Explosive cyclogenesis and large-scale circulation changes: implications for atmospheric blocking. *J. Atmos. Sci.,* **42**, 2701–2717.

———, 1987: Comparative diagnosis of blocking vs. non-blocking planetary-scale circulation changes during synoptic-scale cyclogenesis. *J. Atmos. Sci.,* **44**, 124–139.

Crocker, A. M., W. L. Godson, and C.M. Penner 1947: Frontal contour charts. *J. Meteo.,* **4**, 95–99.

David, C. L., 1976: A study of upper air parameters at the time of tornadoes. *Mon. Wea. Rev*., **104**, 540–545.

desJardins, M. L., K. F. Brill, and S. S. Schotz, 1991: Use of GEMPAK on UNIX workstations. *Proc. Seventh Int. Conf. On Interactive Information and Processing Systems for Meteorology, Oceanography, and Hydrology*, New Orleans, LA, *Amer. Meteor. Soc.*, 449–453.

Dole, R. M., 1986: Persistent anomalies of the extratropical Northern Hemisphere wintertime circulation: Structure. *Mon. Wea. Rev.*, **114**, 178–207.

——— and N. D. Gordon, 1983: Persistent anomalies of the extratropical Northern Hemisphere wintertime circulation: Geographical distribution and regional persistence characteristics. *Mon. Wea. Rev.*, **111**, 1567–1586.

Doyle J. D., and M. A. Shapiro, 1999: Flow response to large scale topography: The Greenland tip jet. *Tellus*, **51A**, 728–748.

Eliassen, A., and E. Kleinschmidt, 1957: Dynamic Meteorology, *Handbuch der Physik,* Vol. 48, Springer-Verlag, 154 pp.

Environmental Modeling Center, Global Climate and Weather Modeling Branch, 2003: The GFS atmospheric model. NCEP office note 442, 14 pp. [Available online at http://www.emc.ncep.noaa.gov/officenotes/newernotes/on442.pdf.].

Fracasso, A. R., 2004: Case studies of cool season 500 hPa cutoff cyclone precipitation distribution. Masters of Science Thesis, Department of Earth and Atmospheric Sciences, University at Albany/SUNY, Albany, NY, 121 pp.

Fritsch, J. M. and R. R. Carbone, 2004: Improving quantitative precipitation forecasts in the warm season: A USWRP research and development strategy. *Bull. Amer. Meteor. Soc.*, **85**, 955–965.

——— and L.A. Giordano, 1991: Strong tornadoes and flash-flood-producing rainstorms during the warm season in the Mid-Atlantic region, *Wea. Forecasting*, **6**, 437–455.

———, R. A. Houze Jr., R. Adler, H. Bluestein, L. F. Bosart, J. Brown, F. Carr, C. Davis, R. H. Johnson, N. Junker, Y.-H. Kuo, S. Rutledge, J. Smith, Z. Toth, J. W. Wilson, E. Zipser, and D. Zrnic, 1998: Quantitative Precipitation Forecasting: Report of the Eighth Prospectus Development Team, U.S. Weather Research Program. *Bull. Amer. Meteor. Soc.*, **79**, 285–299.

Geng, Q. and M. Sugi, 2001: Variability of the North Atlantic cyclone activity in winter analyzed from the NCEP/NCAR Reanalysis data. *J. Climate.* **14**, 3863–3873.

Grumm, R. H. and R. Hart, 2001: Standardized anomalies applied to significant cold season weather events: Preliminary Findings. *Wea. Forecasting*, **16**, 736–754.

Hawes, J. T. and S. J. Colucci 1986: An examination of 500 mb cyclones and anticyclones in National Meteorological Center prediction models. *Mon. Wea. Rev.,* **114**, 2163–2175.

Higgins, R. W., J. E. Janowiack, and Y. P. Yao, 1996: A gridded hourly precipitation data base for the United States (1963–1993). NCEP/Climate Prediction Center Atlas 1, National Centers for Environmental Prediction, 46 pp.

Hodges, K. I., 1994: A general method for tracking analysis and its application to meteorological data. *Mon. Wea. Rev.,* **122**, 2573–2586.

Hoskins, B. J. and K. I. Hodges, 2002: New perspectives on the Northern Hemisphere winter storm tracks. *J. Atmos. Sci.,* **59**, 1041–1061.

——— and ———, 2005: A new perspective on Southern Hemisphere storm tracks. *J. Climate,* **18**, 4108–4129.

———, M. E. McIntyre and W.A. Robertson, 1985: On the use and significance of isentropic potential vorticity maps. *Quart. J. Roy. Meteorol. Soc.*, **111**, 877–946.

Hsieh, Y. P., 1949: An investigation of a selected cold vortex over North America. *J. Meteorol.,* **6**, 401–410.

Jensenius Jr., J. S., 1990: A statistical comparison of the forecasts produced by the NGM and LFM for the 1987/88 Cool Season. *Wea. Forecasting*, **1**, 116–127.

Johns, R. H., 1982: A synoptic climatology of northwest-flow severe weather outbreaks. Part I: Nature and significance. *Mon. Wea. Rev.*, **110**, 1653–1663.

———, 1984: A synoptic climatology of northwest-flow severe weather outbreaks. Part II: Meteorological parameters and synoptic patterns. *Mon. Wea. Rev.*, **112**, 449–464.

Jorgensen, D. L., W. H. Klein and A. F. Korte 1967: synoptic climatology of precipitation from 700 mb lows for the intermountain West. *J. Appl. Meteor.,* **6**, 782–790.

Junker, N. W. and E. Hoke, 1990: An examination of Nested Grid Model precipitation forecasts in the presence of moderate-to-strong low-level southerly inflow. *Wea. Forecasting*, **5**, 333–345.

———, M. J. Brennan, F. Pereira, M. J. Bodner, and R. H. Grumm, 2009: Assessing the potential for rare precipitation events with standardized anomalies and ensemble guidance at the Hydrometeorological Prediction Center. *Bull. Amer. Meteor. Soc.*, **77**, 437–471.

———, R. H. Grumm, R. Hart, L. F. Bosart, K. M. Bell, and F. J. Pereira, 2008: Use of standardized anomaly fields to anticipate extreme rainfall in the mountains of northern California. Wea. Forecasting, **23**, 336–356.

Kalnay, E., M. Kanamitsu, R. Kistler, W. Collins, D. Deaven, L. Gandin, M. Iredell, S. Saha, G. White, J. Woollen, Y. Zhu, A. Leetmaa, B. Reynolds, M. Chelliah, W. Ebisuzaki, W. Higgins, J. Janowiak, K. C. Mo, C. Ropelewski, J. Wang, R. Jenne, and D. Joseph, 1996: The NCEP/NCAR 40-year reanalysis project. *Bull. Amer. Meteor. Soc.*, **77**, 437–471.

Kerr, I. S., 1953: Some features of upper level depressions. *Tech. Note. Meteorol. New Zealand,* No. 106.

Keyser, D. and M. A. Shapiro, 1986: A review of the structure and dynamics of upper-level frontal zones. *Mon. Wea. Rev.,* **114**, 452–499.

Kistler, R., E. Kalnay, W. Collins, S. Saha, G. White, J. Woolen, M. Chelliah, W. Ebisuzaki, M. Kanamitsu, V. Kousky, H. Van den Dool, R. Jenne, and M. Fiorino, 2001: The NCEP–NCAR 50-year reanalysis: Monthly means CD-ROM and documentation. *Bull. Amer. Meteor. Soc.*, **82**, 247–267.

Klein, T., and G. Heinemann, 2002: Interaction of katabatic winds and mesocyclones near the eastern coast of Greenland. *Meteor. Appl.,* **9**, 407–422.

Klein, W. H., D. L. Jorgensen, and A. F. Korte, 1968: Relation between upper-air lows and winter precipitation in the western plateau states. *Mon. Wea. Rev*., **96**, 162–168.

König, W., R. Sausen and F. Sielmann, 1993: Objective identification of cyclones in GCM simulations. *J. Climate,* **6**, 2217–2231.

Konrad C. E. and S. J. Colucci, 1988: Synoptic climatology of 500 mb circulation changes during explosive cyclogenesis. *Mon. Wea. Rev.,* **116**, 1431–1443.

Korte, A. F., D. L. Jorgensen, and W. H. Klein, 1972: Synoptic climatological studies of precipitation in the plateau states from 850, 700, and 500 mb lows during spring. *NOAA Tech. Memorandum,* NWS TDL-48, 130 pp.

Najuch, J., 2004: Forecasting heavy precipitation associated with warm-season cutoff cyclones. Masters of Science Thesis, Department of Earth and Atmospheric Sciences, University at Albany/SUNY, Albany, NY, 112 pp.

Novak, M. J., L. F. Bosart, D. Keyser, K. D. LaPenta and T. A. Wasula, 2002: Climatology of warm-season cutoff cyclones and case study diagnosis of 14–17 July 2000. *19th Conf. On Weather Analysis and Forecasting, 12–16 Aug 2002, San Antonio, TX.*

Otkin, J. A., and J. E. Martin, 2004: A synoptic climatology of the subtropical kona storm. *Mon. Wea. Rev.,* **132**, 1502–1517.

Palmén, E., 1949: Origin and structure of high-level cyclones south of the maximum westerlies. *Tellus*, **1**, 22–39.

——— and K. M. Nagler, 1949: The formation and structure of large-scale disturbances in the westerlies**.** *J. Meteorol.*, **6**, 227–242.

——— and Newton, 1969: *Atmospheric Circulation:* The Academic Press, New York, New York. 603 pp.

Parker, S. S., J. T. Hawes, S. J. Colucci, and B. P. Hayden, 1989: Climatology of 500 mb cyclones and anticyclones 1950–1985. *Mon. Wea. Rev.,* **117**, 558–571.

Peltonen, T., 1963: A case study of an intense upper cyclone over eastern and northern Europe in November 1959. *Geophysica (Helsinki),* **8**, 225–251.

Pielke, R. A., and M. Segal, Mesoscale circulations forced by differential terrain heating, *Mesoscale Meteorology and Forecasting*, edited by P. Ray, chap. 22, pp. 516–548, *Amer. Meteor. Soc*., Boston, Mass., 1986.

Reitan, C. H., 1974: Frequencies of cyclones and cyclogenesis for North America, 1951–1970. *Mon. Wea. Rev.,* **102**, 861–868.

Rex, D.F., 1950: Blocking action in the middle troposphere and its effect on regional climate, I. An Aerology Study of Blocking Action. *Tellus,* **3**, 196–211.

Rogers, E., and L. F. Bosart, 1986: An investigation of explosively deepening oceanic cyclones. *Mon. Wea. Rev.,* **66**, 702–718.

Rossby, C. G., 1940: Planetary flow patterns in the atmosphere. *Quart. J. Roy. Meteorol Soc.*, **66**, Suppl. 68–87.

Sanders, F. and J. R. Gyakum, 1980: Synoptic-dynamic climatology of the bomb. *Mon. Wea. Rev.*, **108**, 1589–1606.

Simpson, R. H., 1952: Evolution of the Kona storm: A subtropical cyclone. *J. Meteor.*, **9**, 24–35.

Sinclair, M. R., 1997: Objective identification of cyclones and their circulation, intensity, and climatology. *Wea. Forecasting,* **12**, 595–612.

Smith, B. A., 2003: Cutoff Cyclones: A Global and Regional Climatology and Two Case Studies. Masters of Science Thesis, Department of Earth and Atmospheric Sciences, University at Albany/SUNY, Albany, NY, 165 pp.

Taljaard, J. J., 1985: Cut-off lows in the South African region. *South African Weather Bureau Tech Paper No. 14,* 153 pp.

Tennant, W. J., and J. Van Heerden, 1994: The influence of orography and local sea-surface temperature anomalies on the development of the 1987 Natal floods: A general circulation model study. *S. African J. Sci.,* **90**, 45–49.

Thorncroft, C. D., B. J. Hoskins, and M.E. McIntyre, 1993: Two paradigms of baroclinic wave life cycles. *Quart. J. Roy. Meteorol. Soc.*, **119**, 17–56.

Thorpe, A. J., 1986: Synoptic scale disturbances with circular symmetry. *Mon. Wea. Rev.,* **114**, 1384–1389.

Trenberth, K. E., 1991: Storm tracks in the Southern Hemisphere. *J. Atmos. Sci.,* **48**, 2159–2178.

van Loon, H., 1956: Blocking action in the Southern Hemisphere. *Notos*, **6**, 171–175.

Wilson, P. H., 2008: Warm-Season Lake-/Sea-Breeze Severe Weather in the Northeast. Masters of Science Thesis, Department of Earth and Atmospheric Sciences, University at Albany/SUNY, Albany, NY, 115 pp.